



KADIR HAS UNIVERSITY
GRADUATE SCHOOL OF SCIENCE AND ENGINEERING
BIOINFORMATICS AND GENETICS

***IN SILICO* MODELING OF DOPAMINE TRANSPORTER
AND DESIGN OF NOVEL NEUROPROTECTIVE DRUGS
FOR PARKINSON'S DISEASE**

TEODORA ĐIKIĆ

PhD THESIS

ISTANBUL, NOVEMBER, 2017

***IN SILICO* MODELING OF DOPAMINE TRANSPORTER
AND DESIGN OF NOVEL NEUROPROTECTIVE DRUGS
FOR PARKINSON'S DISEASE**

TEODORA ĐIKIĆ

PhD THESIS

Submitted to the Graduate School of Science and Engineering of Kadir Has University
in partial fulfillment of the requirements for the degree of PhD in the
BIOINFORMATICS AND GENETICS

ISTANBUL, NOVEMBER, 2017

I, TEODORA ĐIKIĆ

Hereby declare that this PhD Thesis is my own original work and that due references have been appropriately provided on all supporting literature and resources.

Hereby declare that both printed and electronic copies of my work will be kept in Kadir Has Information Center under the following condition as indicated below:

The full content of my thesis/project will not be accessible for 5 years. If no extension is required by the end of this period, the full content of my thesis will be automatically accessible from everywhere by all means.

TEODORA ĐIKIĆ

30.11.2017. Teodora Đikić

DATE AND SIGNATURE

ACCEPTANCE AND APPROVAL

This work entitled *IN SILICO* MODELING OF DOPAMINE TRANSPORTER, AND DESIGN OF NOVEL NEUROPROTECTIVE DRUGS FOR PARKINSON'S DISEASE prepared by TEODORA ĐIKIĆ has been judged to be successful at the defense exam held on 30th November 2017 and accepted by our jury as **PhD THESIS**.

Prof. Dr. Kemal Yelekçi (Kadir Has University)



Prof. Dr. Safiye Saę Erdem (Marmara University)



Prof. Dr. Pemra Doruker (Boęaziçi University)



Doę. Dr. Ebru Demet Akten Akdoęan (Kadir Has University)



Y. Doę. Dr. Őebnem EŐsiz Gökhan (Kadir Has University)



I certify that the above signatures belong to the faculty members named above.



Doę. Dr. Ebru Demet Akten Akdoęan
Institute Director

DATE OF APPROVAL: 30/November/2017

TABLE OF CONTENTS

Abstract	i
Özet	ii
Acknowledgements	iii
List of Tables	vi
List of Figures	vii
List of Abbreviations	x
1. Chapter 1: Introduction	1
2. Chapter 2: Parkinson's disease	4
2.1. Parkinson's disease	4
2.2. Pathogenesis.....	6
2.3. Apoptosis and necrosis	9
2.4. Oxidative stress.....	11
2.5. Mitochondrial damage and aging.....	14
2.6. Neurotoxins.....	17
2.7. α -Synuclein.....	17
2.8. Current therapies.....	19
2.9. Future perspectives.....	22
2.10. The idea of our study.....	24
3. Chapter 3: Dopamine transporter	26
3.1. Dopaminergic neurons.....	26
3.2. Dopamine transporter.....	29
3.3. Transport cycle.....	31
3.4. Interactions of DAT with other proteins.....	32
3.5. Pharmacology.....	35
4. Materials and Methods	41
4.1. Homology modeling.....	42
4.1.1. Building of hDAT model.....	44
4.2. Molecular docking.....	44
4.3. Molecular dynamics simulation.....	48
4.3.1. Molecular dynamics simulation of DAT.....	51
4.4. Virtual screening.....	53
4.4.1. Data set preparation.....	54
4.4.2. LDA-based SBVS.....	55
4.4.3. Pharmacophore-based LBVS.....	56
4.5. <i>In vitro</i> assays.....	58
4.4.6. HEK-DAT cell culture and ASP+ uptake.....	58
4.5. Design of novel hDAT substrates.....	61
5. Results and Discussion	63
5.1. Establishing new hDAT 3D models	63
5.2. Searching for the best conformation.....	70
5.3. Identification of promising hDAT substrate candidates.....	73
5.4. Evaluation of the model using fluorescent <i>in vitro</i> assays.....	81
5.5. Novel hDAT substrates/MAO inhibitors with potential neuroprotective activity.....	85
6. Conclusion	92
References	95

Curriculum Vitae	113
List of Publications	114
List of presentations	114
Appendix A	116
Appendix B	122
Appendix C	127



IN SILICO MODELING OF DOPAMINE TRANSPORTER AND DESIGN OF NOVEL NEUROPROTECTIVE DRUGS FOR PARKINSON'S DISEASE

ABSTRACT

Parkinson's disease (PD) is characterized by the loss of dopamine-generating neurons in the *substantia nigra* (SN) and *corpus striatum* (CS). Current treatments alleviate PD symptoms rather than exerting neuroprotective effect on dopaminergic neurons. New drugs targeting the dopaminergic neurons by specific uptake through the human dopamine transporter (hDAT) could represent a viable strategy for establishing selective neuroprotection. Molecules able to increase the bioactive amount of extracellular dopamine (DA), thereby enhancing and compensating a loss of dopaminergic neurotransmission, and to exert neuroprotective response because of their accumulation in the cytoplasm, are required.

By means of homology modeling, molecular docking and molecular dynamics simulations, we have generated 3D structure models of hDAT in complex with substrate and inhibitors. Our results clearly reveal differences in binding kinetics of these compounds to the hDAT in the open and closed conformations, critical for future drug design. The established *in silico* approach allowed the identification of three promising substrate compounds that were subsequently analyzed for their efficiency in inhibiting hDAT-dependent fluorescent substrate uptake, through *in vitro* live cell imaging experiments. Taken together, our work presents the first implementation of a combined *in silico/in vitro*-approach enabling the selection of promising dopaminergic neuron specific substrates.

Key words: hDAT, substrates, inhibitors, molecular dynamic simulation, drug design, neuroprotection

İN SİLİCO OLARAK PARKİNSON HASTALIĞI İÇİN YENİ NÖROPROTEKTİF İLAÇ TASARIMI VE DOPAMİN TRANSPORTERİNİN MODELLENMESİ

ÖZET

Parkinson hastalığı (PH), *substantia nigra* (SN) ve *corpus striatum* (CS) bölgelerinde dopamin üreten nöronların kaybedilmesi ile karakterize edilen bir olgudur. Yaygın olarak uygulanan tedavi dopamin nöronlarının kaybolmalarının korunması yönünde değilde ortaya çıkan semtoların azaltılmasına yöneliktir. İnsan dopamin tranporterleri (hDAT) yoluyla spesifik olarak sinir hücresine alınan ve dopaminerjik nöronları hedefleyen seçici sinir koruyucu (nöron protektif) ilaçlar geçerli bir strateji olabilir. Tedavide dopaminin hücre dışı biyoaktif miktarını artırabilen dolayısı ile dopaminerjik nörotransmisyonun kaybını dengeleyen ve kuvvetlendiren ve sitoplazmada birikerek nöroprotektif olarak davranabilen moleküller gerekir.

Bu çalışmada homoloji modelleme, moleküler doklama ve moleküler dinamik simülasyon metodları kullanılarak substrat ve inhibitörle komplekslenmiş hDAT'ın üç boyutlu (3D) yapı modelleri bulunmuştur.

Gelecekte yapılacak ilaç tasarımlarında önemli olan bileşiklerin farklı bağlanma kinetiklerini açıklayabilen hDAT'ın açık ve kapalı konformasyonları oluşturulmuştur. *In silico* yaklaşımla elde edilmiş olan yapılar bileşik veri bankası taraması sonucunda bize ümit vadeden üç substrat molekülünün tespit edilmesine olanak sağlamıştır. Bu substratların *in vitro* canlı hücre görüntü deneyleriyle hDAT'a dayalı fluoressan substratın hücreye geri girişi (uptake) inhibe etme etkileri de analiz edilmiştir. Bütün bu sonuçlar birlikte değerlendirildiğinde çalışmamız *in silico/in vitro* yaklaşımlarını birlikte kullanılarak dopaminerjik nöron spesifik substratların seçiminde bir ilk model oluşturmaktadır.

Anahtar Sözcükler: hDAT, substratlar, inhibitörler, moleküler dinamik simülasyon, ilaç tasarımı, nöroproteksiyon

ACKNOWLEDGEMENTS

First of all, I would like to thank my PhD advisor, Professor Kemal Yelekçi, for supporting me during these past three years. He has always been supportive and has given me the freedom to pursue various projects without objections, and has guided me through the research. Also, he always knew how to calm me down when I was anxious and he has helped me whenever I was in need. Aside from being an exceptional mentor, I have also learned to be a better person from him.

Moreover, I thank to other professors from my department, as well as groups from Molecular Discovery, Perugia and Central Institute of Mental Health, Mannheim who helped me with my project and gave me numerous constructive advices during these past three years.

I would like to thank my partner Đorđe Stojšić for believing in me when I doubted myself, for making me continue when I felt like quitting, and many, many tips that improved my English writing skills.

I would like to give thanks to my family, especially Ljiljana, Miroljub and Kristina Đikić for their trust in me and support all the time.

I would also like to thank my friends, especially Syazzana Arina Mohammad Azmi, Dunja Resanović, Gonca Dilcan, Serkan Altuntaş, Mohammed Osman Abd el Karem and Filip Vujačić for providing the support and friendship that I needed.

All these people and many others (too many to list here but you know who you are!) have made my time in Istanbul great and unforgettable. Next to them three years passed like three weeks.

I dedicate this thesis to them.

This work was sponsored by Marie Curie Fellowship, Training in Neurodegeneration, Therapeutics, Intervention and Neurorepair (TINTIN), Funding Scheme: FP7-MC-ITN with grant number: 608381.

LIST OF TABLES

Table 3.1. Chemical structures of some of DAT substrates.....	38
Table 3.2. Chemical structures of some DAT inhibitors.....	39
Table 4.1. Chemical formulas of neuroprotective compounds.....	62
Table 5.1. Known substrates docked in open and closed hDAT.....	70
Table 5.2. Known inhibitors docked in open and closed hDAT.....	71
Table 5.3. Known substrates docked in different snap-shots of the closed-out conformation.....	72
Table 5.4. Docking results of possible substrates.....	73
Table 5.5. Docking results of novel compounds.....	77
Table A.1.....	116
Table A.2.....	118
Table A.3.....	120
Table B.1.....	126

LIST OF FIGURES

Figure 2.1. Scheme of processes in DA neuron in PD.....	8
Figure 2.2. Apoptotic pathways.....	10
Figure 2.3. Mechanisms of neural necrosis.....	11
Figure 2.4. Mitochondrial Electron Transport Chain.....	15
Figure 2.5. Mechanism of Rasagiline neuroprotection.....	22
Figure 2.6. Dopamine, MPP+, and fluorescent DAT substrate.....	25
Figure 3.1. Dopaminergic pathways in the brain.....	27
Figure 3.2. Dopamine synthesis, release, signaling, and reuptake.....	29
Figure 3.3. DAT transport cycle.....	32
Figure 3.4. DAT and its protein-protein interactions.....	33
Figure 5.1. Sequence alignment.....	64
Figure 5.2. 3D model of hDAT.....	65
Figure 5.3. RMSD and residue RMSF.....	66
Figure 5.4. hDAT-amphetamine complex.....	67
Figure 5.5. hDAT-cocaine complex.....	67
Figure 5.6. hDAT-modafinil complex.....	68
Figure 5.7. Comparisson of hDAT-ligand conformations.....	69
Figure 5.8. Superposition of closed and opened hDAT conformations.....	69
Figure 5.9. SBVS model.....	74
Figure 5.10. LBVS model.....	76
Figure 5.11. Predicted interactions of compounds 1, 2, 3 and 6.....	81
Figure 5.12. HEK-hDAT cells.....	82
Figure 5.13. <i>In vitro</i> results.....	83
Figure 5.14. Exemplary images of compound 6.....	83
Figure 5.15. Alteration/inhibition of ASP+ uptake into HEK-hDAT cells.....	85
Figure 5.16. TK014.....	90
Figure 5.17. TK019.....	90
Figure 5.18. TK016.....	91
Figure A.1.....	117
Figure A.2.....	119

Figure A.3.....121
Figure C.1.....127



LIST OF ABBREVIATIONS

3-MT	3-methoxytyramine
POPC	1,2-palmitoyl-oleoyl- <i>sn</i> -glycero-3-phosphocholine
ADHD	Attention Deficit and Hyperactivity Disorders
MPTP	1-methyl-4-phenyl-1,2,3,6-tetrahydropyridine
MPP ⁺	1-methyl-4-phenylpyridinium cation
DCP	3,4-dichlorophenethylamine
DOPAL	3,4-dihydroxyphenylacetaldehyde
DOPAC	3,4-dihydroxyphenylacetic acid
DNA	Deoxyribonucleic Acid
MDEA	3,4-methylenedioxy-N-methylamphetamine
MDMA	3,4-Methylenedioxymethamphetamine
ASP ⁺	4-(4-(dimethylamino)-styryl)-N-methylpyridinium
6-APB	6-(2-aminopropyl)benzofuran
Ach	Acetylcholine
ATP	Adenosine Triphosphate
APP	Amyloid Precursor Protein
Å	Angstrom
AIF	Apoptosis-Inducing Factor
AMBER	Assisted Model Building with Energy Refinement
atm	Atmosphere
BLAST	Basic Local Alignment Search Tool
Bcl-2	B-cell Leukaemia/Lymphoma 2
Bax	BCL2-Associated Protein X
BDNF	Brain-Derived Neurotrophic Factor
CaMK	Calcium Calmodulin-dependent protein kinase
CHARMM	Chemistry at Harvard Molecular Mechanics
COMT	Catechol-O-Methyl Transferase
CNS	Central Nervous System
CS	Corpus Striatum
DA	Dopamine
DAT	Dopamine Transporter
dDAT	drosophila's DAT
ES	Embryonic Stem cells
EC	Extracellular
ERK	Extracellular Signal Regulated Kinase
FLAP	Fingerprints for Ligands and Proteins
FFNs	Fluorescent False Neurotransmitters
FF	Force Fields
GABA	Gamma Aminobutyric Acid

GDNF	Glia cell line-Derived Neurotrophic Factor
GAPDH	Glyceraldehyde-3-Phosphate Dehydrogenase
hDAT	human DAT
HEK	Human Embryonic Kidney cells
IC	Intracellular
IF	Inward-facing
K	Kelvin
kcal	Kilocalorie
LeuT	Leucine Transporter
LBVS	Ligand Based Virtual Screening
LDA	Linear Discriminant Analysis
MDA	Methylenedioxyamphetamine
mtDNA	Mitochondrial DNA
MAPKs	Mitogen-Activated Protein Kinase
MD	Molecular dynamics
MIF	Molecular Interaction Field
MAO	Monoamine Oxidase
NAMD	Nano Scale Molecular Dynamics
nNOS	Neural Nitric Oxide Synthase
NSS	Neurotransmitter Sodium Symporters
NMDA	N-methyl-D-aspartate
MNAP	<i>N</i> -methyl-naphthylaminopropane
NSAID	Nonsteroidal anti-inflammatory drugs
NA	Noradrenaline
NET	Noradrenaline transporter
NR4A2	Nuclear Receptor 4A2
NPT	Number of atoms, Pressure, Temperature
NVE	Number of atoms, Volume, Energy
NVT	Number of atoms, Volume, Temperature
OF	Outward-facing
PD	Parkinson's Disease
PARP1	Poly (ADP-ribose) Polymerase 1
PCA	Principal Component Analysis
PDB	Protein Data Bank
PKC	protein kinase C
DJ-1	Protein/Nucleic Acid Deglycase
ROS	Reactive Oxidative Species
ROC	Receiver Operating Characteristic
ROI	Region Of Interest
RMSD	Root Mean Square Deviation
RMSF	Root Mean Square Fluctuation
5-HT	Serotonin

SERT	Serotonin Transporter
SCL-6	Solute Carrier 6
SE	Standard Error
SEM	Standard Error of Mean
SBVS	Structure Based Virtual Screening
SN	Substantia Nigra
SPF	Survival-Promoting Factors
TFMAP	Trifluoromethylmethcathinone
TH	Tyrosin Hydroxylase
UCH-L1	Ubiquitin C-Terminal Hydrolase L1
VTA	Ventral Tegmental Area
VMAT2	Vesicular Monoamine Transporter 2
VS	Virtual Screening
VMD	Visual Molecular Dynamics

1. INTRODUCTION

Parkinson's disease (PD) is the second most common neurodegenerative disorder of the central nervous system. Typical symptoms include tremor, rigidity and impaired movement. It is characterized by the loss of dopamine-generating neurons in the *substantia nigra* (SN) and *corpus striatum* (CS), and by the accumulation of aggregates containing α -synuclein in the brain. These protein aggregates, named Lewy Bodies, clump together at axons and dendrites in neurons in the SN. They sterically hinder the transport of neurotransmitter-filled vesicles, which can no longer move along the cytoskeleton. Thus, neurotransmitter release is compromised, with a consequent gradual loss of neuronal function. (Underwood and Cross, 2009) An alternative mechanism of neurodegeneration is via the chemical damage to the membrane lipids by reactive radical species, which leads to membrane leakage. (Barnham et al., 2004) Both pathways contribute to the loss of cell function and neuronal death and are tightly connected. (Pavlin et al., 2016)

The dopamine transporter (DAT) is an integral membrane protein and member of the neurotransmitter sodium symporters (NSS) family. It is expressed in dopaminergic neurons of the central nervous system (CNS). Its fundamental role is the rapid DA reuptake from the extracellular space and thereby termination of DA signaling. DA uptake can be maintained against very large concentration gradients, from 1 to 20 substrate molecules per second. (A. S. Kristensen et al., 2011) After being taken up, enzymatic breakdown of DA to its metabolites is carried out by catechol-O-methyl transferase (COMT) and monoamine oxidase (MAO). MAO breaks down dopamine to 3, 4-dihydroxyphenylacetic acid (DOPAC) by the action of the enzyme aldehyde dehydrogenase. (Juárez Olguín et al., 2016a) Alternatively, cytosolic DA is taken up into vesicles by transport via the vesicular monoamine transporter 2 (VMAT2). (Wimalasena et al., 2008)

The neurotoxin MPTP (**1-methyl-4-phenyl-1,2,3,6-tetrahydropyridine**) is

converted into MPP⁺ (**1-methyl-4-phenylpyridinium cation**) by the enzyme MAO-B. This leads to parkinsonism in primates and non-primates by selective killing of dopaminergic neurons in the SN. MPP⁺-induced neurodegeneration is specific to dopamine neurons, since after DAT-dependent uptake it accumulates in mitochondria. MPP⁺ inhibits complex I in the electron transport chain, subsequently reducing adenosine triphosphate (ATP) production and causing oxidative stress. (Wiemerslage et al., 2013) Since the death of DA neurons is the major hallmark of PD, designing new neuroprotective drugs that use this pathway to enter DA neurons may yield potential molecular targets for the treatment of PD. Using this transport pathway as a basis we may design new drugs that specifically accumulate in the dopaminergic neurons. We could modify the structure of DAT substrates to act as antioxidants, scavenging ROS (Reactive Oxidative Species). (Juárez Olguín et al., 2016a) Alternatively, we can add groups that are enhancing the expression of anti-apoptotic protein Bcl-2 (like rasagiline). (Akao et al., 2002a, p. 2) Newly designed molecules would increase the bioactive amount of extracellular DA by competing for DAT-dependent uptake, thereby enhancing and compensating a loss of dopaminergic neurotransmission. Additionally, they may also start neuroprotective response due to their accumulation in the cytoplasm. In contrast to this, DAT inhibiting molecules may only compensate for the loss of DA signaling by reducing DA re-uptake.

To identify promising DAT uptake-dependent candidate molecules, it is necessary to establish a reliable screening model that addresses discriminant characteristics of DAT inhibitors and substrates. The classic alternating access model implies that the transporter protein shuttles through at least three conformational states during the transport cycle: (i) an outward-open conformation where the substrate binding pocket is accessible to the extracellular medium, (ii) an occluded conformation, where access to the pocket is blocked from either side, and (iii) an inward-facing conformation, where the pocket is open to the intracellular medium. (A. S. Kristensen et al., 2011) Therefore, candidate compounds have to be screened to determine and analyze their binding characteristics to different DAT conformations. Compounds with similar structures may bind to the various conformational states of DAT during the transport cycle with different binding affinities. Such occurrences would lead to differentially effective neuroprotection based on DAT's

transport capacity for a specific compound. Thus it is thus necessary to identify the specific transporter state leading to efficient compound uptake. (A. S. Kristensen et al., 2011)

In the current study we combined different *in silico* approaches i.e. homology modeling, docking, virtual screening and molecular dynamics, to identify new potential DAT substrates. We have used this approach to perform screening of compounds in order to identify candidates that, based on their hDAT binding characteristics, may be substrates that are, DAT-dependently accumulated in the cytoplasm. The simulation led to the identification of 99 potential substrates. In order to validate our *in silico* results, we have monitored the effect of the six most promising candidates on hDAT-dependent fluorescent substrate ASP⁺ (4-(4-(dimethylamino)-styryl)-N-methylpyridinium) uptake *in vitro*. *In vitro* assays with ASP⁺ confirmed that these compounds alter DA uptake, which means that they are competing with DA for DAT transport. The obtained results suggest a new way of searching DAT substrates. Afterwards, we used this knowledge to design novel potentially neuroprotective candidates. We combined the neuroprotective propargylamine moiety with DAT substrate part. DAT substrate part should act as a carrier of the neuroprotective group for the specific pharmacodelivery of the drug into the dopaminergic neuron.

2. PARKINSON'S DISEASE

2.1. Parkinson's disease

Parkinson's disease (PD) is the second most common neurodegenerative disorder in the world, with prevalence of 0.3% in industrialized countries, and 1% of people older than 60 years. (Sveinbjornsdottir, 2016) The main risk factor for PD is aging (Rijk et al., 1995); other risk factors include head trauma and exposure to certain environmental toxins. (Rang and Dale, 2007) In 95% of PD cases there is no genetic linkage but in the other 5% of cases it is inherited. (Dauer and Przedborski, 2003) Significant evidences suggest that genetic factors can increase predisposition to the disease. (Foltynie et al., 2002) Mutations in PRKN (gene for the parkin protein) and SNCA (gene encoding the α -synuclein protein) genes are crucial for the not only the manifestation of the disease, but also, for its progress and course. (Oczkowska et al., 2013) At present, 5 genes (α -synuclein (PARK1), parkin (PARK2), Ubiquitin C-Terminal Hydrolase L1 (UCH-L1), Protein/nucleic acid deglycase (DJ-1) and Nuclear Receptor 4A2 (NR4A2)) have been identified in familial Parkinson's disease. (Dekker et al., 2003; Polymeropoulos et al., 1997) Currently, 18 specific chromosomal regions (chromosomal locus), are labelled PARK, and numbered in chronological order of their identification (PARK1 - PARK18). The responsible gene has not yet been identified for all of the loci, nor do all of the identified genes contain causative or disease-determining mutations (i.e., variations in some of these genes are considered to be genetic risk factors, that can increase the risk of developing PD, rather than being a cause of it). (Christine Klein and Westenberger, 2012)

The clinical manifestation of PD can be seen after the pathology has already reached an advanced stage. (Braak et al., 2003) It is characterized by motor and non-motor symptoms.

- The motor symptoms are: **hypokinesia** (slowness of initiation of voluntary movements with progressive reduction in speed and amplitude of repetitive actions), **akinesia** (absence of voluntary movements), **rigidity** (increased resistance to passive movements of limbs), **tremor** (shaking), **postural instability**, **hypomimia** (“face like a mask”) etc. (Dauer and Przedborski, 2003; Hughes et al., 1992)
- Pre-motor symptoms can appear, before the motor symptoms and the diagnosis is made, and they include: **apathy** (lack of emotional involvement and interest), **excessive daytime sleepiness** and other sleep problems, and **constipation**, **anhedonia** (inability to experience pleasure), **memory problems**, **loss of sense of smell and taste**, **mood disturbances**, **excessive sweating**, **fatigue**, **pain**, **depression** and **anxiety**. (Sveinbjornsdottir, 2016)

Early in the course of the disease, symptoms are generally unilateral and mild, and the response to drug treatment is good. Later, even though symptoms progress and motor symptoms appear in the contralateral side, patients can function well, with basic therapy. This period is known as the “*honeymoon period*”. As the disease progresses, treatment becomes heavier and drug response becomes ineffective. The anti-parkinsonian drugs can induce potentially disabling dyskinesia. The disease more and more affects the quality of life and leads to dependency on medication for basic daily activities. (Hughes et al., 1992)

PD has typical neuropathological brain changes. It is characterized by the loss of dopamine-generating neurons in the *substantia nigra* (SN) and *corpus striatum* (CS), which results in decrease of dopamine (DA) levels in the brain. When the symptoms occur, 60-80% of dopaminergic neurons have already been lost. (Dauer and Przedborski, 2003) Decreased levels of other neurotransmitters have also been noticed, especially noradrenaline (NA) and serotonin (5-HT), but to a much lesser extent than DA. Hypokinesia is the symptom which is mainly connected to the decrease of DA. Other symptoms like rigidity and tremor have more complex mechanism and they are connected to other neurotransmitters (acetylcholine (Ach), noradrenaline (NA), serotonin (5-HT), gamma-aminobutyric acid (GABA)). Striatal cholinergic neurons are also included in the pathogenesis of PD. DA is strongly inhibiting hyperactivity of cholinergic neurons. Clearly, in PD there is a lack of DA, accordingly there is an excess of Ach. (Rang and Dale, 2007)

Moreover, inclusion bodies (called Lewy bodies) can be found in PD brain. In the pre-symptomatic stages of the disease, they are limited to the *medulla oblongata/pontine tegmentum* and olfactory bulb/anterior olfactory nucleus. With the progression of the disease, *substantia nigra* and other nuclei of the midbrain and forebrain become affected. Patients develop clinical symptoms of the disease at this stage. In the end stage, the process enters the neocortex and causes a wide variety of clinical manifestations. (Braak et al., 2003) The etiology and pathogenesis of PD will be explained more thoroughly in the following sections.

2.2. Pathogenesis

PD is a complex disease and the exact mechanism remains unknown. It is believed that the main pathological hallmark of PD is death of dopaminergic neurons. (Dauer and Przedborski, 2003) Neurodegeneration and Lewy body (LB) formation are the cause of the neuronal death. (Pavlin et al., 2016) Besides DA neurons, neurodegeneration is also found in noradrenergic, serotonergic and cholinergic neurons. (Dauer and Przedborski, 2003) Neuropathological studies of PD related neurodegeneration gave a possible explanation to the pathogenesis of the disease:

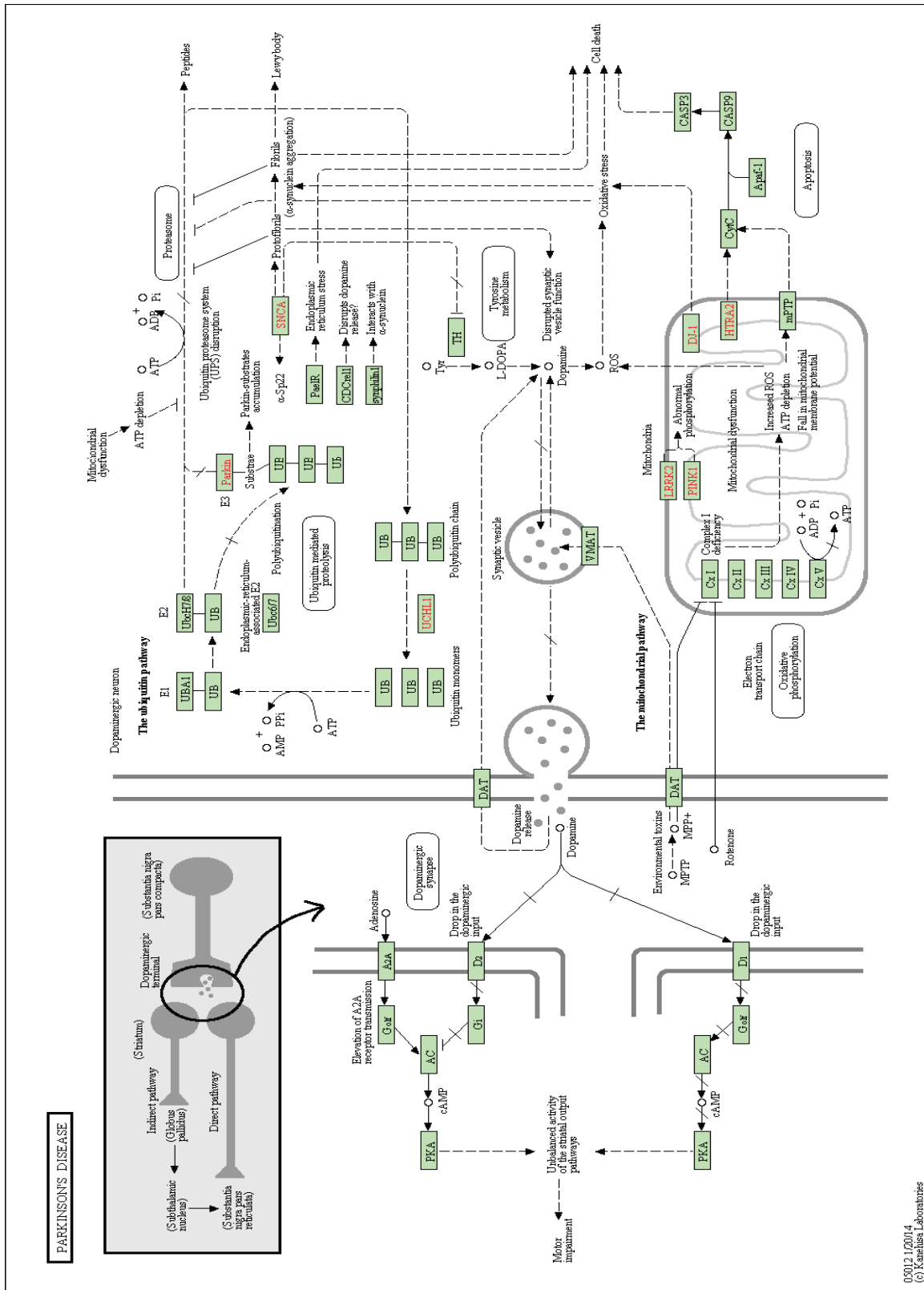
1. PD associated loss of dopaminergic neurons has a distinguishing topology which is different from the pattern that can be seen in normal ageing;
2. The degree of terminal loss in the striatum appears to be higher than the magnitude of SN dopaminergic neural loss;
3. Mechanism of synaptic DA clearance seems to be more dependent on dopamine transporter (DAT) in the striatum, than in other areas of the brain; (Dauer and Przedborski, 2003)

The pathogenesis involves several critical abnormalities, each of which could be the result of genetic or environmental factors. (Tanner et al., 2011) On the other hand, it is possible that endogenous toxins (which are side products of normal biochemical processes in the

cell) might form toxic substances due to exposure or inherited variations in metabolic pathways. A source of these endogenous toxins might be the normal metabolism of DA, where free radicals are formed. (Dauer and Przedborski, 2003) However, two main hypotheses of pathogenesis of PD and death of SN neurons are:

1. Misfolding and aggregation of proteins;
2. Mitochondrial dysfunction and oxidative stress, including toxic oxidized DA species. (Dauer and Przedborski, 2003)

Both these mechanisms are connected. Firstly, reactive oxidative species (ROS) oxidize heavy atom ions, which enhances the interaction with α -synuclein, promoting folding to β -form and giving rise to insoluble protein aggregates, and prevents the function of vesicular transport leading to gradual neuronal death. In the second pathway, ROS react with methylene groups of the nonpolar part of the lipid bilayer of cell and mitochondrial wall, resulting in membrane leakage, followed by the loss of resting potential and neuron death. (Pavlin et al., 2016)



03012.1/2011.4
© Kanazusa Laboratories

Figure 2.1 Scheme of processes in DA neuron in PD; Source: <http://www.genome.jp/kegg/pathway.html> (“KEGG PATHWAY: Parkinson’s disease - Homo sapiens (human),” n.d.)

2.3. Apoptosis and Necrosis

Apoptosis is programmed, ATP-dependent cell death. It results in the formation of apoptotic bodies containing the degraded contents of the dead cell. Thanks to the apoptotic bodies it does not cause inflammatory response. Once the apoptosis has started proper execution requires the coordinated activation and execution of multiple sub-processes. (Hengartner, 2000) In neurons, it is usually a p53 dependent process. Namely, p53 is a transcription factor which binds to DNA in a sequence-specific manner to activate transcription of target genes. (Benchimol, 2001) Cellular stress and reactive oxygen species (ROS) induce the loss of mitochondrial membrane integrity and the release of cytochrome c into the cytosol which results in apoptosome activation. Cytochrome c release is regulated by pro-apoptotic (Bax) and anti-apoptotic (Bcl-2) protein families. Bax is up-regulated through p53-mediated damage responses, while Bcl-2 is down-regulated. (Hengartner, 2000) It results in the formation of the cytochrome c-Apaf-1-caspase 9 complex. ROS can trigger the expression of p53-induced genes (PIGs) and multiple signaling cascades, inclusive of protein kinase C (PKC), mitogen-activated protein kinase (MAPKs), tyrosine kinases, Ras and phospholipase C (PLC) in neurons. (Davies and Morris, 2004; C. Klein and Westenberger, 2012) A caspase-independent form of apoptosis is also possible in neurons. Apoptosis-inducing factor (AIF) is a mitochondrial effector of apoptotic cell death. AIF is a flavoprotein located in the inter-membrane space of the mitochondria. When the apoptosis is induced it transfers to the nucleus, where it causes major DNA fragmentation and, finally, cell death. (Susin et al., 1999) Different mechanisms of apoptosis are shown on the **Figure 2.2**. When and where apoptosis will take place depends on the nature, level of stress, and the ability of the cell to respond to it. For example, older cells will be less resistant to increasing oxidative stress; cells with higher metabolic requirements may have an higher level of oxidative damage, etc. (Davies and Morris, 2004)

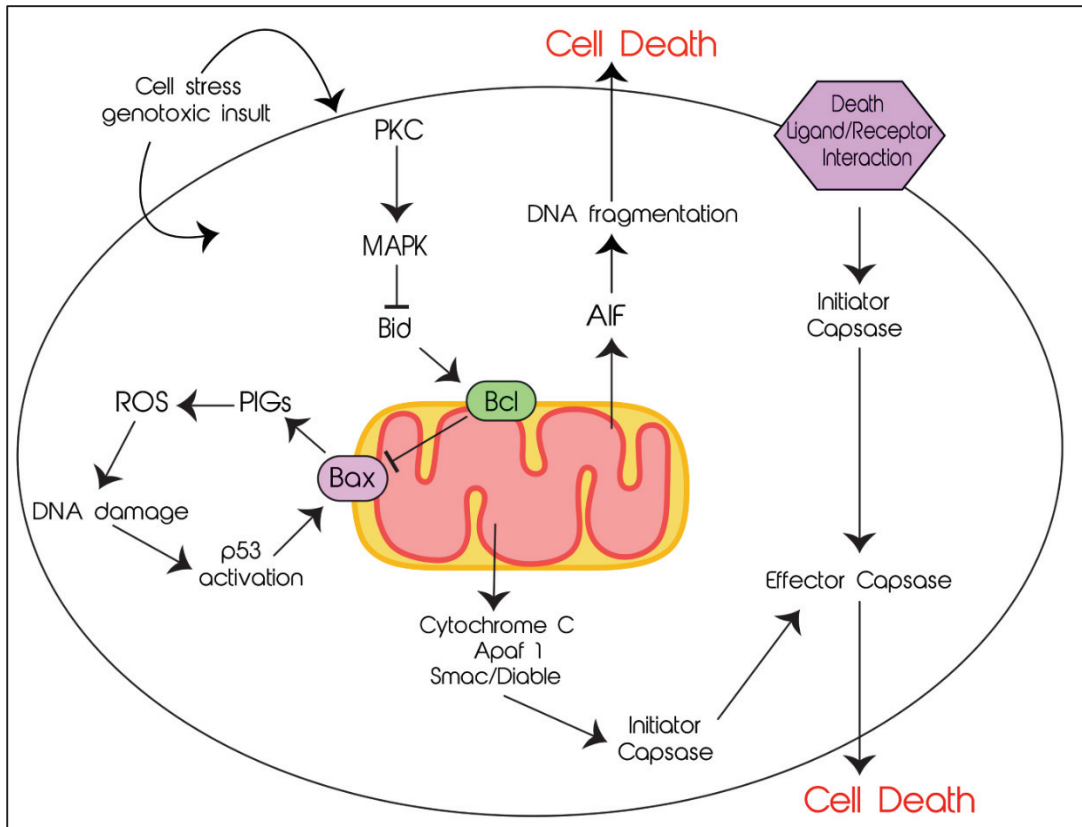


Figure 2.2 Apoptotic pathways; Lethal stress initiates a number of possible mechanisms to effect programmed cell death responses which results in formation of apoptosome that protect neighboring cells from injury. It can be p53 dependent or induced by mitochondrial AIF protein.

Unlike apoptosis necrosis (**Figure 2.3**) is a premature cell death that results from extreme adverse stimuli (e.g. exposure to toxins, ischemia, etc.). It is not as controlled as apoptosis, there is no formation of apoptotic bodies within the cell, and consequently, it causes an inflammatory reaction. Necrosis results in complete disintegration of the affected cells, release of the intracellular contents to the extracellular medium and an associated inflammatory response. The extent of cell loss due to necrosis is significant. (Davies and Morris, 2004) Neuronal necrosis is effected by an increase in cytosolic Ca^{2+} . Cytosolic Ca^{2+} activates lytic enzymes (such as calpains), and enters the mitochondria, where it inhibits the respiratory cycle and the ATP production. This leads to an increase in the production of ROS, activation of nitric oxide synthase (NOS) and nitric oxide (NO) production and finally membrane lysis, neurotransmitter release and spillage of toxic content on neighboring cells. (Kim et al., 2003)

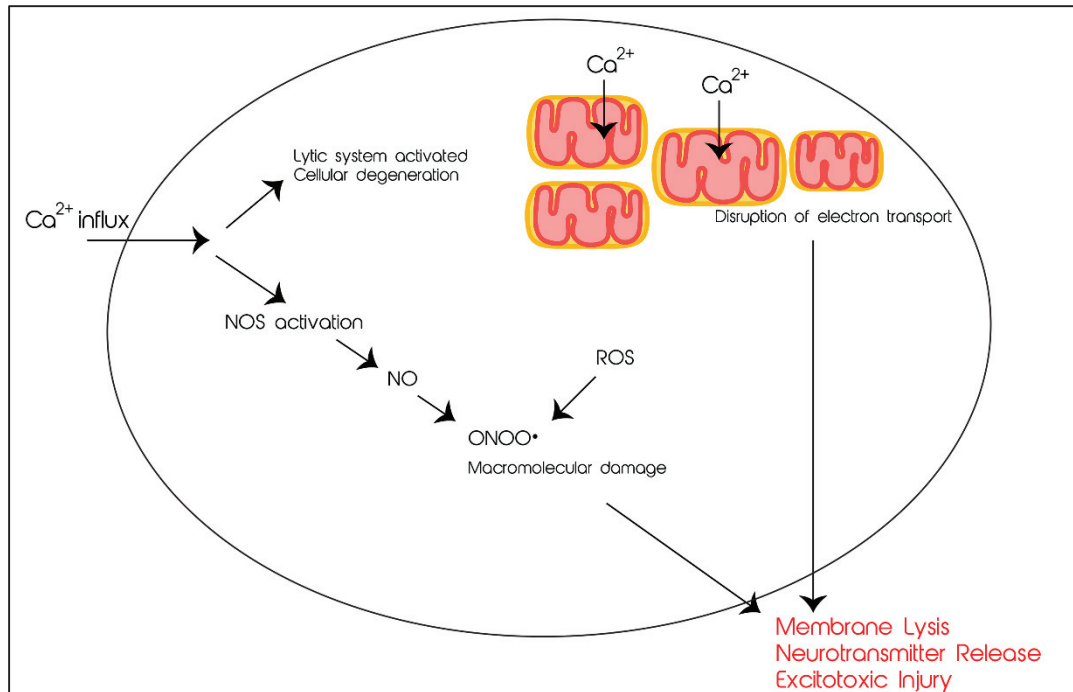


Figure 2.3 Mechanisms of neural necrosis; Large stress causes Ca^{2+} influx which leads to the series of events resulting in disruption of respiratory cycle and ATP production, cell death, inflammation and finally excitotoxic injury in surrounding cells.

2.4. Oxidative Stress

The most famous model of neuronal death has been proposed by Coyle and Puttfarcken in 1993. It is known as ‘cumulative damage hypotheses’. It says that individual neurons accumulate fibrils and oxidative damage with time, until a damage threshold is reached and the cell can no longer cope with the biochemical stress and dies. (Coyle and Puttfarcken, 1993a) A decade later the new model, was proposed by Clarke et al. in 2000. He based his model on a loss of function as the result of random neuronal loss. He explained that neuronal loss, occurs essentially at the same rate over time, and independent of disease state progression. (Clarke et al., 2000) The drawback of both of these models is that none of them takes ageing into account, at both cellular and organ level, as a factor to be equated into how neurons die or how this might relate to pathogenesis. (Davies and Morris, 2004)

Nowadays, it is known that the internal damage is due to oxidative stress, caused by various free radical species that can even be generated by elements of the normal biochemistry of the cell and accumulate over time. For example:

- Glutamate, the main excitatory neurotransmitter is an important source of ROS; excessive activation of glutamate-gated ion channels may cause neurodegeneration. (Coyle and Puttfarcken, 1993b)
- Complex III of the electron transport chain in mitochondria, flavoproteins, cytochrome p450 and other oxidases are ideal source of free radicals. They are tightly coupled to avoid partial reduction of free oxygen, but any intrusion can contribute to oxidative stress; (Swerdlow et al., 1996)
- Nitric oxide synthase (NOS) and prostaglandin H synthase (PGHS) also generate free radicals.
- An additional source of free radicals is auto-oxidation of catecholamines (dopamine, adrenaline, noradrenaline);
- Furthermore, inflammatory cells - activated leucocytes can contribute to the generation of free radicals, and are associated with chronic inflammation arising from activation of immune system, etc.

The main free radicals present under physiological conditions are reactive oxygen species (ROS), (superoxide ($\bullet\text{O}_2^-$), hydroxyl radicals ($\bullet\text{OH}$), alkoxy radicals ($\text{RO}\bullet$)) and reactive nitrogen species (ONOO^- , $\text{NO}\bullet$, and $\text{NO}_2\bullet$). Hydrogen peroxide (H_2O_2) is also produced. Superoxide and hydrogen peroxide are not extremely toxic. It was suggested that the peroxynitrite radical (ONOO^-) is most likely to cause neurotoxicity. (Beckman et al., 1994) It can be rapidly formed when superoxide and $\text{NO}\bullet$ are in the same cellular compartment. Afterwards, it reacts strongly with proteins to form nitrotyrosine. (Davies and Morris, 2004; Halliwell, 2006; Pavlin et al., 2016) Furthermore, interestingly for our study, peroxynitrite has been shown to inactivate the dopamine transporter in a neuronal cell line in vitro. (Park et al., 2002)

Free radicals do have biologically useful purposes: cell signaling, enzyme function, phagocytosis, and regulation. (Halliwell and Gutteridge, 2015) Unfortunately, they can

damage all major macromolecules of the cell. Cells vary widely in their activity and in their use of glycolysis, mitochondrial, electron transport or other form of energy generation. Some cells, like dopaminergic neurons are more susceptible. The degradation pathway of excess dopamine forms neurotoxic o-quinones. Their toxicity comes from the formation of the dopamine o-hydroquinone free radical, which reacts with proteins to make quino-proteins. (Coyle and Puttfarcken, 1993a; Davies and Morris, 2004)

Cells have defense mechanisms against free radical damage. There are various antioxidant defense systems that convert free radicals into harmless chemicals (Halliwell and Gutteridge, 2015). These are:

- low molecular weight agents: polyphenols, tocopherol, carotenoids, glutathione, bilirubin, ubiquinol, melatonin, and lipoic acid;
- proteins: iron and copper sequestration proteins (transferrin, lactoferrin, ferritin, haemopexin, caeruloplasmin);
- enzymes: superoxide dismutase (SOD), catalase (CAT), peroxiredoxins, thioredoxins, glutaredoxins, and glutathione peroxidases (GPx). (Davies and Morris, 2004)

The major extracellular antioxidant - ascorbate and L-carnosine are released with certain neurotransmitters. Dopamine has antioxidant activity at synapses where it is released. (Davies and Morris, 2004) SOD is an important enzyme that maintains the concentration of the superoxide radical at physiological levels by catalyzing its reduction to H_2O_2 and O_2 under acidic conditions. H_2O_2 is not only product of SOD but also NOS and MAO, (concentration within the cell is 10^{-9} to 10^{-7} M) therefore the activity of CAT and GPx are of vital importance. CAT is peroxisomal enzyme found in nearly all aerobic organisms, it plays a central role in homeostasis of ROS. The onset of PD might be explained by the non-enzymatic oxidation of dopamine in the CAT lacking regions. Additionally, H_2O_2 can be consumed by various hemoproteins, such as heme-peroxidases, hemoglobin, myoglobin and cytochrome-c. (Pavlin et al., 2016) Should the damage occur anyway, the cell can either repair the damage, or dispose of the damaged molecule. (Davies and Morris, 2004)

The protein degradation systems of the cell (proteasomes and lysosomes) are crucial for long-term survival. Partial failure of the ubiquitin tagging system for protein removal results in the eventual death dopaminergic neurons. Mutations in the parkin gene, encoding an E3 ubiquitin ligase, and in the gene encoding UCH-L1 (ubiquitin carboxy-terminal hydrolase) can lead to an early onset of PD. Damaged lipids are also processed in lysosomes. Lysosomes have been reported to be particularly prone to free radical oxidative stress (Bahr and Bendiske, 2002), and loss of lysosomal and proteasomal processing capacity could be a factor in the onset of PD. (Davies and Morris, 2004)

A further disposal mechanism of the cell is the sequestration of dangerous chemicals damaged proteins or other cellular components, in disposal organelles or cellular inclusion bodies. The quinone by-products of dopamine degradation are further converted into the inert neuromelanin polymer, and stored as pigment granules (characteristic black color of SN cells). It has been suggested that dopamine quinone is normally degraded by 5-cysteinylation and 5-glutathionization. However, in times of severe oxidative stress, when the cysteine and glutathione pool is depleted, quinone is shifted into neuromelanin biosynthesis. (Cheng et al., 1996) There is a possibility that the characteristic Lewy bodies of PD are the cell's way of isolating α -synuclein that is difficult to clear from the cell. Nevertheless, the aggregation of potentially cytotoxic abnormal proteins indicates that defect in protein handling appears to be a common factor in PD. All in all, stress from damaged, unwanted proteins is an important factor in cellular ageing and pathogenesis of neurodegenerative disorders. (McNaught et al., 2001; Olanow and Brundin, 2013)

2.5. Mitochondrial Damage and Aging

Mitochondrion is one of the most complex subcellular organelles, it has its own DNA, and plays key roles in many cellular functions such as energy production, fatty acid metabolism, pyrimidine biosynthesis, calcium homeostasis, and cell signaling. The most important function of the mitochondria is the production of proton gradient for ATP synthesis. This is accomplished by the sequential transfer of electrons from succinate,

NADH and other electron rich sources to the final reduction of molecular O_2 to H_2O . (Gibson, 2005) The respiratory chain consists of four protein complexes: reduced nicotinamide adenine dinucleotide (NADH) dehydrogenase-ubiquinone oxidoreductase (**complex I**), succinate dehydrogenase-ubiquinone oxidoreductase (**complex II**), ubiquinone-cytochrome *c* oxidoreductase (**complex III**), and cytochrome *c* oxidase (**complex IV**). Finally, there is ATP synthase that is recently named complex V. (Perier and Vila, 2012) The mitochondrial electron transport chain is shown on **Figure 2.4**.

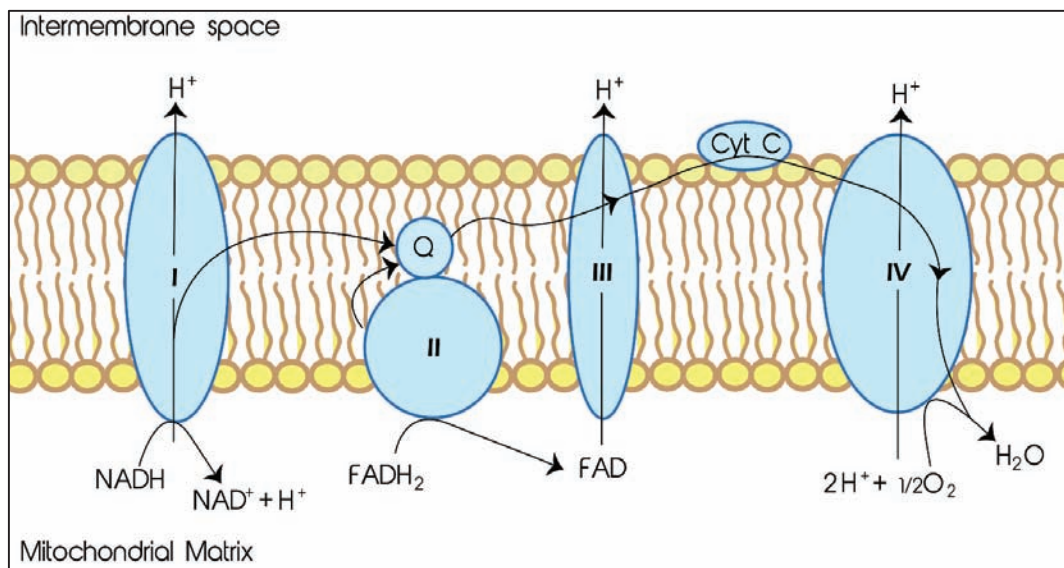


Figure 2.4 Mitochondrial Electron Transport Chain; Electrons are passed from one complex of the transport chain to another through a series of redox reactions. Energy released in these reactions is used to make ATP.

There are numerous theories about mitochondrial damage, disruption of the electron transport and aging. Even though many research has been done, mitochondrion still remains an active point of interest.

Mutation in mitochondrial DNA occurs at a much higher rate than in chromosomal DNA. (Linnane et al., 1989, 1990) Mitochondrial DNA (mtDNA), which is close to a major source of free radicals, could be the first to suffer oxidative damage, but there is no direct evidence of this. Oxidative damage to mtDNA may accumulate and be amplified by replication of mitochondria resulting in a mutant macromolecules with advancing age. (Menzies and Gold, 1971) Respiratory deficiency and degeneration may also arise as a consequence of mitochondrial electron and proton leak. (Jastroch et al., 2010) All these

factors (decrease in mitochondrial respiratory activity, mitochondrial oxidative damage, and an increase in mitochondrial mutations) are a strong correlate of ageing. (Davies and Morris, 2004)

It has been suggested, but remains unclear whether mitochondrial DNA, proteins, and lipids are really the primary site of early oxidative damage in the cell. Indeed, evidence from caloric restriction studies indicates that emphasizing energy production via the mitochondrial electron transport chain reduces metabolic rate and oxidative stress. Nevertheless, the role of the mitochondrion in apoptosis, once damage becomes severe, is well established. (Davies and Morris, 2004)

Oxidation of Complex I reduces its activity and is one of the first biochemical defects observed in humans and animal models with PD. Exposure of drug addicts to 1-methyl-4-phenyl-1,2,3,4-tetrahydropyridine (MPTP), an inhibitor of mitochondrial complex I, resulted in an acute and irreversible parkinsonian syndrome similar to PD. (Langston et al., 1983) Also, chronic exposure of rats to rotenone (potent complex I inhibitor) produces nigrostriatal dopaminergic neurodegeneration. (Betarbet et al., 2000) Clearly, defective mitochondrial respiration leads to PD because of depletion of cellular ATP levels and increased production of ROS. (Perier and Vila, 2012)

More recent data using a dopaminergic cell line under conditions of glutathione depletion indicate that nitric oxide, could be the primary agent responsible for Complex I modification, most likely through *S*-nitrosylation of one or more key cysteine residues. (Hsu et al., 2005) In the same time, it was found that the modification of cysteine in DJ-1 (a protein with anti-oxidant activities) is linked to one form of early onset PD. Afterwards, it has been suggested that DJ-1 protects against cell death. (Canet-Avilés et al., 2004, p. 1)

Furthermore, mitochondrial proteins do have a role in apoptotic cell death. (Newmeyer and Ferguson-Miller, 2003) As mentioned above, through the release of proteins such as cytochrome-c and apoptosis-inducing factor (AIF) during programmed cell death, these proapoptotic proteins combine with other cellular components (for example, caspases and Bax) to complete the apoptotic cascade. (Gibson, 2005; Yuan and Yankner, 2000)

2.6. Neurotoxins

Mitochondrial dysfunction and oxidative stress are pathophysiologic mechanisms implicated in experimental models and genetic forms of PD. Several neurotoxins are used to induce PD in experimental animal models. (Tanner et al., 2011) Exposure to pesticides might be one of the environmental risk factors for PD. Rotenone inhibits mitochondrial complex I, paraquat causes oxidative stress, and they both induce the loss of nigral DA neurons and behavioral changes associated with human PD in experimental animals. Yet despite experimental studies none of these pesticides has been associated with PD in humans. (Tanner et al., 2011) The neurotoxin MPTP is converted into MPP⁺ (1-methyl-4-phenylpyridinium) by enzyme MAO-B which leads to parkinsonism in primates, through selective killing of DA neurons in the SN. MPP⁺-induced neurodegeneration is specific to dopamine neurons, because it selectively enters through DAT and is then accumulated into mitochondria where it inhibits complex I reducing ATP production and causing oxidative stress. (Wiemerslage et al., 2013) Manganese ions accelerate the oxidation of catecholamines in order to produce quinolones, semiquinolones and oxygen radicals. This has been suggested to explain the degeneration of catecholaminergic neurons that has been reported as symptom of manganese-intoxication, which caused parkinsonism. (Crossgrove and Zheng, 2004; Halliwell, 2006)

2.7. α -Synuclein

As mentioned before, PD is characterized by the presence of protein aggregates. (Rang and Dale, 2007) There is formation of abnormal spherical bodies - Lewy bodies (LB), and a thread-like - Lewy neuritis (LN) in the soma of the affected neuron. (Braak et al., 2003) Damage to specific subnuclei of the SN, with severe obliteration of their neuromelanin projection neurons, frequently is considered to be the most important hallmark of PD. (Braak et al., 2003) These aggregates are highly compacted and resistant to digestion even by protein kinase K (which degrades many proteins in the native state), and α -synuclein is the major protein component of these aggregates. It has 140 amino acids and it is abundantly expressed in all the brain. It is found in nearly all compartments

of the neuron, but mostly in presynaptic terminals, where it is believed to play a role in vesicular trafficking and release. (Hansen and Li, 2012)

Within cells, α -synuclein normally adopts an α -helical conformation. However, under certain circumstances, the protein can undergo extreme conformational transition to a β -sheet-rich structure that polymerizes to form toxic oligomers and amyloid plaques. It can, also, transfer to unaffected nerve cells, where it seems to act as a template to promote misfolding of host α -synuclein. This leads to the formation of larger aggregates, neuronal dysfunction, and neurodegeneration. (Olanow and Brundin, 2013) Many factors are responsible for plaque formation. There is a growing evidence that important stimulus for plaque formation is presence of heavy metal ions in their oxidized state. It is well established that amyloid plaques contain concentrations of copper, iron and zinc. Oxidized forms of iron and copper bind to α -synuclein and trigger conformational changes associated with the formation of amyloid plaques. Zinc is involved in the enzymatic cleavage of amyloid precursor protein (APP), a precursor of α -synuclein. (Pavlin et al., 2016)

Various studies trying to connect α -synuclein, oxidative stress and PD have been done. Certain study showed that it inhibits the refilling of the rapidly releasable pool of synaptic vesicles at nerve terminals. (Abeliovich et al., 1993) Other studies indicated that α -synuclein may be required for the genesis and/or maintenance of presynaptic vesicles. (Cabin et al., 2002) There is evidence that it plays a role in formation of the membrane through regulation of phospholipase D (PLD) activity. PLD hydrolyzes phosphatidylcholine into phosphatidic acid and diacylglycerol. (Ahn et al., 2002) One of the most interesting result was that α -synuclein knockout mice are resistant to MPTP toxicity. Knockdown of α -synuclein reduced the availability of DAT on the neuronal surface and decreased the total number of intracellular vesicles by but increased the density of vesicular monoamine transporter (VMAT₂). (Fountain et al., 2008) The increase in vesicular uptake and storing of MPP⁺ may lead to the resistance in the absence of α -synuclein. This would imply that α -synuclein is the cause of the inhibition in dopamine storage. On the other hand, there is a possibility that the direct action of α -synuclein in mitochondrion may be the cause. From all these data, it has been

hypothesized that mutations of α -synuclein might lead to reduced dopamine storage in vesicles. (Lotharius and Brundin, 2002) This would increase the concentration of cytoplasmic dopamine, thus in turn increasing the oxidative stress on the neuron due to the increased risk of toxic dopamine *o*-hydroquinone radicals. Moreover, α -synuclein overexpression has been shown to enhance dopamine toxicity and increase H₂O₂ induced nitrite production in neuroblastoma cells. (Wersinger and Sidhu, 2003) It should be noted that normal low levels of α -synuclein have been reported several times to be neuroprotective, and human α -synuclein expressed in transgenic mice could protect from paraquat toxicity. (Manning-Bog et al., 2003) The α -synuclein is ubiquitously expressed in the brain, and is present in great amount in presynaptic axon termini. It has proved to be a difficult protein to assign a clear function to. Its best-known property is a tendency to aggregate, and it has been shown that the familial mutant forms aggregate more rapidly and easily. The relevance of aggregation to toxicity is not established, but it is thought that it may result in the proteasome being unable to degrade the protein efficiently, leading to local accumulations and proteasome stress. (Davies and Morris, 2004)

2.8. Current Therapies

Enormous progress has been made in the treatment of PD over the past century, but L-DOPA still remains the most potent drug for controlling the symptoms of PD. **Levodopa** is the prodrug that is converted in dopamine in the brain. It is most commonly prescribed and so far the most potent drug for controlling the symptoms of PD (<https://www.drugbank.ca/>). However, the majority of patients treated with it experience motor complications such as fluctuations and dyskinesia after 5 years. The “wearing-off” effect is the most frequent form of motor fluctuations. It is related with the shortening the half-life of levodopa as a consequence of the loss of striatal dopaminergic terminals. The addition of **carbidopa** (peripheral DOPA decarboxylase inhibitor) enhances the therapeutic benefits of levodopa and delays the onset of motor complications. (Jankovic and Aguilar, 2008) There are 3 strategies to improve levodopa therapy:

1. Reduce the dosage;
2. Use other drugs to ameliorate dyskinesia;
3. Surgery.

The addition of COMT inhibitor, MAO inhibitors or dopamine agonists may be used in treatment of levodopa induced dyskinesia. **COMT inhibitors** like **enatcapon** are usually used in combination with levodopa to prolong DA response. By blocking catechol-o-methyl-transferase, enzyme responsible for degradation of dopamine in the presynaptic neuron, it increases the level of DA in the synaptic cleft. (Jankovic and Aguilar, 2008) **Dopamine agonists** directly activate DA receptor on the postsynaptic neuron, bypassing the dopamine synthesis in the presynaptic terminals. They can be used as monotherapy in early stage of PD. As monotherapy, they provide modest improvements in parkinsonian symptoms, but they can be useful in delaying the start of levodopa therapy for couple of months or years. **Ropinirol** is effective in early therapy. **Pramipexole** has been shown to be safe and effective monotherapy in the early stages of PD. It has been also demonstrated that it shows neuroprotective effects and enhances neurotrophic activity. (Jankovic and Aguilar, 2008) **MAO inhibitor - selegiline** is selective MAO-B inhibitor. By inhibiting MAO-B it blocks intra-neural DA degradation. It can be used as adjuvant therapy with levodopa, or as monotherapy. (Rang and Dale, 2007)

There are also non-dopaminergic therapies for treatment of PD. Neuroprotective therapy is aimed at modifying the etiopathogenesis and therefore slowing down the progression of a neurodegenerative disorder. (Nayak and Henchcliffe, 2008) Neuroprotective strategies can alter or delay the progression of disease, but they have to be implemented in early stages of the disease.(Jankovic and Aguilar, 2008) Rasagiline (N-propargyl-1 (R)-aminoindan) is a novel propargylamine, irreversible, selective monoamine oxidase inhibitor for treatment of PD. Rasagiline inhibits striatal dopamine metabolism, thereby providing relief from motor symptoms of PD (Figure 2.5). (Nayak and Henchcliffe, 2008) Propargylamine moiety of rasagiline protects mitochondrial viability and MPTP by activating mitochondrial B-cell leukemia/lymphoma 2 (Bcl-2) and protein kinase C (PKC), and down-regulating pro-apoptotic BCL2-associated protein X (Bax) caspase 3, poly (ADP-ribose) polymerase 1 (PARP1) and H2AX (a phosphorylated mammalian

histone H2A). One direct consequence is the processing of amyloid precursor protein (APP) through the activation of α -secretase, resulting in increased release of the neuroprotective/neurotrophic soluble APP (sAPP). The activation of PKC might explain the ability of these propargylamines to induce expression of glia cell line-derived neurotrophic factor (GDNF) and brain-derived neurotrophic factor (BDNF) mRNAs, and stimulate the release of GDNF. (Mandel et al., 2005; Youdim et al., 2006) Besides this, some studies also suggested that it inhibits Glyceraldehyde-3-Phosphate Dehydrogenase (GAPDH). (Ou et al., 2009) Today, many drug designers are using rasagiline as a starting compound for novel neuroprotective agents. (Akao et al., 2002b; Luan et al., 2013; Marco-Contelles et al., 2016; Weinreb et al., 2009)

Anticholinergic agents, amantadine, and nicotine may also provide satisfactory symptomatic relief in early phases of the disease, due to the fact that acetyl-cholinergic neurotransmission is also dysregulated in PD. (Jankovic and Aguilar, 2008)

Other suggested methods are gene therapy or surgical methods, as promising strategy for PD. (Chen et al., 2006; Coune et al., 2012) However, since we are mainly focused in drug design of small molecules these strategies will not be further discussed, since they are beyond the scope of our research.

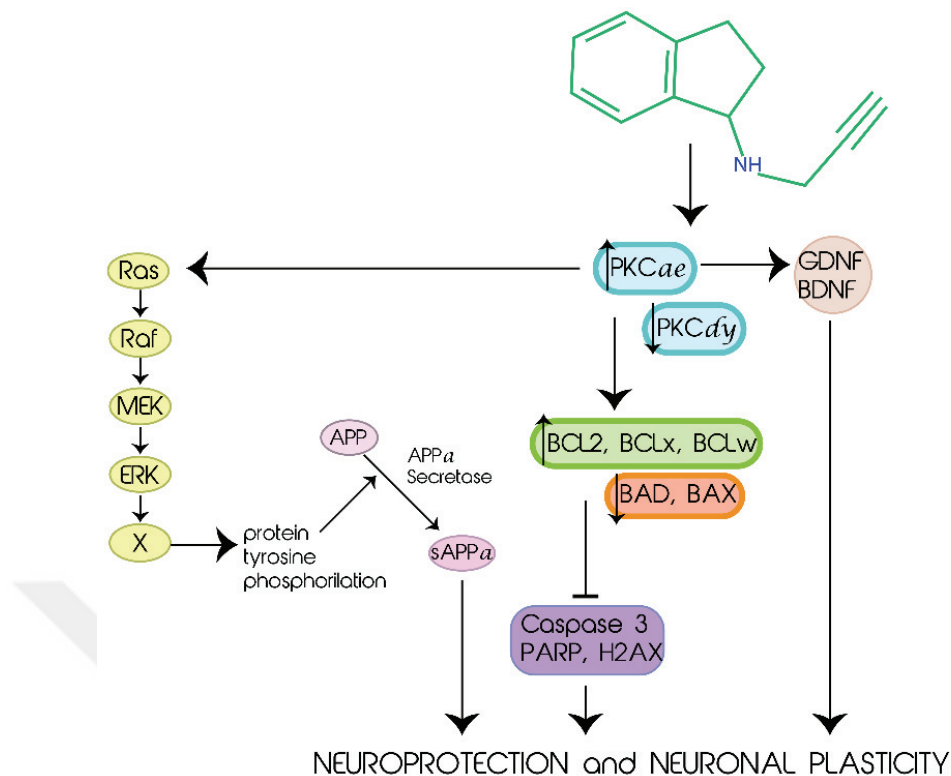


Figure 2.5 Mechanism of Rasagiline neuroprotection: Through the activation of PKC-dependent mitogen-activated protein (MAP) kinase and BCL2 family anti-apoptotic proteins, and downregulation of pro-apoptotic BAD, BCL2-associated protein X (BAX), caspase 3, (PARP1) and H2AX. It also induces the expression of GDNF and BDNF mRNAs, and stimulate the release of GDNF. (Youdim et al., 2006)

2.9. Future Perspectives

A lot of effort has been made in the field of neurodamage/neuroprotection and design of neuroprotective drugs, and various different strategies are being explored, but neurodegenerative disorders, as complex as they are, still remain an inexhaustible source of research opportunities.

Dopamine uptake inhibitors - whether selective or have actions on noradrenaline or serotonin transporters, theoretically represent an attractive way to alleviate parkinsonism and potentially enhance L-DOPA antiparkinsonian action (provided that sufficient dopamine terminals remain within the striatum). (Huot et al., 2016) A dual DAT/ NET inhibitor, was an effective anti-parkinsonian agent as monotherapy in the MPTP-lesioned

cells, but did not enhance L-DOPA anti-parkinsonian action when administered as adjunct therapy. (Pearce et al., 2002)

Reducing oxidative stress and enhancing mitochondrial function: From a pharmacological perspective, mitochondria's role in generating ROS and undergoing oxidative damage to protein, mtDNA and lipids makes it reasonable targets for therapeutic strategies. (Murphy and Smith, 2000; Szewczyk and Wojtczak, 2002) Current drugs strategies that target mitochondria take advantage of the electrochemical gradient from the outer plasma membrane ($\Psi_p = 30\text{--}60\text{ mV}$) to the inner mitochondrial matrix ($\Psi_m = 150\text{--}180\text{ mV}$). This gradient provides a large driving force for the selective targeting and concentration of large lipophilic cations to the mitochondria. (Murphy and Smith, 2000) In another study, Superoxide Dismutase/Catalase Mimetics conferred neuroprotection against selective paraquat-mediated dopaminergic nigral cell death. (Gibson, 2005; Peng et al., 2005)

Neural Nitric Oxide Synthase (nNOS), is a potential target for the treatment of PD. It is expressed in several neuronal subtypes but not in dopaminergic neurons of the nigrostriatal pathway. However, they are surrounded by an abundant network of neuronal cell bodies and fibers that contain nNOS suggesting that any nitric oxide will be used by dopaminergic neurons. (Tieu et al., 2003) Minocycline, a semisynthetic tetracycline, was recently shown to have neuroprotective effects in animal models of stroke/ischemic injury and Huntington's disease. It prevents DA neurodegeneration in the MPTP mouse model of PD. (Du et al., 2001) The inhibition of nNOS is a promising strategy for neuroprotection, yet despite significant efforts, no nNOS inhibitors are in therapeutically use so far.

In various animal models, memantine a **NMDA receptor blocker** has been reported to be a neuroprotective agent that positively impacts both neurodegenerative and vascular processes. While excessive levels of glutamate result in neurotoxicity, in part through the over-activation of NMDARs, memantine - as a partial NMDAR antagonist, blocks the NMDA glutamate receptors to normalize the glutamatergic system and ameliorate cognitive and memory deficits. (Cheng et al., 1996; Olanow and Brundin, 2013)

Adenosine 2a (A2a) receptor antagonists are a new class of nondopaminergic medications currently under evaluation for their ability to improve signs and symptoms of PD. Theoretically, they offer the potential to provide benefits that are not delivered by traditional dopaminergic medications and might avoid dopaminergic side effects. Adenosine A2 receptor antagonists can modulate GABA and glutamate release in basal ganglia and other key neurotransmitters that modulate motor activity. In primete models they have shown improve in motor behavior. They can be administered alone or in combination with dopaminergic drugs. In clinical trials, istradefylline reduces "off" time in patients with PD receiving L-dopa. (Jenner et al., 2009, Hauser, 2011)

As mentioned above **rasagiline derivatives** are becoming very popular since it has been recently discovered that propargylamine group has some neuroprotective effects, design of different drugs with this functional group became very popular. (Marco-Contelles et al., 2016)

There are many other approaches, such as targeting α -synuclein aggregation (Jeřsko et al., 2017; Török et al., 2016), administration of growth factors to promote the survival of remaining midbrain neurons (Stayte et al., 2017), certain NSAIDs (Nonsteroidal anti-inflammatory drugs) may prevent or delay the progression of PD (L'Episcopo et al., 2010), blocking L-type calcium channels located on the plasma membrane of dopaminergic cells (Pasternak et al., 2012), cytochrome c inhibition (Wang et al., 2008, 2009), etc.

2.10. The Idea of Our Study

Design of neuroprotective drugs that use the same pathway like MPP⁺ to enter dopaminergic neurons may be a therapeutic option for PD. By competing with dopamine for DAT, they may also increase dopamine concentration in the synaptic cleft (**Figure 2.6**). After entering and accumulating in dopaminergic neurons these compounds could target various neuroprotective or immunological mechanisms: heavy metal ions (metal chelators); Calcium ions (calcium chelators); Monoamine Oxidase activity (MAO-B

inhibitors); Cyclooxygenase 2 (COX-2 antagonists); Glycogen Synthase Kinase 3 (GSK3 inhibitors), etc. (Juárez Olguín et al., 2016b; Pavlin et al., 2016) Inhibitors only block the dopamine transporter which would provide antiparkinsonic effect only in the beginning, by increasing the level of dopamine in the synaptic cleft, until all the stocks of dopamine are spent. On the other hand by designing the substrates with neuroprotective properties that could accumulate specifically in DA neurons, whose life could be prolonged, and in the same time by competing with dopamine for transport the level of dopamine in the synaptic cleft would be increased.

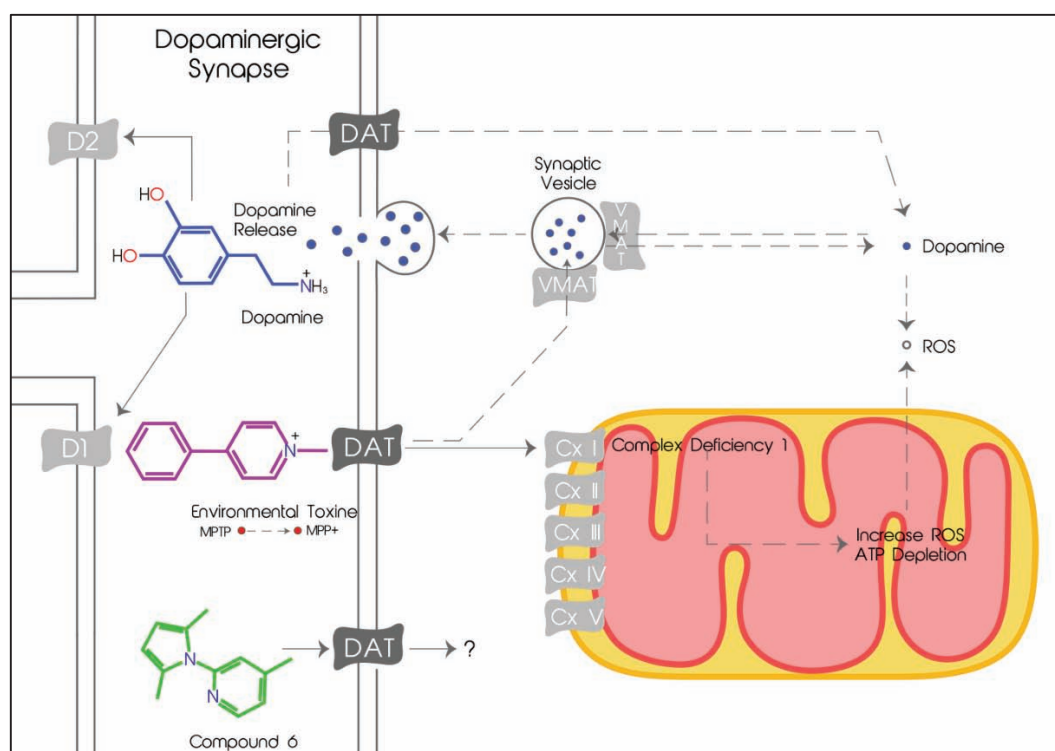


Figure 2.6 Dopamine (blue), MPP⁺ (purple) and fluorescent DAT substrate selected with our *in silico* model (green); All of these compounds are DAT substrates, and all of them take different pathways after entering the DA neuron.

3. DOPAMINE TRANSPORTER

3.1. Dopaminergic Neurons

Dopaminergic neurons of the midbrain are the main source of DA in the mammalian central nervous system (CNS). As mentioned above, selective degeneration of these neurons is associated with PD. They are found in *substantia nigra pars compacta*, which is DA-rich and contains both redox available neuromelanin and a high content of iron (Fe). Although their numbers are few, they play an important role in the control of many brain functions including voluntary movement, mood, stress, reward and addiction. (Chinta and Andersen, 2005)

DA neurons are an anatomically and functionally heterogeneous group of cells. They are localized in the diencephalon, mesencephalon and the olfactory bulb. (Björklund and Lindvall, n.d.) Mesencephalon contains approximately 90% of the total number of brain DA cells. The mesencephalic DA system has been subdivided into several nominal systems (**Figure 3.1**). The best known is the nigrostriatal system, which forms *zona compacta* of the *substantia nigra* and extends into the *caudate-putamen* (dorsal striatum). The nigrostriatal pathway plays a vital role in the control of voluntary motor movement. There are also the mesolimbic and mesocortical dopaminergic systems, made out of dopaminergic cells, present in the ventral tegmental area (VTA). These DA systems are involved in emotion-based behavior, motivation and reward. In principle, they can be considered as totally unrelated neurons and the only thing they have in common is the synthesis of DA. (Chinta and Andersen, 2005)

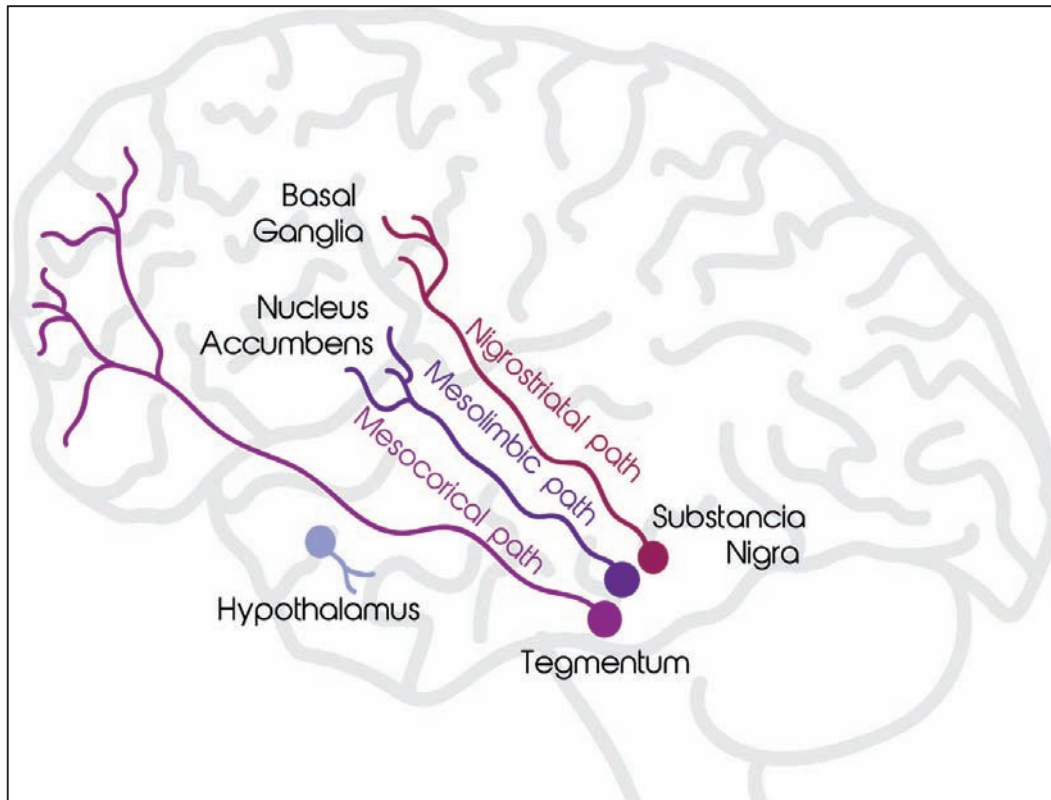


Figure 3.1 Dopaminergic pathways in the brain; Dopamine plays different roles in Nigrostriatal, Mesolimbic and Mesocortical pathways.

DA and other catecholamines are synthesized from amino acid, tyrosine, catalyzed by enzyme tyrosin-hydroxylase (TH). After the synthesis, DA is incorporated into synaptic vesicles, by the action of vesicular monoamine transporter 2 (VMAT2), where it is stored. After that, it is discharged by exocytosis and released into synapse. In the synapse it binds to postsynaptic (D1) and presynaptic neurons (D2). When it binds for postsynaptic receptors the signal is spread to the postsynaptic neuron. Presynaptic receptors with an inhibitory potential, also known as auto-receptors, inhibit the synthesis and release of neurotransmitters in order to maintain the optimal levels of DA. After carrying out its function, it is taken up by DAT or degraded by catechol-O-methyl transferase (COMT). DA in cytosol can then be repacked into vesicles or degraded. The enzymatic break-down of cytosolic DA to its inactive metabolites is carried out by monoamine oxidase (MAO). (Juárez Olguín et al., 2016a) Dopamine synthesis, release, signaling, and reuptake is shown on **Figure 3.2**.

MAOs are flavoenzymes that oxidize monoamines. In the brain, MAO B mainly metabolizes dopamine, while MAO A predominately metabolizes serotonin. However, MAO selectivity is quite poor since, for example, MAO B also metabolizes serotonin, only five times slower than dopamine. On the other hand, experiments have demonstrated that striatal dopamine tissue levels or extracellular levels are increased by the inhibition of MAO-A with clorgyline. In the human brain, MAO-A is found in catecholaminergic neurons, but MAO-B is found in serotonergic neurons and glial cells. Interestingly, DA neurons contain more MAO-A than MAO-B, while for serotonergic neurons the opposite is true. (Pavlin et al., 2016) MAO brakes down dopamine to 3,4-dihydroxyphenylacetaldehyde (DOPAL), which is then degraded to form 3,4-dihydroxyphenylacetic acid (DOPAC) by the action of enzyme aldehyde dehydrogenase. (Juárez Olguín et al., 2016a)

Oxidation of dopamine via MAO generates a series of toxic species including H_2O_2 , oxygen radicals, semiquinones, and quinones. (Chinta and Andersen, 2005; Graham et al., 1978) Furthermore, DOPAC metabolite is probably more toxic than H_2O_2 . The inactivation of DA in the brain (striatum and basal ganglia) is mediated by reuptake by DAT followed by enzymatic action of MAO, which breaks it down to DOPAC. Nevertheless, there are few DATs in the frontal cortex, which leads to breakdown of DA via other pathway. This pathway involves the norepinephrine transporter (NET) on neighboring NA neurons, where DA is then processed by the enzymatic action of COMT that breaks it down to 3-metoxytyramine (3-MT). (Juárez Olguín et al., 2016a)

Due to their high rate of oxygen metabolism, low levels of antioxidants, and high iron concentration, DA neurons are believed to be particularly predisposed to oxidative stress. Mechanisms of generating toxic ROS and ROS generated from DA metabolism, (Halliwell, 2006) increase the formation of reactive metabolites, especially under conditions in which the ratio of available DA to antioxidant capacity is high. (Chinta and Andersen, 2005; Hastings and Zigmond, 1994) DA cell loss is associated with the presence of Lewy bodies, composed of α -synuclein, neurofilaments, and ubiquitin. (Chinta and Andersen, 2005; Goldman et al., 1983) For detail explanation of mechanisms involved in dopaminergic cell death refer to Chapter 2.

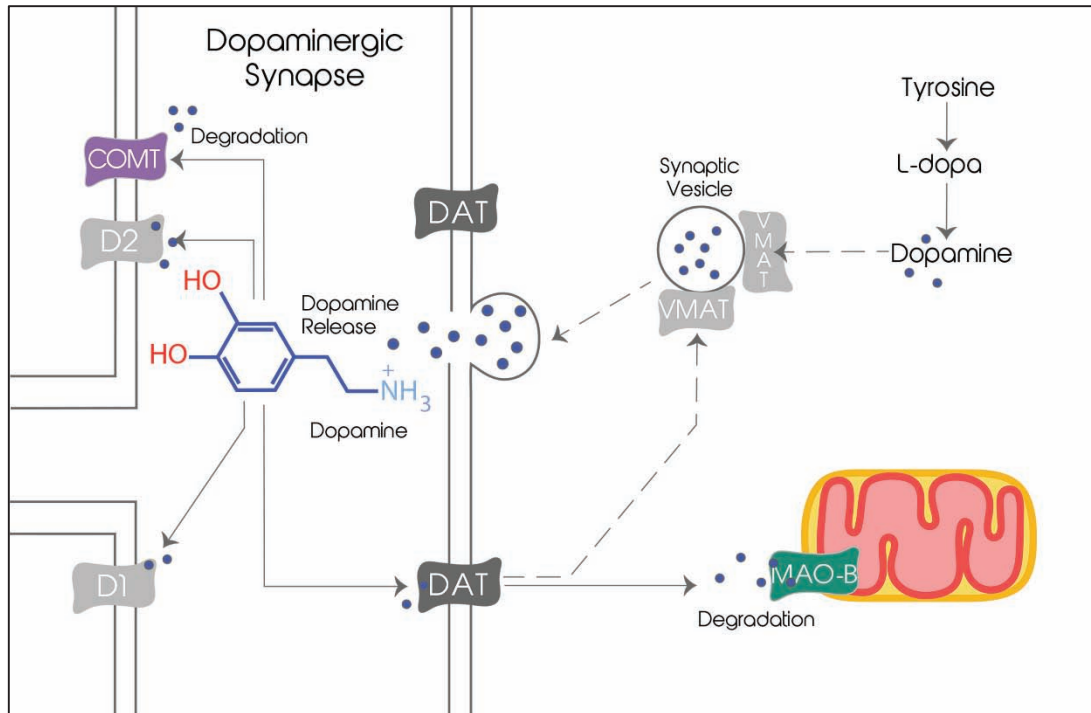


Figure 3.2. Dopamine synthesis, release, signaling, and reuptake; Dopamine synthesis originates from the amino acid tyrosine, which is converted to DOPA by the enzyme tyrosine hydroxylase. Subsequently, DOPA is decarboxylated, by the enzyme L - aromatic amino acid decarboxylase. Dopamine is stored in vesicles through VMAT₂ and released into synapse. After finishing its function it is degraded by MAO-B and COMT.

3.2. Dopamine Transporter

The DAT is a member of solute carrier 6 (SLC6) family of transporters. It is located on the plasma membrane of nerve terminals, where it transports DA across the membrane. The transport cycle is energetically coupled by the use of ion gradients that enable transport of the substrate across the membrane, against its concentration gradient. (Anders S. Kristensen et al., 2011) SLCs are called neurotransmitter sodium transporters (NSS), because they use co-transport of extracellular Na⁺ as driving force for substrate translocation. The first NSS structure published, was X-ray structure of prokaryotic leucine transporter (LeuT). (Yamashita et al., 2005a) LeuT was published in an outward-open, occluded and inward open state. Publication of this model has answered many questions about the structure and mechanisms of NSS transporters. Since then, any studies have been done on homology modeling of transporters from NSS family. (Beuming et al., 2008; Indarte et al., 2008a; Ravna and Sylte, 2012) However, in 2013, the X-ray structure

of drosophila's DAT (dDAT) (Penmatsa et al., 2013), in an outward-open, inhibitor-bound conformational state was finally published. This gave us a better insight into architecture and understanding of molecular mechanisms of this transporter. Even though LeuT and dDAT are very similar there are some very important differences: a kink in TM12 halfway across the membrane bilayer, a latch-like C-terminal domain that caps the cytoplasmic gate and a cholesterol molecule in the groove formed by TMs 1a, 5 and 7. The dDAT is also a chloride anion co-transporter, however this activity is absent in the LeuT (Penmatsa et al., 2013)

The human DAT (hDAT) consists of 620 amino acids, distributed in 12 transmembrane helices (TM). Helices 1–5 and 6-10 have characteristic pseudo-symmetry. Residues in TM1 and TM6 make numerous interactions with the ligands and ions via non helical, hinge like regions located half-way through the membrane. Phenylalanine residues at the curve of TM3 form the hydrophobic pocket of binding site. The variable extracellular loop (EL2) has many N-glycosylation sites, which play an important role in regulation, and one disulfide bond, that has a significant role in trafficking. EL2 and EL4 are harboring zinc binding site.

The substrate recognition (S0) site is located above the gate of the binding site (S1). The aromatic moieties of substrate are accommodated in a hydrophobic region of the binding pocket formed by TM1, 3, 6 and 8. One phenylalanine residue (Phe319 in dDAT, Phe320 in hDAT) forms the gate of the substrate binding pocket. The acidic side chain of Asp residue in this position is strictly required for the function of dDAT, because this residue is involved in a critical interaction with the amino group of the substrate. (Anders S. Kristensen et al., 2011) For the transport two sodium and one chloride ion are required. (Penmatsa et al., 2013) They are located adjacent to the binding site. One cholesterol molecule is located in a groove between TM5 and TM7 and it has a role in modulating the movement that occurs during transport cycle, stabilizing an outward-open state. Another important part is a C-terminal latch that makes extensive interactions with the cytoplasmic side of the transporter, proximal to the gate, and it may modulate transport activity. (Penmatsa et al., 2013)

3.3. Transport Cycle

The explanation of transport cycle became more imaginable when Yamashita, in 2005, (Yamashita et al., 2005a) published the X-ray structure of prokaryotic homolog of SLC6 transporters in an outward-open conformation, (Singh et al., 2007) followed with X-ray structures in occluded (Singh et al., 2008) and in and inward-open conformation (Krishnamurthy and Gouaux, 2012). These X-ray structures were fitting into the classical model of the transport cycle (**Figure 3.3**). The classic alternating access model (Jardetzky, 1966) implies that the transporter protein shuttles through at least three conformational states during the transport cycle:

1. an outward-open conformation where the substrate binding pocket is accessible to the extracellular medium,
2. an occluded conformation, where access to the pocket is blocked from either side,
3. an inward-facing conformation, where the pocket is open to the intracellular medium. (Anders S. Kristensen et al., 2011)

Many *in silico* studies have been done so far, trying to understand transport cycle of NSS family members. (Billesbølle et al., 2015; Borre et al., 2014; Adriana K. Kantcheva et al., 2013; Zhao et al., 2010) The most recent study was carried out by Cheng and Bahar in 2016 on the hDAT homology model, revealed the sequence of events involved in DA reuptake. (Cheng and Bahar, 2015a) Global transitions take place between outward-facing (OF) and inward-facing (IF) states; local conformational switches control the opening/closure of the extracellular (EC) or intracellular (IC) gates in their respective OF and IF states. (Cheng and Bahar, 2015a)

Firstly, DA binds to its recognition site S0 at the upper part of the EC vestibule. Asp79 and Asp476 coordinate the DA amine and carbonyl groups. Afterwards, DA proceeds to S1 binding site where it is settled. This leads to closure of EC outer and inner gates Arg85-Asp476 and Tyr156-Phe320. Binding of DA and its attractive interaction with Asp79 disrupts hydrogen bonds that than free up Tyr156 to pair up with Phe320, and finally the occluded state is spontaneously formed. These conformational switches were followed

by tilting in transmembrane TM1 and TM6, connected to the closure of EC gates. From this state DAT proceeds to more stable occluded state, called holo-occluded state, where ligand is sealed from both EC and IC environment. Ser422 and Asp79 react with DA, which weakens their interaction with Na⁺. The dislocation of Na⁺ started to trigger the permeation of a few IC water molecules which disrupted Asn85-Asn353 hydrogen bond near Na⁺ and Cl⁻, kinking of TM5 and its opening to expose DA to IC medium. Protonation of Asp79 weakens the bonds and leads to final release of DA. (Cheng and Bahar, 2015a)

It is worth mentioning that some authors suggested that DAT can transport DA reversely, from IC to EC compartment (e.g. it is capable of efflux of dopamine). (Robertson et al., 2009a; Kyle C. Schmitt et al., 2013)

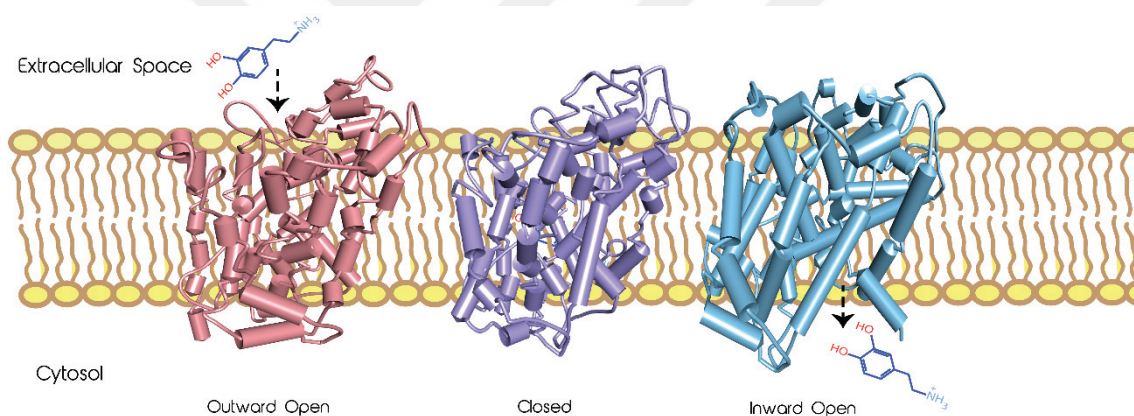


Figure 3.3 DAT transport cycle: classic alternating access model; transporter protein shuttles through at least three conformational states during the transport cycle: outward open, closed and inward open.

3.4. Interactions with Other Proteins

DAT is regulated by multiple signaling systems, among them protein kinase C (PKC) and extracellular signal regulated kinase (ERK) being two of the most well-characterized. (Vaughan and Foster, 2013) The fact that PKC is increasing the transport while ERK is decreasing it signals the characteristic of DAT which enables it to undergo bidirectional regulation. This further indicates that establishment of overall uptake set points

incorporates the signals from different pathways. (Fenollar-Ferrer et al., 2014; Vaughan and Foster, 2013)

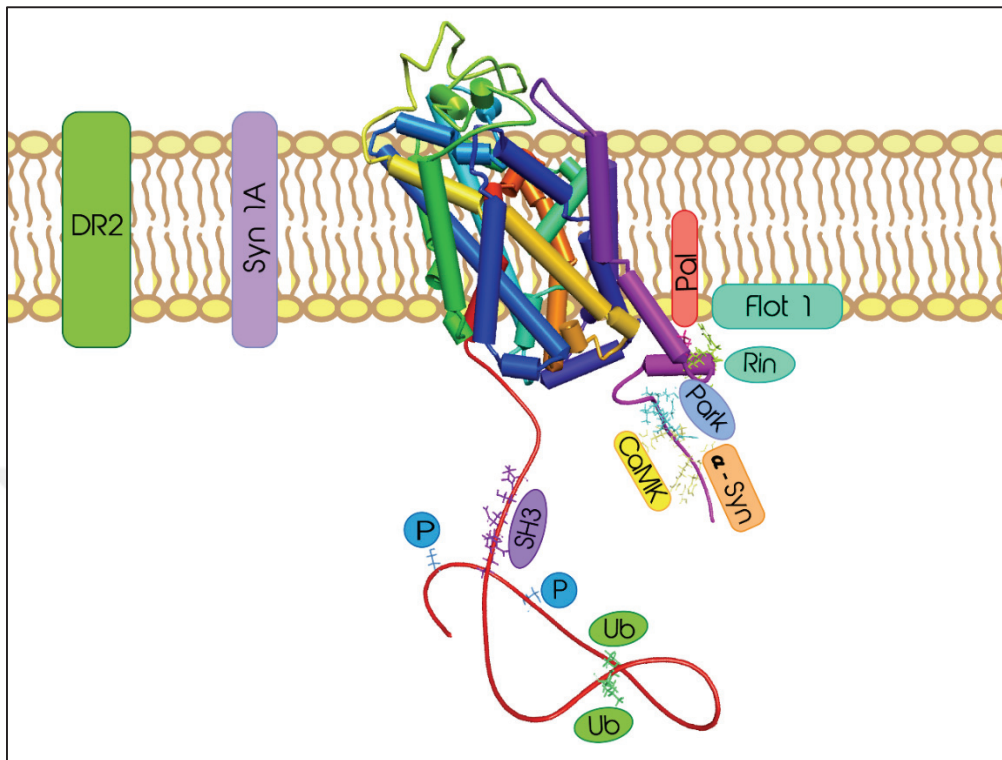


Figure 3.4 DAT and its protein-protein interactions: (Vaughan and Foster, 2013) DAT interacts with Dopamine Receptor 2 (DR2), Syntaxin 1A (Syn1A), Ca^{2+} /calmodulin-dependent protein kinase (CaMK), flotillines (Flot1), plasma membrane-associated GTPase – Rin, α -synuclein (α -syn) and Parkin (PARK); Post-translational modifications shown phosphorylation (P), ubiquitylation (Ub), and palmitoylation (Pal)

Important protein-protein interactions playing a role in regulation of DAT that have been discovered so far are:

- **Protein kinase C (PKC)** quickly down-regulates DA transport capacity through effects on DAT endocytosis, transport velocity, and efflux. Extended activation of PKC forces DAT into lysosomal degradation for long-term regulation of transporter levels. The activity of PKC is regulated by different mechanism and compounds (amphetamines, phorbol esters, proteins flotillines, N-terminal ubiquitination, etc.). (Daniels and Amara, 1999; Fenollar-Ferrer et al., 2014; Hong and Amara, 2013; Sorkina et al., 2013) PKC regulates DA reuptake capacity by multiple processes, such as: endocytotic mechanism driven by phosphorylation of DAT accessory proteins, a kinetic down-regulation mechanism mediated by

Ser7 phosphorylation, and enhancement of efflux. (Vaughan and Foster, 2013) The dynamic balance between endocytosis and recycling controls the concentration of DAT on the surface of the neuron and therefore, modulates DA neurotransmission. (Hong and Amara, 2013) To summarize, the increased activity of PCK, *in vivo*, increases DA levels. (Ramamoorthy et al., 2011; Vaughan and Foster, 2013)

- **Extracellular signal regulated kinase (ERK)** increases DA transport capacity. DAT residue Thr53 regulates substrate reuptake and Thr53, as Thr53Ala mutation, reduces DA transport velocity. This is consistent with the potential for ERK-mediated phosphorylation of this site to increase transport activity. (Foster et al., 2012) D₂ receptors also activate ERK, which promotes DAT surface expression. (Lee et al., 2007; Ramamoorthy et al., 2011)
- Syntaxin 1A is a plasma membrane protein, firstly considered to interact with synaptic vesicle fusion proteins during transmitter release. It is now known to regulate other proteins including neurotransmitter transporters. Syntaxin 1A binds to the distal N-terminus of DAT. The conditions that reduce its levels or prevent its interaction with the transporter lead to multiple effects, including increased uptake and channel activity and decreased efflux and transporter phosphorylation. (Carvelli et al., 2008)

For us, two of the most important interactions are with α -synuclein and Parkin, since the mutations and/or overexpression of these proteins has been noticed in PD patients.

- **α -Synuclein** binds to the distal C-terminus of DAT, where it could compete with Calcium calmodulin-dependent protein kinase (CaMK) and have the effect on related regulatory properties. Recent work indicates that α -synuclein influences DAT-mediated ion currents that may modify DA neuron function. Some studies suggest that α -synuclein accelerates the DA-induced apoptosis through enhanced transport of neurotoxic compounds. (Lee et al., 2001) This interaction is still not

fully understood, due to a fact that many contradictory evidences have been found. (Vaughan and Foster, 2013)

- **Parkin**, the E3 ubiquitin ligase, has a positive role in normal DAT function by regulating transporter ubiquitination and degradation. Mutations of Parkin which cause PD are connected to the loss of DAT quality control via failure of the mutant proteins to ubiquitylate misfolded transporters. This accumulates and induces negative effects on DA uptake, which might be associated with DA toxicity. Parkin interacts with the C-terminus of DAT. It disrupts DAT- β -synuclein interactions and suppresses α -synuclein-induced DA neurotoxicity *in vitro*. (Vaughan and Foster, 2013)

3.5. Pharmacology

The DAT is an important drug target and a lot of research has been carried out on this transporter. Since DA signaling is involved in many aspects of the brain function, its fluctuations had been noticed in numerous neuropsychiatric disorders: attention deficit/hyperactivity disorder (ADHD), PD, depression, anhedonia, and addictive/compulsive disorders, etc. (Kyle C. Schmitt et al., 2013) DAT is a target for several popular medicines as well as some recreational drugs.

DAT ligands include:

- **psychostimulants** (e.g., dextroamphetamine, methylphenidate),
- **antidepressants** (e.g., bupropion, modafinil),
- **anorectics** (e.g., phendimetrazine). (Kyle C. Schmitt et al., 2013)

DAT is a target for addictive drugs including cocaine, amphetamine, and methamphetamine, and for the drugs used in treatment of ADHD, depression, and other dopamine imbalance conditions. (Vaughan and Foster, 2013)

Ligands acting on DAT have, traditionally, been divided into two categories: substrates and inhibitors (**Table 3.1 and 3.2**). Inhibitors are compounds that bind to the transporter and block the substrate translocation, but are not transported themselves. Substrates, on the other hand, are transported into the cell themselves. Despite having different mechanisms of action, both substrates and inhibitors work to increase DA level in synapse. Inhibitors increase the amount of dopamine in the synaptic cleft by blocking its uptake, as mentioned above. Substrates increase the levels of dopamine in the synapse by provoking efflux of dopamine and by competing with it for access to empty DAT. (Kyle C. Schmitt et al., 2013) Both processes induce DA overflow, controlling the strength of DA signaling during drug abuse and therapeutic treatments. (Vaughan and Foster, 2013) DAT inhibitors can be selective and non-selective. Selective DAT inhibitors, like some benzotropine analogs (AHN 2-005), are lacking the reinforcing actions and therefore abuse potential, which is why they are under the consideration as potential ADHD therapy. (Schmeichel et al., 2013) Certain studies suggest that S-phenylpiracetam, a selective DAT inhibitor, could be potentially useful in treating obesity in patients with metabolic syndrome, without locomotor side effects. (Zvejniece et al., 2017) Some DAT selective analogues (GBR 12909 and benzotropine) are suggested as mean for treatment of cocaine addiction. (Aksenov et al., 2008)

Non-selective DAT inhibitors can be grouped into:

- Dual DAT/NAT inhibitors (brasofensine, bupropion, methylphenidate, and nomifensine) are suggested to be used in treatment of ADHD and PD. (Huot et al., 2016; Schmeichel et al., 2013)
- Dual DAT/SERT inhibitors (S-3,4-methylenedioxymethamphetamine (MDMA), UWA-101 and UWA-121, etc.) can enhance L-dopa activity and extend duration of its anti-parkinsonian benefits. (Huot et al., 2012, 2014)
- nonselective DAT/NAT/SERT inhibitors (mazindol, nefazodine, tesofensine, indanamine, bicifadine, etc.) have been considered as potential treatments for PD (Huot et al., 2016), depression, (Marks et al., 2008; Millan, 2009) obesity, (Tizzano et al., 2008) cocaine abuse, (Gardner et al., 2006) chronic pain, (Basile et al., 2007) etc. Unfortunately, due to their unselective mechanism of action they do have a lot of side effects.

Dual DAT/NAT and triple DAT/NAT/SERT inhibitors may have potential for the treatment of parkinsonism as monotherapy. However, the antiparkinsonian efficacy afforded by DAT inhibition may only be momentary and symptomatic. In the clinical settings, both brasofensine and tesofensine effects faded over weeks of repeated treatment. (Huot et al., 2016)

Some authors suggested (Maarten E. A. Reith et al., 2015; Kyle C. Schmitt et al., 2013) that in addition to substrates and inhibitors there are also partial substrates, allosteric modulators of DAT and atypical inhibitors. Studies on substrate-like ligands, (Kyle C. Schmitt et al., 2013) revealed compounds with partial substrate properties. Partial substrates (3,4-methylenedioxy-N-methylamphetamine (MDEA, PAL-193), ethylnaphtilaminopropane (ENAP, PAL-1045), 2S,5S-2-(3-chlorophenyl)-5-methylmorpholine (PAL-738)) are transported by DAT, but are considerably less effective at inducing reverse transport. Various DAT inhibitors (benztropine, modafinil, vanoxerine) have far milder reinforcing and stimulant properties than cocaine-like inhibitors which is why they are considered atypical inhibitors. Alternatively, some authors have suggested that cocaine and methylphenidate are DATs inverse agonists. (Heal et al., 2014) These partial substrates and atypical inhibitors have been suggested as a way of alleviating the abstinence symptoms in treating of cocaine dependence. (Kampman, 2008)

Table 3.1 Chemical structures of some of DAT substrates.

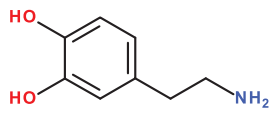
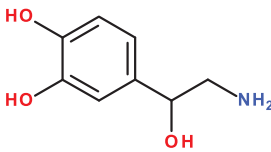
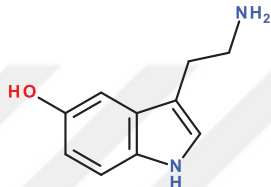
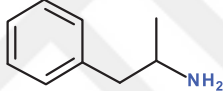
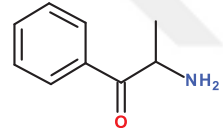
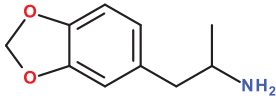
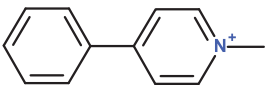
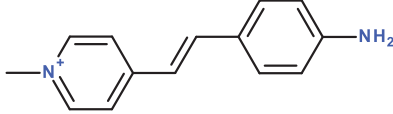
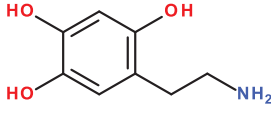
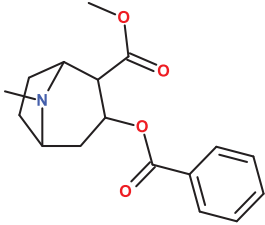
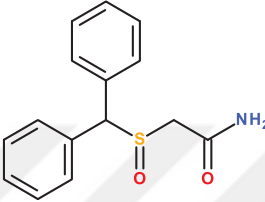
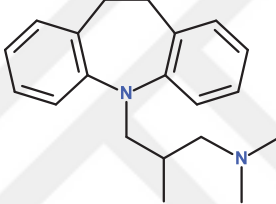
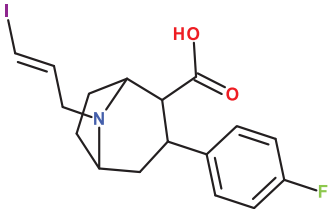
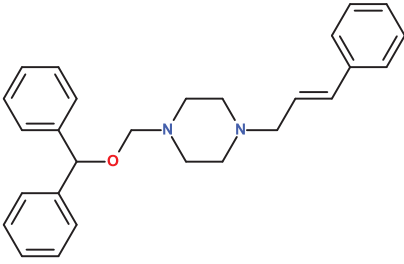
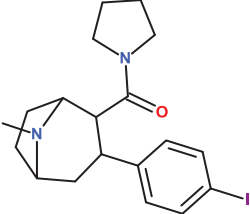
Compounds	Chemical formula
SUBSTRATES	
Neurotransmitters	
dopamine	
noradrenalin	
serotonin	
Amphetamines and its derivatives	
amphetamine	
cathinon	
MDA	
Neurotoxins and related compounds	
MPP+	
ASP+	
6-OH-dopamine	

Table 3.2 Chemical structures of some DAT inhibitors

Compounds	Chemical formula
INHIBITORS	
Nonselective transporter inhibitors	
cocaine	 <p>The chemical structure of cocaine is a tropane alkaloid. It features a bicyclic tropane ring system with a methyl group on the nitrogen. It is substituted with a methyl ester group and a benzoyloxy group.</p>
modafinil	 <p>The chemical structure of modafinil consists of a central carbon atom bonded to a phenyl ring, a benzyl group, a sulfonyl group (SO₂), and a propionamide group (CH₂CH₂CONH₂).</p>
trimipramine	 <p>The chemical structure of trimipramine is a tricyclic antidepressant. It features a central nitrogen atom bonded to two benzene rings and a propyl chain that ends in a dimethylamino group.</p>
Selective Dopamine transporter inhibitors	
altropan	 <p>The chemical structure of altropan is a tropane alkaloid. It features a bicyclic tropane ring system with a methyl group on the nitrogen. It is substituted with a propyl iodide group, a propionic acid group, and a 4-fluorophenyl group.</p>
GBR-12783	 <p>The chemical structure of GBR-12783 is a selective dopamine transporter inhibitor. It features a central piperazine ring substituted with a benzyl group, a propyl group, and a propyl group with a phenyl ring at the end.</p>
RTI-229	 <p>The chemical structure of RTI-229 is a tropane alkaloid. It features a bicyclic tropane ring system with a methyl group on the nitrogen. It is substituted with a pyrrolidine group and a 4-iodophenyl group.</p>

It is possible that altering the conformation of the DAT in different ways can trigger different downstream cellular signaling events. For example, binding of particular ligand increases the probability that the transporter will adopt a given conformation and that ligand-specific conformation would then be transduced via DAT interaction partners and associated scaffolding proteins. The second-messaging cascades, downstream of the DAT have not been completely explained so far, but many DAT-interacting proteins have been discovered. (Eriksen et al., 2010; Hadlock et al., 2010) DAT interaction partners include membrane scaffolding and trafficking proteins, cytosolic kinases, phosphatases, and other signaling proteins, G-protein-coupled receptors, and receptor tyrosine kinases. As pointed out above they are capable of changing DAT levels on the cell surface in real time. They can even selectively modulate specific DAT functions, such as reverse transport. (Eriksen et al., 2010)

Study of ligands with conformation-specific activity will help to reveal the nature of the transporter function of NSS proteins and could lead to improved medications for monoamine-linked disorders. (Kyle C. Schmitt et al., 2013) In the same time, understanding the differences between various drug-induced conformations of the transporter can offer new insights into the principles that determine whether a ligand becomes a substrate or an inhibitor. Structurally related compounds can trap the transporter in different conformational stages during the cycle. Such differences in drug molecular mechanisms can lead to different physiological outcomes. Therefore, with the sufficient knowledge of the structure and function of different conformational states, rational design of novel compounds that target specific transporter states will become within reach. (Anders S. Kristensen et al., 2011)

4. MATERIALS AND METHODS

Drug discovery is a very time-consuming and expensive process. It takes approximately 12 to 15 years and hundreds of millions of dollars for a drug to get on the market. Rational drug design and lead discovery is the first part of this research. **Lead** is the model compound that has positive characteristics such as pharmacological or biological activity but may also, have undesirable properties, like low potency, high toxicity, absorption difficulties, insolubility, etc. The first step is to identify the cause for the disease. Once the relevant biochemical system (**target**) is identified, natural ligand/substrate is usually taken for initial lead compound for the target protein. Today, this process consists of *in silico* (computational), *in vitro* (cell), *in vivo* (animal) studies and finally human clinical trials. (Richard B. Silverman, 2004)

As mentioned earlier, in our research the target is DA neuron, more specifically DAT. To identify new, potential substrate drugs, first we need to identify the discriminant characteristics of inhibitors and substrates. Afterwards we correlate them with the transporters' various conformations, and finally, build models for virtual screening of substrate-like molecules. Accordingly, finding open and closed conformations of hDAT is helpful in the design of next generation of anti-parkinsonian drugs. We speculated that an inhibitor blocks the transporter in an outward open conformation, and thus can only be docked in it, and not in the closed conformation; meanwhile the substrate should be able to bind for an outward-open, closed and inward-open conformation. We also expect less interactions and lower affinity of the substrate for DAT since it needs to be released from it, whereas inhibitor remains bound. Moreover, we will use multiple transporter conformational states for virtual screening, because use of single conformation state provides a scarce image of proteins. This is one of the major limitations in virtual screening, where the recognition of active compounds is significantly affected by the receptor conformation. (Spyrakis et al., 2013a) For the purposes of this work, we used different computational approaches to find the best tools that enable the screening and

design of new substrates for the hDAT, such as homology modeling, docking, molecular dynamic simulations, virtual screening and *in vitro* studies.

4.1. Homology Modeling

Since the X-ray structure of human DAT is still unknown, and the structure of drosophila's DAT has been revealed recently, (Penmatsa et al., 2013) we have employed homology modeling in order to obtain 3D model of our target protein. Homology modeling is rapidly becoming the method of choice for obtaining 3D coordinates of proteins. Knowledge of the 3D structures of proteins provides unique insights into the molecular basis of their functions. (Vyas et al., 2012) The importance of 3D model will be clarified further through explanation of our *in silico* studies.

Homology modeling is the construction of a 3D model of the **target** protein from its amino acid sequence and an experimental X-ray structure of a related corresponding (homologous) protein (the **template**). Normally, evolutionarily associated proteins have similar sequences, and this similarity is called homology. The fact that homologous proteins generally have similar stable tertiary structure is used in homology modeling. (Forrest et al., 2006a; Kaczanowski and Zielenkiewicz, 2010) High-quality structural models can be created when the target and the template are closely related. (Fiser, 2010) The process of homology modeling contains four chronological steps:

1. **Template selection and fold assignment:** this can be accomplished by searching for homologous protein sequences and/or structures with tools such as BLAST (Basic Local Alignment Search Tool) and PSI-BLAST (<https://blast.ncbi.nlm.nih.gov/Blast.cgi>). The target can be compared with protein structure databases such as PDB (Protein Data Bank) (<https://www.rcsb.org/pdb/>). Then, structurally conserved and variable regions are identified. The variable regions usually come from loops and turns at the exterior of the protein, **and** are further away from binding site.

2. **Alignment of target with the template:** for 30% minimum sequence identity between a target and a template, proteins are expected to have similar structures if the aligned region is long enough. When two proteins have more than 50% sequence identity the quality of model is generally considered excellent. (Pevsner, 2015)
3. **Model building:** different approaches are employed, such as rigid-body assembly, segment matching, modeling by satisfaction of spatial restraints and comparative model building. Rigid-body assembly model building relies on the natural division of the protein structure into conserved core regions and variable loops, and flexible amino acid side chains on the backbone. The model is then constructed from core regions and from loops and sidechains, which are taken from “cutting” related structures. Segment matching is based on the constructing a model by using a subset of conserved atoms’ positions from the template structures as guiding positions, to calculate the coordinates of other atoms and by identifying and assembling short parts of the protein chain. (Havel and Snow, 1991) Modeling by satisfaction of spatial restraints translates sequence alignments (from the alignment of the target sequence with the template structures) into distance and chirality constraints, which are then used as input for distance geometry calculations. The model is calculated by an optimization method relying on conjugate gradients and molecular dynamics. (Sali and Blundell, 1993) The commonly used programme, MODELLER is using this method. (Webb and Sali, 2016) Generalized comparative modeling starts with predicting contacts and secondary structure for the template-aligned regions, and possibly for the unaligned regions and then searches the conformational space guided by a distance geometry and clustering, to overcome alignment mistakes. (Kolinski et al., 2001)
4. **Model evaluation:** assessing whether the certain structure is likely, based on general knowledge of protein structure principles (bond length, angle, peptide bonds, local environment for hydrophobic/hydrophilic residues, etc.) (Pevsner, 2015)

4.1.1. Building of hDAT Model

We have retrieved sequence of our target protein, hDAT, from UniProt databank (QO1959 SCGA3_HUMAN) (<http://www.uniprot.org/>) and X-ray structure of our template, dDAT, from Protein Data Bank (PDB code: 4M48). Sequences were aligned using “Align Sequences” toolkit from BIOVIA DS 4.5 (<http://accelrys.com/>). BIOVIA DS is the commercial program that combines several platforms which allow simple usage in the process of drug design (homology modeling, protein and ligand preparation, visualization, picture production, etc.). The secondary structure alignment was set to TRANSMEM as for trans-membrane proteins. The sequence identity and similarity was estimated as equal to 49.6% and 69.2%, respectively. The model was built using “Homology Modeling” protocol in BIOVIA DS 4.5. The first 57 and last 20 amino acids were omitted because there was no corresponding homolog. Omitting these extra-membrane amino acids is allowed, since they are far away from the transporters’ ligand-binding pocket. Two Na⁺ ions, one Cl⁻ ion and 1 molecule of cholesterol were included, and 10 homology models were created and verified with MODELLER plug-in. The model having the best DOPE and normalized DOPE score (-79899.35 and -1.3418, respectively) was selected. One loop, between Phe187 and Thr210 was refined by the use of the “Refine Loops” protocol, and the CHARMM22 Force Field was applied to relax the steric hindrance between amino acids side chains. The model was then minimized using the “Clean Geometry” toolkit to avoid any further steric hindrance of amino acids side chains. Finally, the protein was prepared in the “Prepare Protein” protocol and protonated at pH = 7.4.

4.2. Molecular Docking

We have used molecular docking in several phases during our *in silico* studies. Molecular docking (later referred to as docking) is a “computational technique that predicts the preferred orientation of one molecule towards another.” (Lengauer and Rarey, 1996) Ligand-protein docking is based on sampling different conformations of small molecules in binding sites of the protein. Scoring functions are used to evaluate which of these

conformations best fits to the protein binding site. (Warren et al., 2006) It calculates and ranks the complexes that are coming from the associations between a target protein of known 3D structure and a certain ligand. (Sousa et al., 2006) Recent progresses in the field of X-ray crystallography and NMR techniques caused the significant increase in the number of known 3D structures of proteins; with known 3D structure the docking became a choice tool in drug design.

Docking protocols consist of **search algorithm** and a **scoring function**. (Sousa et al., 2006) Firstly, docking algorithms are used to orient small molecules in the active site. Organic molecules, even comparatively very basic ones, pose many conformational degrees of freedom. Sampling these degrees of freedom has to be carried out with adequate accuracy to determine the conformation that best fits the protein binding pocket. Sampling must also be fast enough to evaluate thousands of compounds in a given docking run. Lastly, scoring functions are applied to estimate the biological activity through the assessment of interactions between ligands and potential targets. (Kitchen et al., 2004) In this work, we have used three different programs in order to find the one with most suitable scoring function for our protein. (Nikolic et al., 2016):

- **AutoDock 4.2** (<http://autodock.scripps.edu/>) uses a semi empirical force field based on the AMBER force field. (Weiner and Kollman, 1981) It uses a molecular mechanics model for enthalpic contributions such as vdW and hydrogen bonding, and an empirical model for entropic changes upon binding. Each component is multiplied by empirical weights found from the calibration against a set of known binding constants. AutoDock uses a Lamarckian genetic algorithm for the conformational search. (Goodsell et al., 1996; Morris et al., 1998, 2009) The scoring function of Autodock is represented in following equation:

$$\Delta G = \Delta G_{vdW} \sum_{ij} \left(\frac{A_{ij}}{r_{ij}^2} - \frac{B_{ij}}{r_{ij}^2} \right) + \Delta G_{h-bond} \sum_{ij} E(t) \left(\frac{C_{ij}}{r_{ij}^{12}} - \frac{D_{ij}}{r_{ij}^{10}} \right) + \Delta G_{elec} \sum_{ij} \frac{q_i q_j}{\epsilon r_{ij}^2} + \Delta G_{tor} N_{tor} + \Delta G_{sol} \sum_{ij} (S_i V_j + S_j V_i) e^{-\frac{r_{ij}^2}{2\sigma^2}} \quad (4.1)$$

where ΔG stands for free energy of binding, r_{ij} is the magnitude of the distance between i and j atoms, q_i and q_j are the charge at points i and j respectively, in C and ϵ_0 is the permittivity of a vacuum, S - solvation term for atom V - atomic fragmental volume of atom σ - Gaussian distance constant; it is a sum of van der Waals, hydrogen bonds, Electrostatics (Coulomb's Law), torsions and desolvation energies.

- **GOLD** v5.2.2 (<http://csg.sph.umich.edu/abecasis/Gold/>) (Genetic Optimization for Ligand Docking) uses several different scoring functions. **GoldScore** fitness function predicts peptide binding positions. It is based on H-bonding, vdW energies and ligand torsion strain terms. For example the **ChemScore** fitness function predicts the total free energy change upon peptide binding to the predetermined binding site. **ChemPLP** is the ChemScore hydrogen bonding term and uses multiple linear potentials to model vdW and repulsive terms; calculation speed is fast and more effective than the other scoring functions for both pose prediction and virtual screening. GOLD uses the genetic algorithm procedure for conformational search. (Jones et al., 1995, 1997)
- The **FLAPdock** (<http://www.moldiscovery.com/software/flap/>) approach splits the ligand into fragments, generates conformations for them, and predicts a set of poses for these fragments and their conformations. The remaining fragments are then added and conformational space explored by varying the torsion angles of the bond that is being joined. The results are scored according to a global scoring function that combines MIF (Molecular Interaction Fields) similarity, dissimilarity, and energetic terms. Results are filtered if there is a high energy of overlap with the receptor atoms, and clustered according to their similarity. The N best results are retained at each stage, to increase the search efficiency, and in the end typically tens of thousands of potential conformers and poses of the ligand are explored. In FLAPdock a global S-Score has been parameterized and validated on many targets including those in the DUD datasets. The score includes describing hydrogen-bonding interactions, hydrophobic interactions, shape,

Lennard-Jones (LJ) non-polar attractive and repulsive interactions, and the electrostatic-interactions. (FLAP manual, Cross and Cruciani, 2010)

Three ligands, commonly used for hDAT modeling: **amphetamine** (a substrate and psychostimulant) (Robertson et al., 2009b), **modafinil** (an atypical inhibitor) (Madras et al., 2006) and **cocaine** (an inhibitor) were docked into apo hDAT model with AutoDock 4.2 (<http://autodock.scripps.edu/>). (Morris et al., 2009) Cocaine and amphetamine were modeled with a positive charge, as they are protonated at pH=7.4. The coordinates of alpha carbon of Phe326 were used for grid-centering; grid box was set to be 50 grid points (each grid point is 0.375Å apart) in all directions to allow the ligand to rotate freely in binding pocket. All the compounds were situated in the central binding pocket halfway into the membrane, lined by Phe155 Tyr156, Phe320, Phe326 and Ser422 residues.

To identify the most probable open-out and closed transporter conformation, known substrates and inhibitors were docked into a set of ten conformations extracted by the MD trajectories in all three docking programs mentioned above. The number of conformations was first reduced by performing a regular sampling (one out of 100 structures) and then picking them according to the distance between Phe326 and Tyr156. In this analysis, for docking in AutoDock the size of the grid box was set to be between 40 - 60 grid points. For docking in GOLD the size of the binding site was set to 10 - 12Å, centered on Phe326. The parameters for binding pocket for FLAPdock were set to be 2Å for substrates and 6Å for inhibitors around the reference ligand were taken as the binding pocket.

In order to identify new possible substrates, 150 compounds obtained after virtual screening were docked into previously identified probable open-out and closed open-out and closed conformations.

For docking in AutoDock and GOLD all the compounds and proteins were prepared in BIOVIA DS 2016, using the “Prepare Protein” and “Prepare Ligand” protocols. For FLAPdock ligands were imported into the database, protonated at pH=7.4, and “Fix PDB” protocol was used for preparation of the transporter.

4.3. Molecular Dynamics Simulation

To understand how the docked ligands, interact with the DAT transporter, and to obtain information about the main conformational changes in the protein upon ligand binding, the hDAT, both complexes and apo-hDAT (empty) were submitted to 40 ns Molecular dynamics simulations.

Molecular dynamics (MD) is a computer simulation method for studying the physical movements of atoms and molecules, which enables us to understand the structure and dynamics with detail (on the scales where motion of individual atoms can be tracked). The atoms and molecules are allowed to interact for a fixed period of time, to give a view of the dynamic evolution of the system. The trajectories of atoms and molecules are calculated by solving of Newton's equations of motion for the entire system of interacting atoms. Forces between the particles and their potential energies are calculated by using interatomic potentials or molecular mechanics force fields. (Alder and Wainwright, 1959; Andreas Kukol, 2008; Rahman, 1964) The most important fact of simulation is that it provides a way to test whether theoretical models predict experimental observations. It is not enough to work with individual structures, but the system has to be expanded to generate a representative ensemble of structures at certain experimental conditions (temperature and pressure). MD simulation has the advantage of accurately reproducing kinetics of non-equilibrium properties. Usually, a starting configuration is very far from equilibrium. For this reason, it is necessary to start with energy minimization before the molecular dynamic simulation. If minimization is not done, large forces would cause the simulation to collapse or change the system. (Andreas Kukol, 2008)

All MD simulations rely on force fields (FF) to describe the time evolution of bond lengths, bond angles and torsions, also the non-bonding van der Waals and electrostatic interactions between atoms. FF is a series of equations and related constants that are describing dependence of the energy of a molecule on the coordinates of its particles. (González, 2011) FF methods (also called molecular mechanics) ignore the electronic motion (quantum mechanics) and calculate the energy of the system as a function of the

nuclear position only. Molecular Mechanics is thus used to perform calculations on systems that contain large number of atoms. (Andrew R. Leach, 2001) Nowadays, improvements in computational resources are permitting longer MD simulations. Combined with modern improvements in the quality of force field parameters, they have produced some advances in protein structure prediction and modeling. (Beauchamp et al., 2012; Piana et al., 2014; Raval et al., 2012) A force field consists of set of equations, given below, and used to calculate the potential energy and forces from particle coordinates, as well as a collection of parameters used in equations (**Equation 4.2**). All common FF subdivide potential functions into two classes:

1. Non-bonded interactions - covalent bond-stretching, angle-bending, torsion potential, improper torsions;
2. Non-bonded interactions - Lennard Jones repulsion and dispersion and Coulomb electrostatics.

$$\begin{aligned}
 E = & \sum_{bonds} K_b (b - b_0)^2 + \sum_{angles} K_\theta (\theta - \theta_0)^2 + \sum_{\substack{improper \\ dihedrals}} K_\varphi (\varphi - \varphi_0)^2 + \\
 & \sum_{dihedrals} \sum_{n=1}^6 K_{\phi,n} (1 + \cos(n\phi - \delta_n)) + \sum_{\substack{nonbonded \\ pairs\ ij}} \frac{q_i q_j}{4\pi D r_{ij}} + \\
 & \sum_{\substack{nonbonded \\ pairs\ ij}} \epsilon_{ij} \left[\left(\frac{R_{min,ij}}{r_{ij}} \right)^{12} - 2 \left(\frac{R_{min,ij}}{r_{ij}} \right)^6 \right] \quad (4.2)
 \end{aligned}$$

Where energy E is sum of energies of bonded and non-bonded interactions. First four terms denote intramolecular contributions to the total energy (bond stretching, angle bending, and dihedral and improper torsions); the last two terms denote the hydrophobic and repulsive contribution to the total energy (Columbic interactions and Lennard-Jones potential)

It is important to point out that the FFs are empirical - there is no “correct” form of FF. (Andrew R. Leach, 2001) Recent advancements have enabled simulation studies of protein systems on biophysically-relevant timescales (hundreds of μ s), which resulted in

the need to incorporate new, improved FFs. Although early FF development was limited by the lack of direct comparisons between simulation and experiment, recent work has demonstrated direct calculation of NMR observables from protein simulations. (Beauchamp et al., 2012) Several force fields were found to provide rather accurate representations of the structure and dynamics of a number of small globular proteins on the sub-microsecond timescale. (Piana et al., 2014) Most commonly used FFs today are CHARMM (Yin and MacKerell, 1998) and AMBER (Weiner et al., 1984) FFs, as they cover the broad spectrum of atoms.

Setting up and running MD simulation consist of following, sequential steps:

1. **Setting up the system.** First of all, the initial positions and velocities of each atom in the system has to be identified. This information can be obtained from 3D structure of our molecule. After preparing the system the boundary conditions should be set by setting the periodic boundary conditions where the simulation box is surrounded by an endless number of replicas of itself. Only the atoms inside the main box are considered, but as soon as one of the atoms abandons the cell, an image particle enters from the opposite side to replace it. Afterwards, it is necessary to select the working ensemble. Possible ensembles are: NVE (where number of particles (N), volume (V) and energy (E) is kept constant), NVT (constant temperature (T)) or NPT (constant pressure) .
2. **Equilibration:** The initial configuration will not be representative of the conditions that we want to explore, so it is necessary to make sure that the system has reached the equilibrated state before continuing. This can be done by setting NPT simulation in order to allow the system to achieve the equilibrium density corresponding to the desired pressure and temperature.
3. **Production:** Once the system is equilibrated at desired temperature and pressure the production start. Usually it is done in NVT environment. The trajectory of the molecule is extracted from this step. (González, 2011)

Our simulations were carried out with Nano Scale Molecular Dynamics (**NAMD**) software. NAMD is a computational software for molecular dynamic simulation developed by Theoretical and Computational Biophysics Group and Parallel Programing

Laboratory at the University of Illinois. It is a parallel molecular dynamics code (Charm++) designed for high-performance simulation of large systems. It uses both AMBER and CHARMM force fields. It is widely known for high performance simulation of biomolecules in realistic environment of more than 100.000 atoms. (Phillips et al., 2005)

4.3.1. MD Simulation of DAT

As mentioned in Chapter 3, DAT is a membrane protein, and there is not enough information on membrane proteins in the PDB database because of difficulties associated with expression and crystallization. Moreover, most membrane proteins undergo large conformational changes in order to complete their function. Therefore, MD simulations can provide useful additional information. Recently, there have been substantial advancements in the simulation of lipid bilayer and membrane proteins embedded in them.(Andreas Kukol, 2008) It is important to mention that the time frame of typical MD simulation (10-100 ns) is smaller than the turnover rates of membrane transporter proteins (0.1 – 10 s). MD simulations are, therefore unlikely to predict the structural rearrangements during a complete translocation cycle. However, they are still used for exploring the proposed changes of the interaction networks for the intra- and extracellular gates.(Khalili-Araghi et al., 2009) The process and running of such simulations can be divided into four steps:

1. The preparation of the protein,
2. The preparation of lipid,
3. The insertion of the protein inside the lipid bilayer and establishing of a stable system,
4. Running the simulation. (Andreas Kukol, 2008)

As mentioned above, the system was prepared with Visual Molecular Dynamics (VMD) and all the simulations were performed with Nano Scale Molecular Dynamics (NAMD) (Phillips et al., 2005) version 2.8 (<http://www.ks.uiuc.edu/Research/namd/>). The protein

was located within a 1,2-palmitoyl-oleoyl-*sn*-glycero-3-phosphocholine (POPC) membrane (100x100x100) using the OPM web service (<http://opm.phar.umich.edu/>). The topology files for the ligands were generated using the CGENFF web service (<https://cgenff.paramchem.org/>). Crystallographic water molecules were preserved, and the entire system was solvated using the TIP3P water model and neutralized by addition of NaCl to an ionic concentration of 0.2 M.

Since we were using a membrane patch that has not been equilibrated, firstly we performed a simulation in which everything (water, ions, protein, lipid head groups) except lipid tails was fixed. In this way, we induced the appropriate disorder of a fluid-like bilayer. Minimization was performed for 1000 steps. The default NAMD minimizer uses sophisticated conjugate gradient with line search algorithm. After minimization, we reinitiated velocities according to the desired temperature of 310 K, using Langevin dynamics with damping coefficient of 5/ps. Finally, dynamics was run for 0.5 ns (using a 2-fs time step). Our second run with NAMD was a “minimization” run, which simply guided the system to the nearest local energy minimum in configuration space. It was then followed by an equilibration with the protein constrained, so as to permit the environment to relax first. Harmonics constraints were applied using a PDB file that tags the atoms which are to be restrained. The use of such harmonic constraints permits lipids, water, and ions to adapt to the protein in its form. We applied forces to keep water molecules from entering the membrane hydrophobic region. This step also ran minimization 1000 steps, followed by 1 ns of dynamics. After minimization and equilibration with the protein constrained, we obtained a system in which lipids are well packed around the protein, while water has not entered forbidden regions. We proceeded to release the harmonic constraints and further equilibrate the whole system. We have eliminated the minimization step in the next simulation. With protein equilibrated we performed a 40-ns long production run in NPT environment, where temperature was set to 310 K, and pressure to 1 atm.

4.4. Virtual Screening

We used Virtual Screening (VS) methods to screen the libraries for potential hDAT substrates that could be used later on as the lead in design of novel neuroprotective compounds. VS is an important tool that finds novel lead compounds. It is a computational technique that surfs through large libraries of small molecules to find compounds that are most likely to bind to a specific protein. (Reddy et al., 2007; Walters et al., 1998) *In silico* screening speeds up modern lead identification and lead optimization, allowing us to choose and design new drugs in a time and cost effective manner. (Rester, 2008; Walters et al., 1998) Two major methods for VS are: Structure-Based VS and Ligand-Based VS. (McInnes, 2007) Both of these approaches have advantages and disadvantages; the combination of SB and LB approaches is becoming more and more popular recently. (Nikolic et al., 2016)

- **Structure-Based Virtual Screening (SBVS)** is based on the knowledge of the 3D structure of the target protein. Today, the structure based methods are enabled by the huge number of 3D structural information that can be found in the Protein Database - PDB. (McInnes, 2007) Using the 3D structural information of the protein target, we are now able to explore the basic molecular interactions, involved in ligand-protein binding, and understand experimental results up to atomic levels. In SBVS, large libraries of commercially available drug-like compounds that are computationally screened against proteins of known structure, and those that are predicted to bind well can be experimentally tested. (Lionta et al., 2014)
- **Ligand-Based Virtual Screening (LBVS)** is usually used when the three-dimensional (3D) structures of drug targets are not available, and it is based on various statistical methods. 3D Structure-Activity Relationships (3D QSAR) and pharmacophore modeling are the most important and widely used tools in ligand-based drug design. They can provide crucial insights into the nature of the interactions between drug target and ligand molecule and provide predictive models, suitable for lead compound optimization. The known ligand molecules

that bind to the drug target are studied in order to understand their structural and physical and chemical properties. This is done in order to correlate these properties with the desired pharmacological activity of those ligands. (Acharya et al., 2011)

During this project, we have combined these two approaches in order to get more precise results. First, we have screened the library using flexible SBVS, after which we have rescreened the results using pharmacophore LB approach. All VS experiments were performed with **FLAP** (Fingerprints for Ligands and Proteins), developed and licensed by Molecular Discovery Ltd (<http://www.moldiscovery.com/>). Several VS campaigns were successfully performed with FLAP and are reported in the literature. (Spyrakis et al., 2013c, 2013b, 2014) FLAP describes small molecules and protein binding sites in terms of four-point pharmacophoric fingerprints, extracted from the molecular interaction fields (MIFs), and calculated by GRID. (Pj, 1985) The information contained in the MIFs is extracted and condensed in quadruplets of pharmacophoric points, used to compare, align, and superimpose different chemical entities, which can be either small molecules or macromolecules, usually described in terms of pockets.

4.4.1. Data Sets Preparation

Fifty common substrates were obtained from the literature (Cook et al., 2002; Cozzi et al., 2013; Glennon, 2014; Howell and Negus, 2014; Kohut et al., 2013; López-Arnau et al., 2012; Mavel et al., 2012; Maarten E.A. Reith et al., 2015; Rothman, 2003; Schloss et al., 2015; Seddik et al., 2013) and from the ChEMBL website (<https://www.ebi.ac.uk/chembl/>) and used to build LDA and pharmacophore-based models. (Bento et al., 2014) For each substrate (classified as active molecules), the most likely tautomer and protomer at pH = 7.4 was calculated by MoKa. (Milletti et al., 2010) Afterwards, fifty decoys were generated for each substrate (active molecule) using the decoy generator tool available, within the DUD-E (Mysinger et al., 2012) website (<http://dude.docking.org/>). Decoys are inactive compounds, computed on the basis of similar physical properties but different chemical structures from substrate analogues, in order to test the validity of our model. Twenty-five active molecules and fifty decoys

were randomly selected and used to build the training set. The test set comprised all available active molecules and decoys. For the pharmacophore-based VS, alongside decoys, test set was extended with inhibitors.

4.4.2. LDA-Based SBVS

Previously mentioned MD simulation is a powerful tool for researching intrinsic protein dynamics and helps to provide information on protein flexibility in drug design and VS. A new method for flexible SBVS has been recently developed. An integrated MD - FLAP (molecular dynamics–fingerprints for ligand and proteins) approach that combines molecular dynamics, clustering and linear discriminant analysis, for improving accuracy and efficacy in VS. To take into account protein flexibility in VS, the entire trajectory was clustered according to the variability of the MIFs within the pocket. The pocket was defined by FLAPsite implemented within FLAP and the MIFs calculated for all the pocket conformations generated by the dynamics. Principal Component Analysis (PCA) was used to cluster the conformations and select the most representative medoids for each cluster. Ten clusters were generated and ten medoids selected to represent protein flexibility. The linear discriminant analysis (LDA), approach implemented in FLAP, was used to select the templates and the FLAP scores that are able to discriminate between an active and decoy molecules in the training set. Different template/FLAP score combinations were used to generate LDA models. The models were validated using the test set. Eventually, the best results in prediction were obtained with a 1 template/3 scores model, and the selected FLAP scores were H, H*DRY*N1, H*O*DRY (shape, hydrophobic interactions and hydrogen bond donor/acceptor). The same model was then used to screen the entire Specs library. When VS is carried out using an LDA model, FLAP will produce “Activity Class” predictions for each candidate, alongside the usual output forms and a corresponding LDA-R score, ranking the compounds from the most active (highest score) to the most inactive (lowest score). When the inclusion of multiple structures improves VS predictions, the LDA-R score ranking shows the highest enrichment. (“A Pipeline To Enhance Ligand Virtual Screening,” n.d.) The most promising 1000 compounds were selected and submitted to further pharmacophore-based

virtual screening.

4.4.3 Pharmacophore-Based VS

Only some parts of the lead compound may be involved in the appropriate receptor interactions. Those groups on a molecule that interact with a receptor and are responsible for the activity are called pharmacophore. (Richard B. Silverman, 2004) **Pharmacophore** is therefore defined as “an ensemble of steric and electronic features that is necessary to ensure the optimal supramolecular interactions with a specific biological target and to trigger (or block) its biological response.” It is important to point out that pharmacophore is not a real molecule but an abstract description of molecular features that is necessary for its biological activity. (Ganellin et al., 1998)

The pharmacophore model was built using the 50 substrates mentioned above. Pharmacophore model was created in FLAP-2.0.0 using FLAPpharm protocol (<http://www.moldiscovery.com/>). FLAPpharm generates a detailed conformational ensemble for each structure, filters these conformations to keep the ones with the most similar pharmacophore and performs a prune tree search to find common alignment models. After creating the alignment models, a pharmacophoric pseudo-molecule is generated. The model consists of the most common atomic locations as pharmacophoric points as well as MIFs and pseudo-MIFs. FLAPpharm models use a parameterized scoring function that is a weighted sum of shape, hydrophobic, hydrogen-bond donor and hydrogen-bond acceptors MIF similarities.

Molecules were aligned to each other in order to find the optimal MIF similarity across the set, then subsequently pharmacophore was extracted, and the least fitting molecules were excluded. By excluding these molecules, one by one, 8 pharmacophore models were created, out of which 5 had S-score greater than 1. The structures of the following substrates were included in the best performing pharmacophore model: 3-fluoroamphetamine, 3-methyl-tryptamine, 4-fluoro-tryptamine, 5-fluoro- α -ethyltryptamine, 5-chloro- α -methyltryptamine, 5-fluoro- α -methyltryptamine, 6-(2-aminopropyl)benzofuran

(6-APB), 6-hydroxy-dopamine, 6-fluorotryptamine, α -ethyltryptamine, amphetamine, cathine, cathinone, dopamine, 3,4-dichlorophenethylamine (DCP), fluorescent fake neurotransmitter (FFN102), (*N*-ethyl)-1-(2-naphthyl)-propan-2-amine (ENAP), ephedrine, m-octopamine, m-metoxyamphetamine, methylenedioxyamphetamine (MDA), 3,4-Methylenedioxyamphetamine (MDMA), metamphetamine, metcathinone, mefedrone, (*N*-methyl)-1-(2-naphthyl)-propan-2-amine (MNAP), 1-(2-naphthyl)-propan-2-amine (NAP), noradrenalin, norphenfluoramine, phenmetrazine, phenethylamine, phentermine, phenflouramine, tyramine, tryptamine.

To validate these models and to choose the best one that differentiates between active and inactive compounds, three different datasets were created. One dataset contained 50 substrates and 77 inhibitors (Cook et al., 2002; Cozzi et al., 2013; Glennon, 2014; Howell and Negus, 2014; Kohut et al., 2013; López-Arnau et al., 2012; Mavel et al., 2012; Maarten E.A. Reith et al., 2015; Rothman, 2003; Schloss et al., 2015; Seddik et al., 2013), second dataset contained 50 substrates and 2500 decoys and the third dataset contained all three. Since we are interested in finding substrates only, we marked substrates as active while both inhibitors and decoys were marked as inactive compounds. Model was chosen according to the LBVS enrichment.

The obtained models were then used to screen the Specs database, which is part of the ZINC archive (<http://zinc.docking.org/>), (Irwin et al., 2012) looking for new possible hDAT substrates. This database provides affordable molecules in terms of purity and availability (Spyrakis et al., 2013c, 2014) and contains molecules with significant chemical and geometric diversity. A set of about 300,000 compounds was downloaded and filtered based on the principles of drug-likeness using $\text{LogP} < 5$, and $150 < \text{MW} < 500$ as cut-offs.

4.5. *In Vitro* Assays

The most promising potential hDAT substrates were bought and tested in *in vitro* experiments. We have based our *in vitro* experiments on fluorescent microscopy and ASP+ (4-(4-(dimethylamino)-styryl)-N-methylpyridinium) assays.

Fluorescence microscopy is a major tool for monitoring cell physiology. The theory behind fluorescence includes the absorption of light energy (a photon) by an indicator followed by the emission of some of this light energy (as another photon) a few nanoseconds later. Due to certain energy loss in this process, the emitted photon has less energy than the absorbed photon. Light with a short wavelength (toward the blue) has higher energy than light with a long wavelength (toward the red). The development of various transmitted light microscopy approaches emphasized the natural contrast of cells in order to make them more visible. However, the introduction of fluorescence microscopy, using a variety of fluorescent indicators that can be specific for proteins, lipids, or ions, (Giepmans et al., 2006; Palmer and Tsien, 2006) has allowed us to visualize cell physiology. (Sanderson et al., 2014) In our *in vitro* studies we used the fluorescent features of compounds (e.g the ability/inability to show the fluorescence) to track whether the compounds will be up-taken by DAT.

4.5.1. HEK-hDAT Cell Culture and ASP+ Uptake

The fluorescent organic compound ASP+ is a substrate for the monoamine transporters that has been applied in various studies to visualize neurotransmitter uptake in monoaminergic neurons in real-time live cell imaging, including DAT-dependent uptake of dopamine. (Inyushin et al., 2013; Lau et al., 2015; Matthaues et al., 2015; Oz et al., 2010; Schwartz et al., 2003) Here we applied ASP+ live cell imaging to determine whether our compounds compete with ASP+ as substrates for hDAT *in vitro* surroundings and thereby decrease the amount of detectable ASP+ fluorescence.

Two different cell lines have been used for our *in vitro* experiments. First, we tested the fluorescence of purchased compounds, and one out of six emitted fluorescents. Five compounds were then tested with ASP⁺ uptake assays. The last compound could not be tested due to interference and it was imaged in Mouse ES cell-derived dopaminergic neurons.

For ASP⁺ experiment we used **HEK (Human Embryonic Kidney cells) 293**. They are a specific cell line, derived from human embryonic kidney cells. HEK 293 cell line and its derivatives are used in experiments ranging from signal transduction and protein interaction studies over viral packaging to rapid small-scale protein expression and biopharmaceutical production. (Lin et al., 2014) They have been transformed by exposing cells to cropped fragments of adenovirus type 5 DNA by Graham in 1973. (Graham et al., 1977) Later on, it has been discovered that HEK-293 cells have an unexpected relationship to neurons. (Shaw et al., 2002) HEK -293 cells stably transfected with the human DAT are commonly used in *in vitro* experiments such as DAT inhibition, DA release, transport rates, etc. (Sitte et al., 1998) The HEK-293 cells stably expressing the recombinant human DAT (HEK-hDAT) (Hummerich et al., 2004) were maintained in Dulbecco's modified Eagle's medium, supplemented with 10% fetal bovine serum, penicillin (100U/mL), streptomycin (100µg/mL), and geneticin (G418, 200µg/mL) at 37°C in 95% humidified air with 5% CO₂. The HEK-hDAT cells were incubated for 10 min with compounds 1, 2 or 3 (0µM, 1, 10 and 30µM) at 37 °C. Subsequently, the cells were loaded with ASP⁺ for 30 s. The cells were washed with medium before imaging. The ASP⁺ was added at the concentration of 10 µM.

Mouse Embryonic Stem (ES) cells that were differentiated into midbrain dopaminergic neurons according to established protocols (Baizabal and Covarrubias, 2009; Lau et al., 2015; Lee et al., 2000; Martí et al., 2017) were used for imaging the fluorescent compound. ES cells, pluripotent cell lines derived from the inner cell mass of blastocysts, are able to differentiate into the endodermal, mesodermal and ectodermal lineage. In order to establish an *in vitro* system of functional dopaminergic neurons, called survival-promoting factors (SPF), were applied to differentiating pluripotent embryonic stem cells. They were found to increase the number and viability of tyrosine hydroxylase (TH) - and

dopamine transporter (DAT)-positive dopamine producing neurons. The system may be used in pharmacological assays to analyze the activity of medical drugs for treatment of Parkinson's disease, or to identify the effects of toxic factors to dopaminergic neurons by in vitro analyses. The system may also be helpful in high-throughput screening assays using cDNA microarrays to identify regulatory genes and mechanisms involved in the differentiation of dopaminergic neurons. (Rolletschek et al., 2001) Mouse ES cell-derived dopaminergic neurons were generated as described by Martí et al. (Martí et al., 2017) Briefly, the growth-factor-based differentiation protocol comprised three stages: (1) generation of neuronal stem spheres, (2) selection of dopaminergic progenitors, and (3) terminal differentiation of dopaminergic neurons. During stages 1 and 2, culture medium was supplemented with growth factors that drive neuronal differentiation along the dopaminergic pathway. Terminal differentiation was induced by withdrawal of growth factors and yielded mature neurons after 14 days. Overall, differentiation from stem cell to mature neurons took 28 days. ES cell-derived dopaminergic neurons were incubated with compound 6 for 10 min at 37°C before image acquisition.

Images and data analyses for experiments with ASP+ were performed as described previously. (Lau et al., 2015) Live-cell imaging of HEK-hDAT cells was performed using a Leica TCS SP5 imaging system attached to a DM IRE2 microscope equipped with an incubation chamber (Ibidi, Planegg, Germany). Excitation laser was a DPSS laser (561nm). Confocal z-stacks were acquired with sections taken every 0.5 μm with a 63 \times magnification. During image acquisition of control ASP+ fluorescence intensities, the photomultiplier sensitivity was set to acquire non-saturated pixel value to allow quantitative image acquisition. To ensure quantitative ASP+ imaging for dose response tracing, images of each respective compound were acquired with their own internal controls. Images were exported as tiff-files and imported to NIH **ImageJ** (NIH, Bethesda, USA) for quantification of ASP+ fluorescence intensities. Regions of interest (ROI) were selected with the freehand selection tool. For all ROIs, the integrated fluorescence densities were determined after cutting off background fluorescence. Data from at least 10 ROI were averaged for each 35mm μ -dish imaged (Ibidi, Planegg, Germany).(Martí et al., 2017) ASP+ fluorescence intensities are given as the mean \pm SEM. Statistical analysis was performed by one-way ANOVA followed by post hoc Tukey tests using

GraphPad Prism software (GraphPad Software, Inc., La Jolla, USA). $P < 0.05$ was considered significant. Each set of experiments was performed three times.

4.5. Design of Novel hDAT Substrates

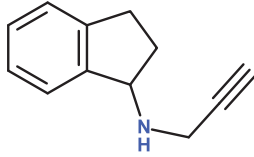
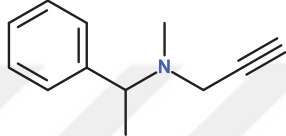
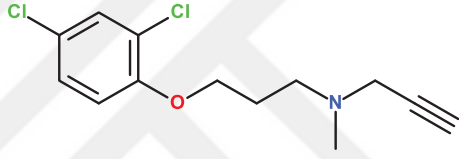
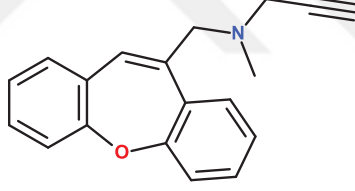
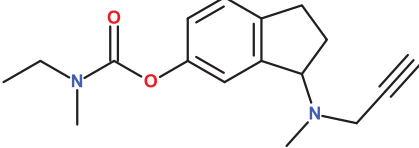
Previously, it has been noticed that compounds having propargylamine group demonstrate neuroprotective effects. Based on this observation, studies have been done in order to evaluate Structure-Activity Relation (SAR) of the propargylamine moiety and neuroprotection. (Luan et al., 2013) This neuroprotection has been confirmed both *in vitro* and *in vivo*. (Baranyi et al., 2016; Blandini, 2005; Huleatt et al., 2015; Luan et al., 2013) Using this knowledge we have designed new compounds combining the scaffold of hDAT's substrate and the MAO-B inhibitors with propargylamine group which is proven to be neuroprotective. The exact mechanism of neuroprotection of this moiety remains unknown and possible mechanism has been described previously in Chapter 2. In the **Table 4.1** chemical structures of some neuroprotective compounds are shown.

To design our compounds we have used different structures of known DAT substrates, and we attached propargylamine moiety on the amino group of the substrate. We hope that DAT-substrate part of the molecule will behave as carrier for the neuroprotective group. This way, using “The Trojan Horse” approach we will “*sneak in*” neuroprotective compound into DA neuron where it will accumulate, protecting the cell.

To evaluate our compounds, and predict their activity *in silico*, first we docked these compounds into previously determined open and closed conformation of hDAT, to check whether they could be potential substrates. Afterwards, we docked successful candidates into MAO-A and MAO-B. Docking was done in AutoDock 4.2. The X-ray structures of human MAO-A and MAO-B were downloaded from PDB (**2Z5X**, **2V5Z** respectively). (Binda et al., 2007; Son et al., 2008) Both enzymes were prepared in **BIOVIA DS 4.5**. One monomer of each protein was taken. The water molecules, ligands, and unnecessary ions were deleted, while one molecule of FAD was retained since it participates in ligand binding interactions. Energies of enzymes were then minimized using “Energy Minimize” toolkit. Minimized and cleaned enzymes were then submitted to “Prepare

Protein” protocol. Prepared 3D models of MAO-A and MAO-B were further used for docking studies.

Table 4.1 Chemical structures of neuroprotective compounds; all these neuroprotective compounds contain propargylamine moiety

Neuroprotective drugs	Chemical formula
Rasagilin	
Selegilin	
Chlorgilin	
Omigapil	
Ladostigil	

5. RESULTS AND DISCUSSION

5.1. Establishing a New hDAT 3D Model

A new homology model was established for hDAT based on its known amino acid sequence using dDAT as a template. The sequence identity and similarity between dDAT and hDAT was estimated equal to 49.6% and 69.2%, respectively (**Figure 1**). Based on the sequence 10 models were built, and the best model was selected according to the best DOPE and normalized DOPE score (-79899.35 and -1.3418, respectively). In order to get a more precise model for structure-based drug design we have extended the homology model of hDAT using molecular dynamics simulation, to optimize two conformational structures namely, open-out, inhibitor-bound and closed, substrate bound. Homology model of hDAT dipped in membrane bilayer environment, prepared for MD simulation is presented in the **Figure 5.2**.

The stability of hDAT models were evaluated by root-mean-square-deviation (RMSD) from the initial structure and residue root-mean-square-fluctuation (RMSF) values (**Figure 5.3**). RMSD values were stabilized after approximately 5000 time steps (10 ns), and were around 4 Å from the reference conformation. From residue RMSF we concluded that residues in the extracellular loops were most flexible and had most influence on RMSD changes. RMSD and RMSF values of hDAT models in 40 ns MD simulation are shown in the **Figure 5.3**.

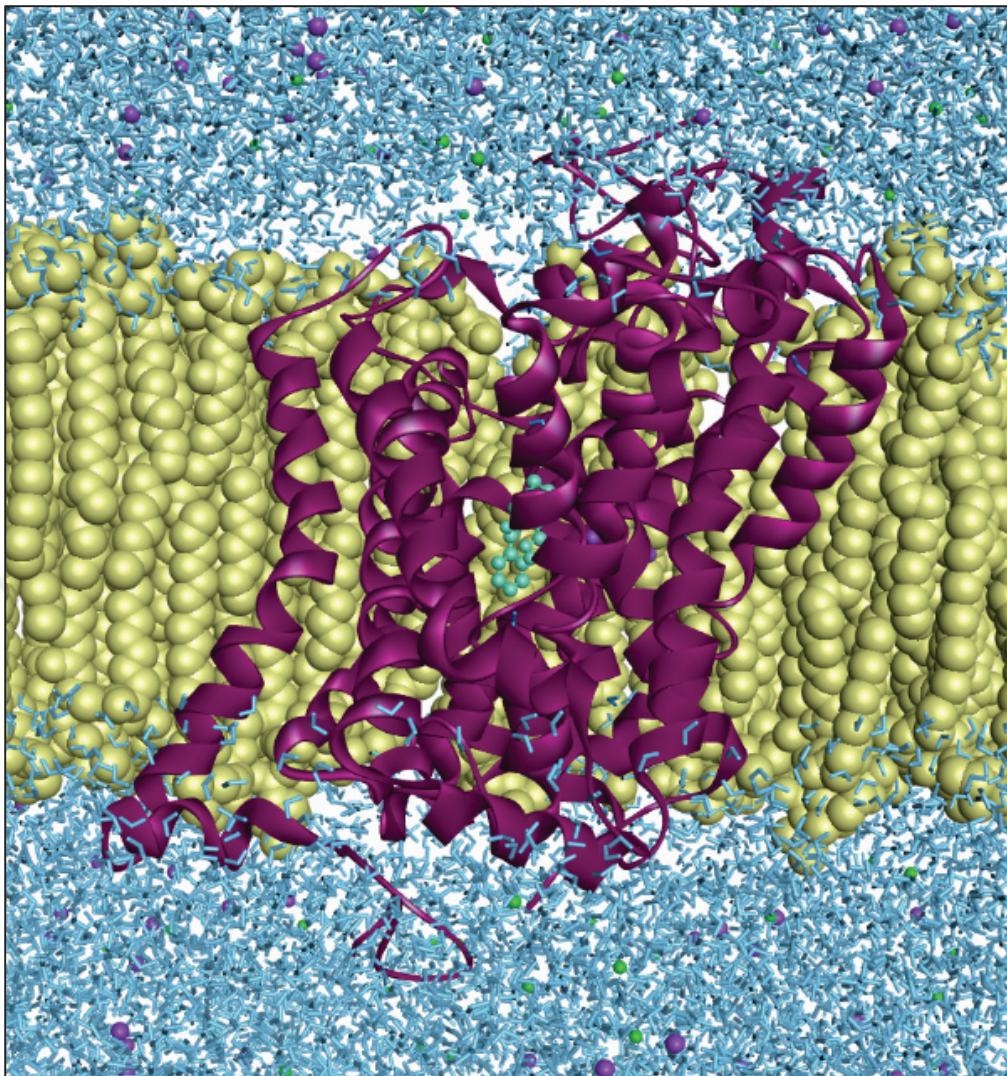


Figure 5.2 3D model of hDAT with ligand in the binding pocket imbedded in the lipid membrane prepared for the NAMD simulation.

We have noticed different behavior of the transporter when substrate is bound in contrast to empty transporter and also inhibitor bound transporter.

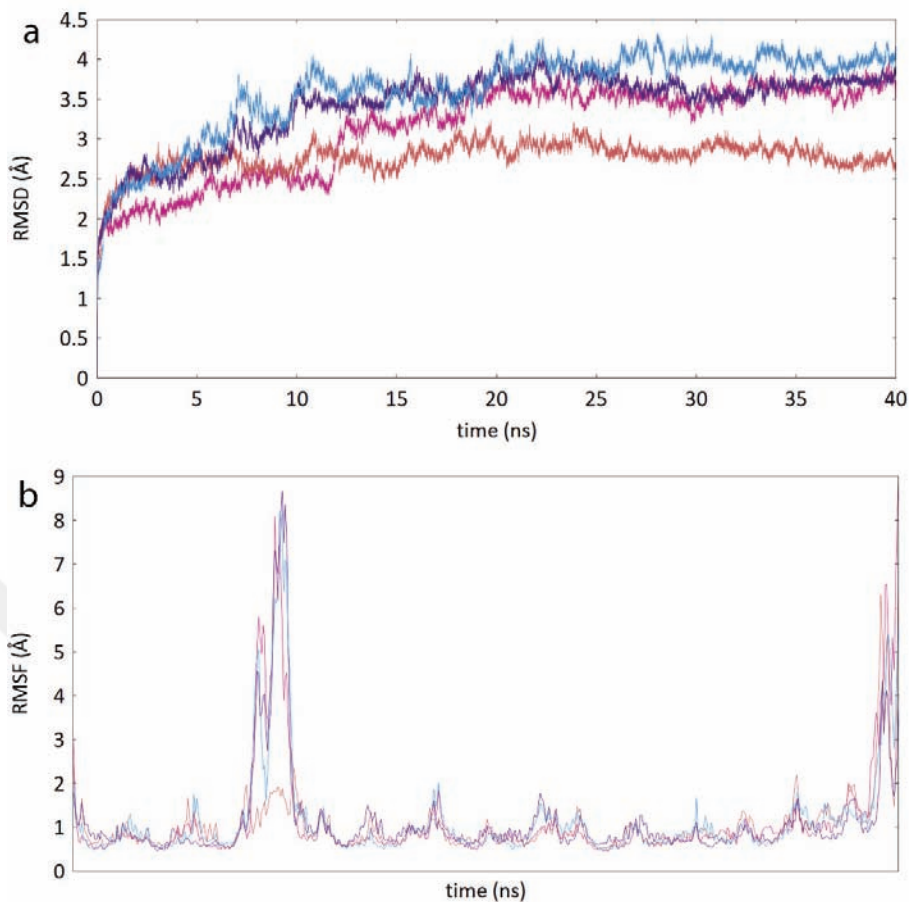


Figure 5.3 RMSD (right) and residue RMSF values of hDAT (a) empty transporter in purple, hDAT-amphetamine – blue, hDAT-cocaine - pink and hDAT-modafinil – orange complexes. The RMSD stabilized around 4 Å (for all the simulations) from the reference conformation after approximately 5000 time steps (10 ns). From the RMSF measurement (b) we reasonably observed that the most flexible residues were located in the extracellular loops.

hDAT - Substrate complex: After stabilization of RMSD in the DAT-substrate complex, we noticed closing of the residues of the binding pocket (**Figure 5.4**). Specifically, residue Phe320 flips and closes the gate above the substrate and flipping of the Phe320 residue causes tilting of the TM-6 domain. We also observed dehydration of the binding pocket due to hydrophobic interactions of Phe155, Tyr156, Phe320 and Phe326.

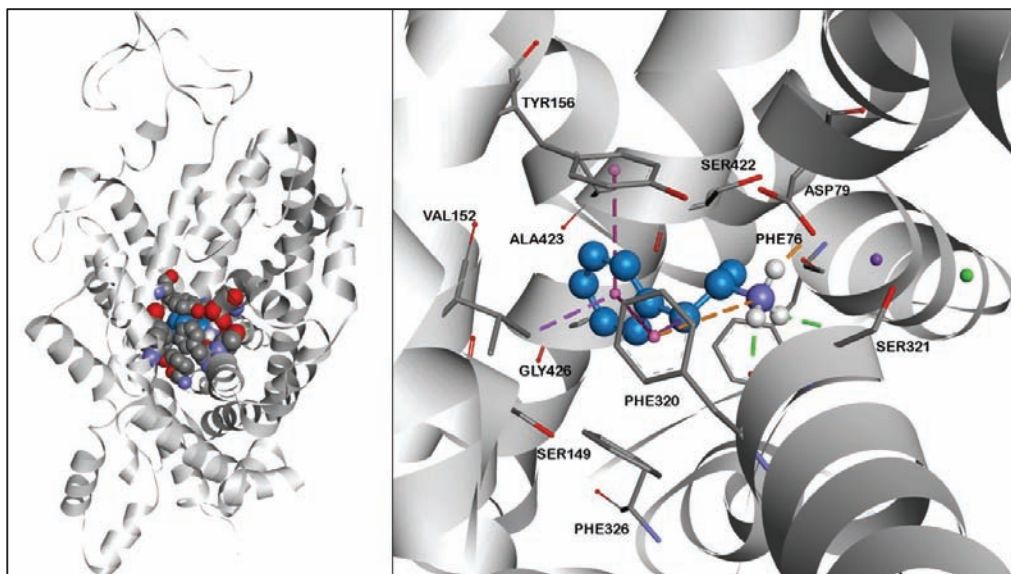


Figure 5.4 hDAT-amphetamine complex; Binding of amphetamine causes Phe320 to close the binding pocket and tilt trans-membrane domain 6 in the hDAT. RMSD and residue RMSF values of hDAT-amphetamine transporter in 40 ns simulation; Interactions of amphetamine and hDAT in the binding pocket; upper and side view of hDAT in closed conformation with bound amphetamine.

hDAT - Inhibitor complex: The typical and atypical inhibitors - cocaine and modafinil, respectively, displayed similar molecular dynamics behavior with the hDAT. Both inhibitors block the transporter in the outward-open conformation (**Figures 5.5. and 5.6**). For visualization of interactions we used pictures generated in BIOVIA Discovery Studio 2016.

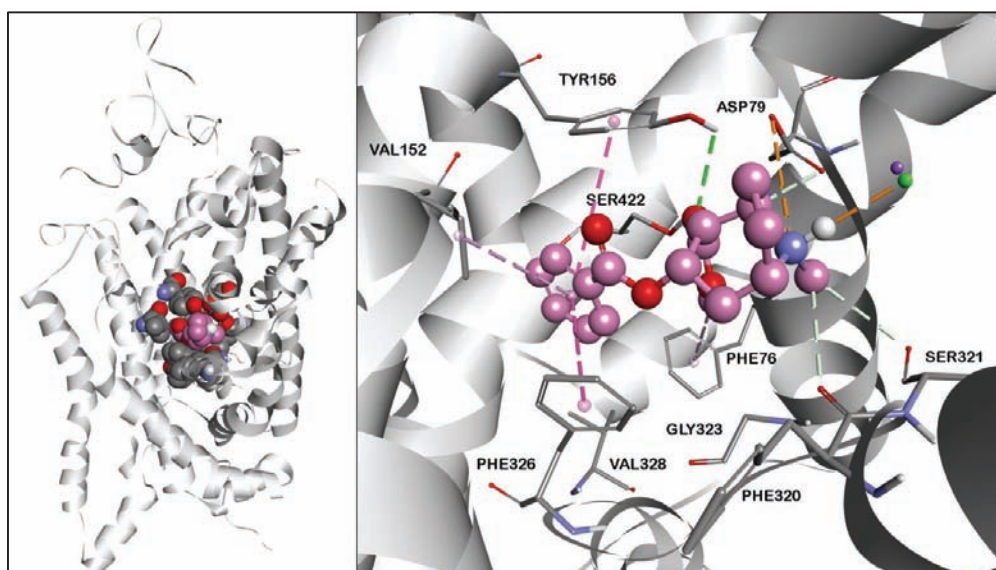


Figure 5.5 hDAT-cocaine complex; Cocaine maintains an outward-open conformation in the hDAT. Interactions of cocaine and hDAT in the binding pocket are shown; upper and side view of hDAT in outward-open conformation with bound cocaine.

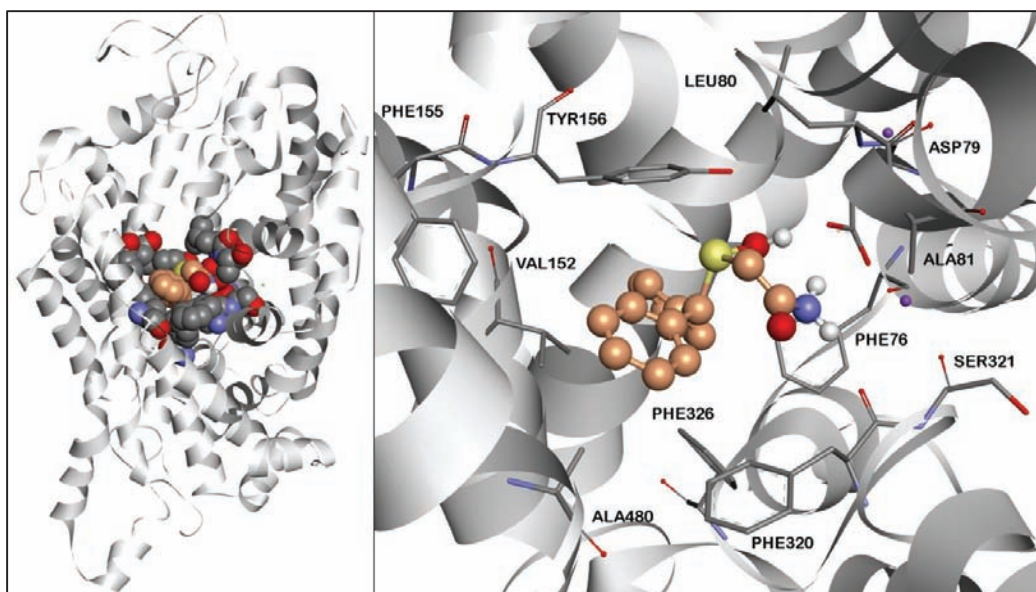


Figure 5.6 hDAT-modafinil complex; Modafinil maintains an outward-open conformation in the hDAT. Interactions of modafinil and hDAT in the binding pocket are shown; upper and side view of hDAT in outward-open conformation with bound modafinil.

Comparison of hDAT-ligand conformations: The main differences were a flipping of the Phe320 amino acid side chain, tilting of TM6 (**Figure 5.7**), a decreased distance between Phe320 and Tyr156 and a decreasing of solvent accessible surface area. We measured the distance between Phe320 and Tyr156 in VMD. A comparison of the substrate bound structure with the inhibitor bound structure and empty DAT structure shows that the distance between Phe320 and Tyr156 (aminoacids that are closing pocket) decreases. For amphetamine-hDAT complex the distance is 5 Å, after 10 ns, which is maintained, while in all other cases it is around 13 Å (**Figure 5.8**). Since the distance in the empty transporter staying at 13 Å, we conclude that ligand binding is necessary to cause a conformational change. The solvent Accessible Surface Area (SASA) of amino acids in the binding pocket (Phe76, Val78 Asp79, Ser142, Val152, Gly153, Tyr156, Phe320, Ser321, Phe326, Val328 and Ser422) was also measured in VMD with a probe radius of 1.4 Å (**Figure 5.8**). The results show lower SASA of residues in the binding pocket when substrate is bound to the hDAT.

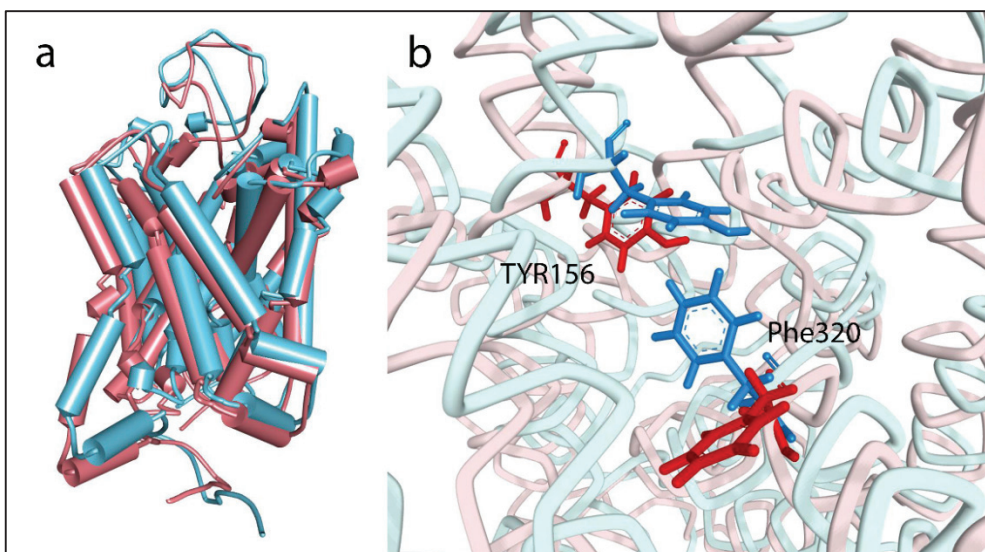


Figure 5.7 Superposition of closed (blue) and opened (pink) hDAT conformations: Residues Tyr156 and Phe320 are closing the gate in the closed hDAT conformation.

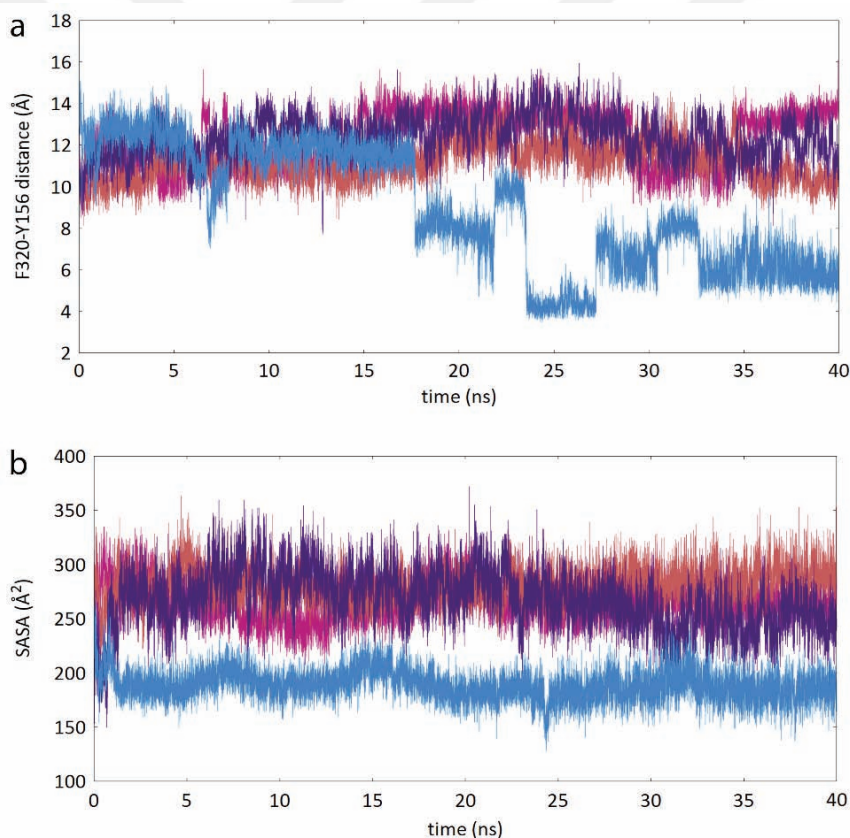


Figure 5.8 Comparison of hDAT-ligand conformations: (a) Comparison of F320 and Y156 distance in hDAT-amphetamine (blue), hDAT-cocaine (pink), hDAT-modafinil (orange) complexes and empty hDAT (purple) transporter. Amphetamine decreases the F320 to Y156 distance when bound to hDAT. (b) Comparison of SASA values shows that the hDAT- amphetamine complex (blue) displaces H₂O from the binding pocket whereas the hDAT- cocaine (pink), hDAT-modafinil (orange) complexes and empty hDAT (purple) maintain H₂O in the binding pocket.

Since the empty transporter acts similarly to the inhibitor bound transporter these results may suggest that binding of substrate causes the conformational change from an outward-open state to outward-closed state.

5.2. Searching For The Best Conformation

From previous findings we speculated that if compound is a substrate it has a higher affinity for the closed conformation, while if a compound is an inhibitor access into the closed conformation is prohibited. After obtaining the molecular dynamics results, we collected 10000 frames from last 10 ns of simulation. 100 frames were randomly chosen by BIOVIA DS 2016. Ten frames out of 100 were chosen manually based on the distance between Phe320 and Tyr156. Known substrates and inhibitors were docked in these conformations, to determine which frame from each simulation differentiates the best between inhibitors and substrates e.g. gives the best representation of open and closed conformation.

Monitoring of docking into these two conformations can differentiate whether the compound is an inhibitor or a substrate (**Table 5.1 and 5.2**). Tables above show that inhibitors display strong affinity as evidenced by their docking scores when docked into the open conformation, while lower affinity values or no values when docked to the closed conformation. Substrates show higher affinity for closed conformation, when docked. Values for the binding of substrates are not as high as inhibitors, even in closed conformation. This suggests that inhibitors are binding more strongly and with more interactions than substrates, which is expected since substrate needs to be released from the pocket. The AutoDock program gives the most relevant results, so it will be our tool of choice in further work with these conformations. Based on docking of the known compounds into these two conformations may classify the compounds as a substrate or an inhibitor. Namely, substrates show binding energies at around -7 kcal/mol (or more positive) for both hDAT conformations. The inhibitors show around -8 kcal/mol (or more negative) for open conformation and much less, or no binding for closed conformation (**APPENDIX A**).

Table 5.1 Known substrates docked in open (blocked with cocaine and modafinil) and closed (closure induced with amphetamine) conformations of DA.

SUBSTRATES									
compounds	hDAT-open1 (cocaine blocked)			hDAT-open2 (modafinil blocked)			hDAT-closed (amphetamine)		
	Auto Dock	GOLD	FLAP	Auto Dock	GOL D	FLAP	Auto Dock	GOL D	FLAP
	ΔG kcal/mol	Chem PLP	S score	ΔG kcal/mol	Chem PLP	S score	ΔG kcal/mol	chemP LP	S score
3-fluoroamphetamine	-4.95	53.22	1.544	-5.21	40.38	1.524	-6.17	56.22	1.572
3-methylamphetamine	-5.41	56.38	1.577	-5.56	44.96	1.527	-6.61	56.02	1.002
3-TFMAP	-5.56	51.56	1.199	-5.3	48.62	1.315	-6.46	32.91	1.585
4-fluorotryptamine	-5.48	57.13	1.544	-5.37	45.31	1.392	-6.45	52.96	1.249
4-methylaminorex	-6.09	51.05	1.38	-5.7	47.68	1.582	-6.13	49.84	1.032
5-fluoro-a-ethyltryptamine	-6.09	56.75	1.486	-6.36	65.64	1.392	-7.09	56.37	1.545
5-fluoro-a-methyltryptamine	-6.03	59.93	1.549	-6.01	62.4	1.356	-7.06	52.19	1.543
6-OH-dopamin	-4.76	49.15	1.481	-5.72	41.35	1.582	-5.58	43.74	1.535
6-APB	-5.96	59.41	1.241	-6.31	46.08	1.21	-7.08	54.16	1.258
amphetamine	-4.98	49.2	1.561	-5.22	40.57	1.515	-6.11	51.76	1.573
ASP+	-5.38	60.1		-6.43	51.82	1.278	-4	21.81	/
4-benzpiperidine	-5.79	56.6	1.554	-6.61	59.73	1.452	-7.42	54.9	1.52
cathine	-5.01	50.53	1.278	-5.12	41.73	1.488	-6.13	49.2	1.272
cathinon	-5.18	48.86	1.333	-5.12	41.35	1.357	-6.3	50.34	1.287
DCP	-5.54	57.66	1.556	-5.95	43.9	1.531	-6.86	53.16	1.539
dextroamphetamine	-5	49.25	1.561	-5.21	40.62	1.529	-6.12	51.75	1.573
dopamin	-5.31	56.33	1.498	-4.61	38.88	1.302	-6.22	50.51	1.537
ephedrine	-4.89	47.47	1.318	-4.76	46.75	1.431	-6.25	49.05	1.251
fenflouramine	-5.18	55.82	1.475	-5.68	52.52	1.467	-6.59	39.73	1.426
FN102	-5.19	58.29	1.344	-6.41	50.72	1.344	-6.27	23.65	0.788
metcathinone	-6.76	49.97	1.195	-5.19	45.19	1.367	-6.41	49.99	1.322
MDA	-5.67	53.62	1.221	-5.9	46.87	1.141	-6.76	47.02	1.282
MDMFA	-5.43	50.25	1.203	-5.99	51.49	1.154	-6.76	43.35	1.187
mefendrone	-5.43	54.58	1.226	-5.3	46.2	1.481	-6.86	48.12	1.252
m-metoxo amphetamine	-5.25	53.97	1.243	-5.61	45.81	1.225	-6.41	51.02	1.246
metamphetamine	-4.82	49.72	1.561	-5.19	45.31	1.52	-6.24	51.83	1.516
methylone	-5.37	55.82	1.396	-5.58	47.59	1.359	-6.87	40.83	1.42
MNAP	-6.27	65.11	1.519	-7.26	44.85	1.475	-7.58	52.69	1.412
MPTP	-4.9	59.99	1.465	-5.72	42.7	1.412	-6.28	45.09	1.418
noradrenalin	-4.79	56.05	1.447	-4.71	40.68	1.454	-5.47	48.79	1.526
norfenfloramine	-5.26	53.9	1.492	-5.48	44.44	1.267	-6.25	48.91	1.481
pemoline	-5.18	50.51	1.168	-5.38	54.88		-5.94	49.95	1.26
tyramine	-4.7	52.18	1.546	-4.71	37.85	1.296	-5.68	45.77	1.599

Table 5.2 Known inhibitors docked in open (blocked with cocaine and modafinil) and closed (closure induced with amphetamine) conformations of DAT

INHIBITORS									
compounds	Auto Dock	GOLD	FLAP	Auto Dock	GOL D	FLAP	Auto Dock	GOLD	FLA P
	ΔG kcal/mol	Chem PLP	S-score	ΔG kcal/mol	Chem PLP	S-score	ΔG kcal/mol	Chem PLP	S-scoe
adrafinil	-7.35	71.87	1.287	-7.72	70.59	1.23	-4.11	16.93	/
altroan	-8.14	55.07	1.033	-8.33	66.02	1.064	10.27	-31.08	/
amineptine	-7.43	71.8	1.113	-6.58	79.01	0.981	13.71	2.37	/
armodafinil	-7.47	63.88	1.246	-8.23	75.61	1.232	-5.87	28.63	/
benocyclidine	-9.22	76.3	0.908	-9.46	70.45	0.99	4.14	-16.02	/
benzotropine	-8.09	71.27	1.13	-8.61	69.97	1.022	7.65	-18.16	/
benzpetamine	-7.09	67.84	1.426	-7.39	73.27	1.4	-5.64	36.52	0.733
bupropion	-6.89	51.38	1.19	-6.94	63.19	1.367	-6.66	48.24	0.666
chlorpheniramine	-7	66.69	0.927	-7.69	73.71	1.243	0.27	22.82	/
chlorprocaine	-5.92	61.29	1.204	-6.08	59.67	1.232	-5	36.96	0.679
citalopram	-8.52	70.54	0.984	-8.67	69.1	0.798	15.69	-26.91	/
cocain	-7.74	59.58	1.231	-8.31	65.37	1.01	-2.39	-7.34	/
DBL583	-5.37	112.82	0.869	-8.19	100.8	1.023	448	-50.26	/
duloxetine	-8.36	74.42	1.273	-8.69	79.02	1.208	-3.41	46.55	/
escitalopram	-8.1	66.69	1.193	-7.42	60.33	0.749	5.74	-8.23	/
fenkafamin	-6.75	61.98	1.551	-7.18	61.24	1.545	-6.66	39.36	1.421
GBR-13069	-6.33	95.62	0.982	-9.85	93.73	1.101	43.77	23.02	/
GBR-13098	-6.42	97.4	1.188	-9.47	95.56	0.892	29.29	22.76	/
GBR-12783	-9.24	94.02	1.232	-10.53	93.61	0.93	69.3	28.56	/
GYKI-52895	-7.54	60.22	1.243	-8.27	50.47	1.22	42.04	-34.12	/
mazindol	-6.85	55.5	1.287	-8.06	63.61	1.22	-0.63	15.59	/
medifoxamine	-6.43	64.58	1.387	-7	70.06	1.14	-4.96	28.16	/
metaphit	-8.63	69.29	0.98	-8.91	69.9	1.10	3.76	-9.96	/
methylphenidat	-6.28	55.68	1.367	-6.64	63.94	1.33	-6.58	26.35	0.682
modafinil	-7.23	66.44	1.278	-7.87	67.71	1.27	-5.15	24.23	/
nefazodie	-8.15	92.47	1.211	-9.46	97.74	1.15	98.93	34.38	/
prokain	-5.76	58.25	1.258	-5.74	62.89	1.35	-5.11	43.43	/
rimcazol	-8.29	71.56	0.953	-10.09	78.41	1.13	-2.11	-2.3	/
RTI55	-7.98	51.84	0.924	-8.31	67.85	1.04	7.74	3.94	/
RTI113	-8.87	73.08	0.973	-9.38	60.84	1.01	8.65	-10.11	/
RTI229	-9.51	64.71	0.764	-9.52	59.05	1.08	5	-43.59	/
sertalin	-8.81	62.99	1.395	-9.19	66.89	1.213	7.99	11.46	/
sibutramin	-7.3	66.14	1.316	-7.61	70.89	1.383	-0.87	14.27	/
trimipramin	-7.75	65.87	1.123	-8.2	60.21	1.383	3.3	-6.11	/
vanorexine	-6.88	93.14	1.162	-9.77	97.94	0.746	89	-41.22	/
venafaxin	-7.02	63.73	1.259	-7.34	60.9	1.228	3.17	-5.38	/
WIN-25978	-7.4	70.16	1.242	-7.06	83.5	1.353	26.94	21.36	/

All proteins in nature are flexible. Since we were using rigid-protein docking, naturally none of the conformations displayed perfect binding for all the substrates, while excluding all the inhibitors and vice versa (APPENDIX A). Example is shown in **Table 5.3**. To take into consideration more conformations that protein is taking during the transport cycle we have decided to use flexible structure based virtual screening.

Table 5.3 Known hDAT substrates docked in different snap-shots of the closed-out conformation. Best scores are marked in blue.

compounds	hDAT closed 1	hDAT closed 3	hDAT closed 5	hDAT closed 6	hDAT closed 7
	ΔG kcal/mol	ΔG kcal/mol	ΔG kcal/mol	ΔG kcal/mol	ΔG kcal/mol
6-OH-dopamin	-5.87	-5.72	-5.76	-6.01	-6.07
amphetamine	-6.26	-6.5	-6.34	-6.16	-6.34
cathinon	-6.53	-6.7	-6.48	-6.28	-6.58
dopamin	-6	-6.23	-5.6	-5.94	-5.96
ephedrine	-6.32	-6.67	-6.43	-6.33	-6.59
fenflouramine	-6.78	-6.98	-6.94	-5.91	-6.63
FN102	5.54	-6.99	-5.9	-6.93	-6.66
metcathinone	-6.56	-6.45	-6.58	-6.35	-6.73
MDA	-7.04	-7.22	-6.9	-6.79	-7.14
metamphetamine	-6.37	-6.49	-6.44	-6.3	-6.42
MNAP	-8.01	-8.56	-7.79	-7.33	-7.73
MPTP	-6.39	-6.15	-5.42	-6.15	-5.52
octopamine	-5.94	-6.22	-5.62	-5.77	-6

5.3. Identification of Promising hDAT Candidates

To identify new compounds that are most likely taken up by hDAT as substrates we combined three different approaches in a pipeline, consisting of flexible LDA-based VS, pharmacophore-VS and docking simulations.

Based on the belief that the inclusion of flexibility in VS generally provides more reliable results (Moroy et al., 2015; Sinko et al., 2011; Spyraakis and Cavasotto, 2015; Totrov and

Abagyan, 2008), we performed a first flexible VS using a recently published methodology, based on the integrated MD-FLAP approach recently developed (Spyrakis JCIM 2015). The transporter flexibility was investigated by means of MD simulation performed on the amphetamine-hDAT complex (closed conformation). Then, for all the possible binding site conformations, the Molecular Interaction Fields were calculated with FLAP²³ and clustered through principal component analysis. Differently from other clustering methodologies based on RMSD and atomic position, this innovative approach allows the identification of the most representative and variable binding site conformations, in terms of geometrical, chemical and energetic properties. In the present case ten different conformations were extracted from the trajectory and used with the initial model as possible reference structure for structure-based virtual screening.

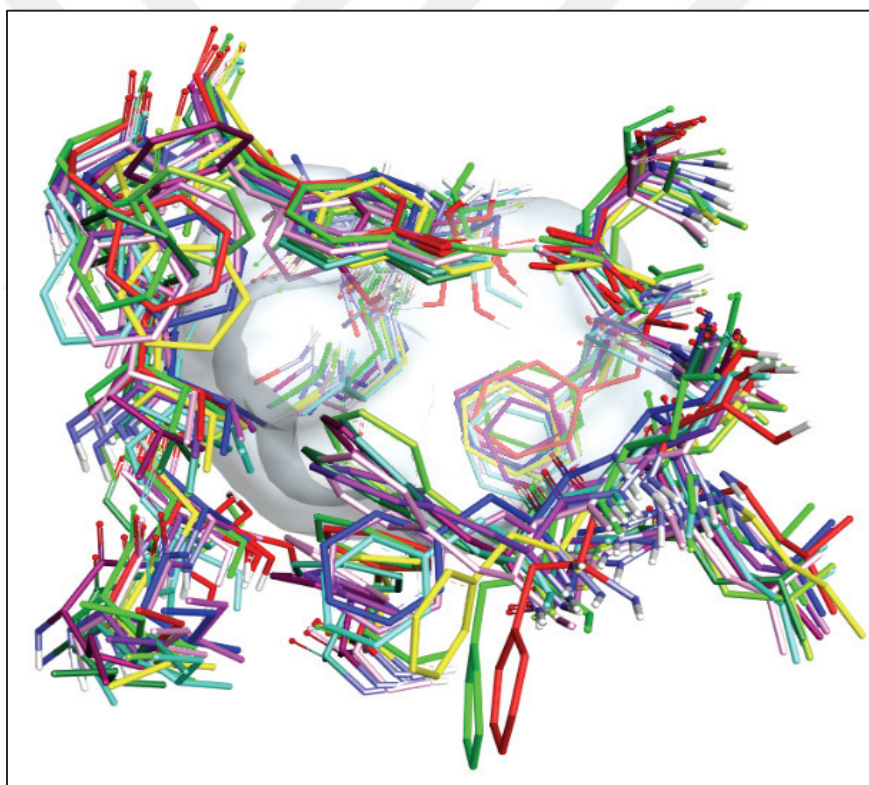


Figure 5.9 SBVS model; Flexible binding pocket of closed hDAT used to create a SBVS model.

The Linear Discriminant Analysis-based protocol implemented in FLAP was applied to automatically choose the combination of conformational templates and FLAP scores were better able to discriminate between active compounds and decoys in a training set (see Material and Methods for further details). Previous analyses reported a 3 template over 3

FLAP-score combination as the one able to provide the best overall and early enrichment. (Spyrakakis et al., 2015) Clearly, the number of templates and FLAP-scores strictly depend on the nature of the target and its intrinsic flexibility. In this specific case a model combining one MD-generated template and three different FLAP-scores provided the best enrichment when used to screen the test set. The enrichment increase obtained with respect to a single receptor conformation VS performed with the starting model was particularly relevant. The overall AUC (Area Under the Curve) moved from 0.57 to 0.91 and the partial ROC enrichment at 1% and 5% moved from 0.04 and 0.10 to 0.14 and 0.71, respectively. The model was thus used to screen the Specs database (part of the ZINC database) looking for new potential hDAT substrates. The model was thus used to screen the Specs database (part of the ZINC database) looking for new potential hDAT substrates. The best scored thousand compounds, according to the LDA-R score, were selected and submitted to the following pharmacophore-based VS.

Out of 9 pharmacophore models that we have created, the best model was selected based on score (score 1.048) and performance. Our pharmacophore model, based on chemical characteristics of substrates, was able to distinguish between substrates and inhibitors, as well as decoys. GlobSum probe was showing good enrichment, both in differentiating between substrates and decoys ($AUC_{(100\%)} = 0.92$; $AUC_{5\%} = 0.66$); substrates and inhibitors ($AUC_{(100\%)} = 0.96$; $AUC_{5\%} = 0.95$); and between both substrates against decoys and inhibitors ($AUC_{(100\%)} = 0.92$; $AUC_{5\%} = 0.64$) which is why GlobSum was chosen to rank the compounds.

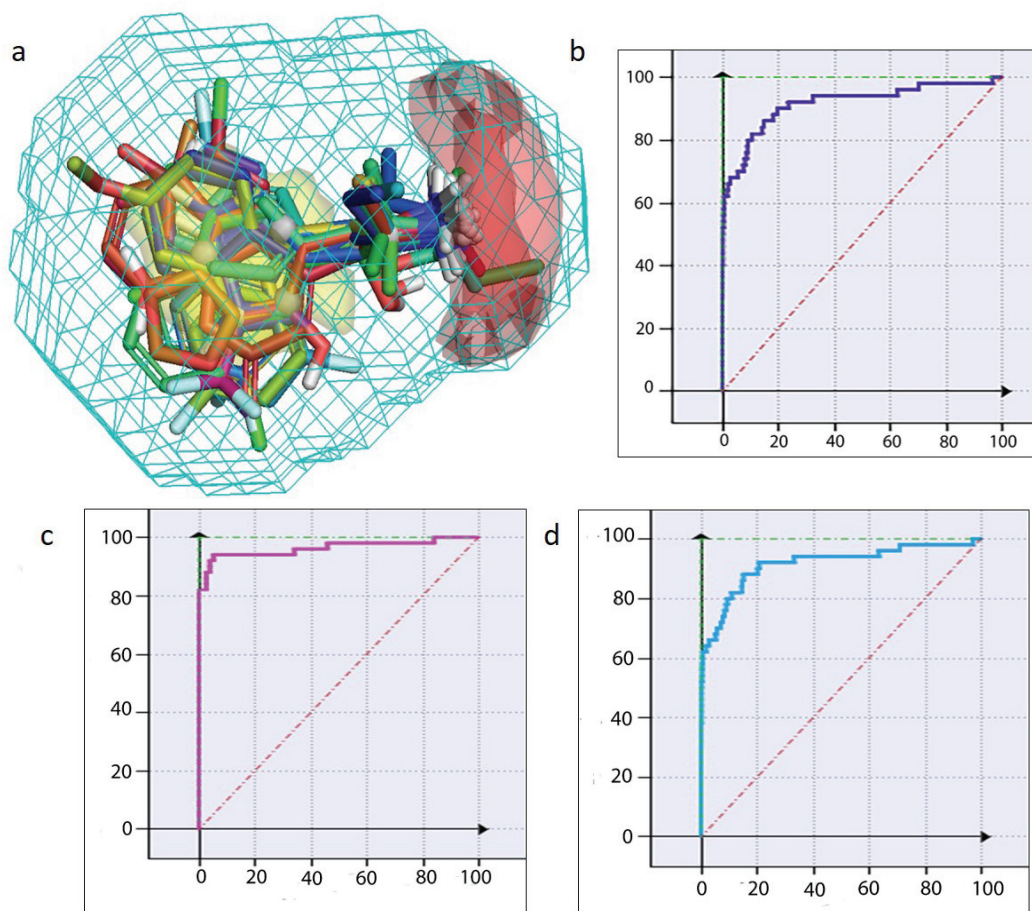
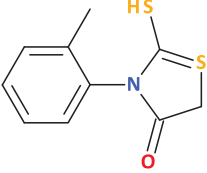
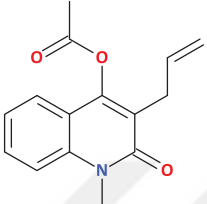
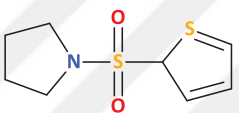
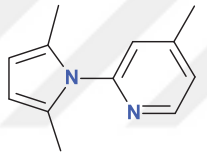
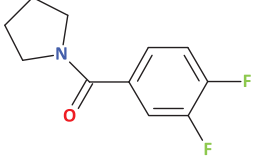
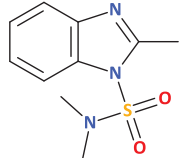
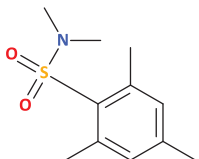
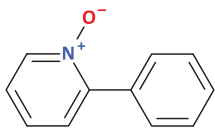
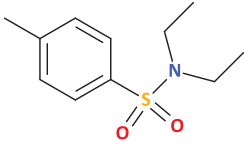
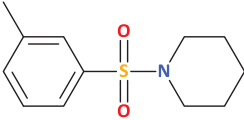
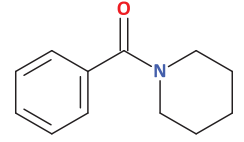
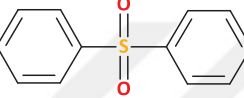
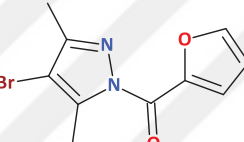
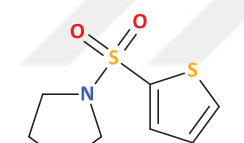
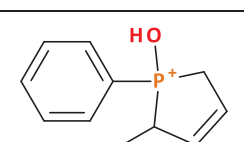
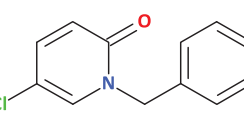
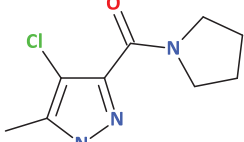


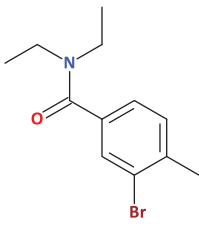
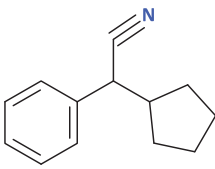
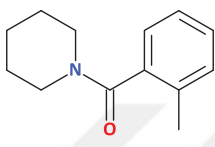
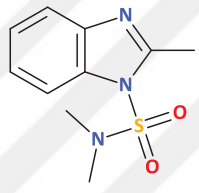
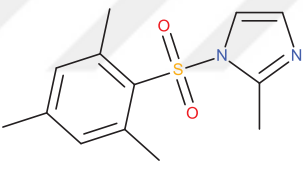
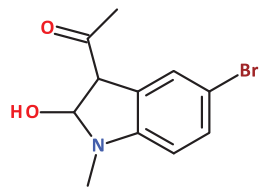
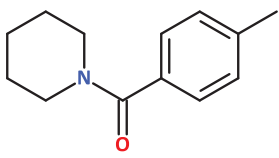
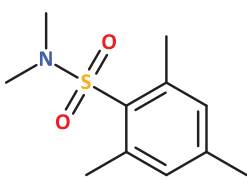
Figure 5.10 LBVS model: Pharmacophore model of hDAT substrates (a). Enrichment plot of GlobSum after LBVS, where x-axis represents % of false positives and y axis represents % of true positives, shows how the pharmacophore model is differentiating between, (b) substrates and non-substrates (c) substrates vs. inhibitors, and (d) substrates vs. decoys

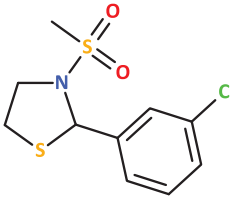
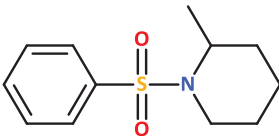
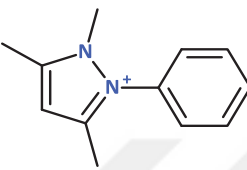
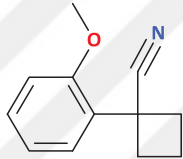
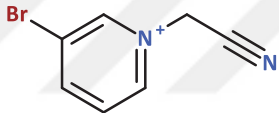
The first 150 candidates (shown in **APPENDIX B**), according to GlobSum, were docked into the open and closed hDAT conformation. The results are shown in **Table 5.4**. We have assumed that the ones that are showing better scores for hDAT-closed are supposed to be substrates, while the ones who give better scores for hDAT-open are most probably inhibitors. According to this assumption we purchased 6 commercially available compounds from Specs. These 6 compounds are underlined in **Table 5.4** and the interactions of four compounds with closed hDAT are shown in the **Figure 5.11**. These compounds were tested *in vitro* in order to evaluate our model.

Table 5.4. Docking results of some of the possible substrates obtained from VS docked in closed and open conformations

COMPOUNDS		hDAT closed	hDAT open
		ΔG (kcal/mol)	ΔG (kcal/mol)
AA_504_32171020		-6.89	-5.44
AB_337_13036340		-6.56	-6.14
AG_690_13705992		-6.61	-5.4
AM_879_11741391		-6.58	-5.38
AO_854_12910145		-6.55	-5.67
AP_124_41027793		-6.72	-6.16
AQ_390_11633955		-6.59	-5.82
AC_907_25005104		-6.82	-5.34

AE_641_00674038		-6.38	-5
<u>AG_205_05879010</u>		-7.15	-6.22
AC_907_25014313		-7.11	-5.77
AE_562_13465017		-7.19	-5.9
AG_205_12367041		-6.68	-6.4
AG_690_13705992		-6.59	-5.4
AH_034_11963070		-7.01	-5.54
AI_204_31701041		-6.56	-5.59
AK_968_40941130		-6.64	-5.59

AN_329_41006735		-6.66	-6.09
<u>AO_080_43441536</u>		-7.08	-5.76
<u>AO_854_40003386</u>		-6.9	-5.5
AP_124_41027793		-6.71	-5.49
<u>AP_263_10166001</u>		-6.97	-6.26
AP_355_43470043		-6.6	-5.69
AQ_390_09693049		-6.81	-5.83
AQ_390_11633955		-6.59	-5.55

AQ_432_41436196		-6.56	-6.25
<u>AP_263_40017925</u>		-7.59	-6.08
AR_360_40250960		-6.62	-5.28
AS_871_11336720		-6.62	-5.32
AT_051_43421379		-6.58	-5.53

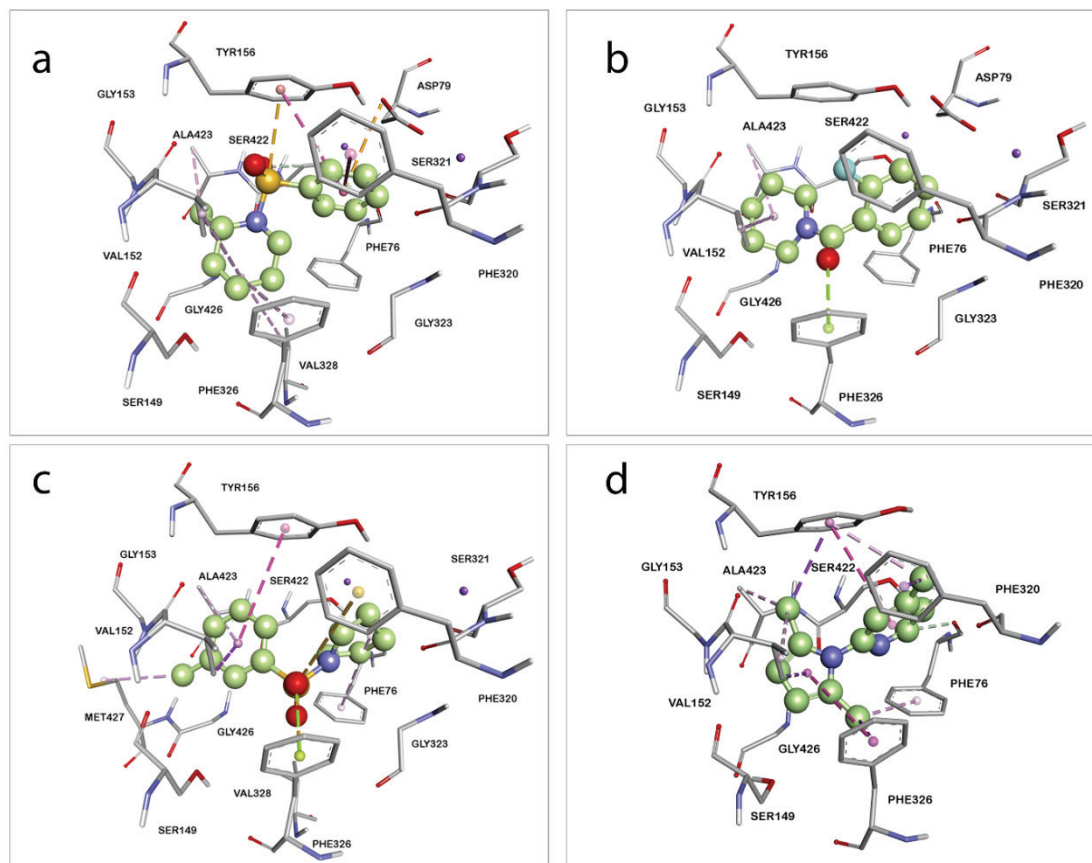


Figure 5.11 Predicted interactions of compounds AG_205_05879010 (a), AO_854_40003386 (b), AP_263_10166001 (c) and AM_879_11741391 (d) in binding pocket of hDAT in closed conformation.

In order to clarify, in further text we will refer to these compounds as: compound 1 (AG_205_05879010), compound 2 (AO_854_40003386), compound 3 (AM_879_11741391), compound 4 (AP_263_10166001), compound 5 (AO_080_43441536), and compound 6 (AM_879_11741391).

5.4. Evaluation of The Model Using Fluorescent *In Vitro* Assays

In order to investigate whether the above mention substrates showed an alteration in transporter function, we measured ASP+ (4-(4-(dimethylamino)-styryl)-N-methylpyridinium) uptake in human embryonic kidney cells expressing human dopamine transporter (HEK-hDAT). HEK-hDAT (**Figure 5.12**) cells were previously cultured in our collaborating laboratory (Hector Institute for Translational Brain Research, Central

Institute of Mental Health, Medical Faculty Mannheim, Heidelberg University, Germany) and where we conducted the *in vitro* experiments.

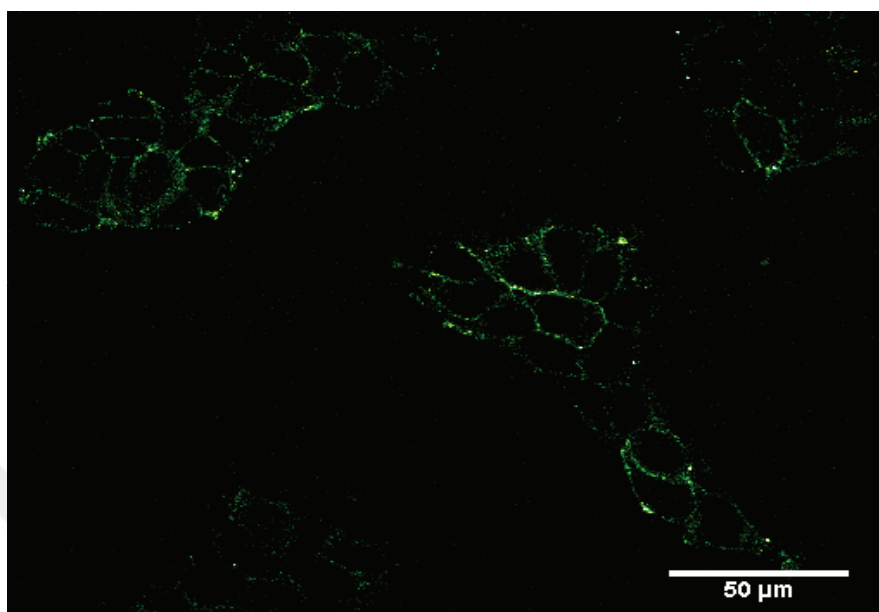


Figure 5.12 HEK-hDAT cells with expressed hDAT: hDAT (green) stained by fluorescent immunoassay, these cells were used for our *in vitro* assays.

Initially we have tested six compounds in ASP+ live cell imaging experiments to quantify to which extend they influence ASP+ uptake in human embryonic kidney cells expressing the hDAT (HEK-hDAT) (**Figure 5.13** and **APPENDIX C**). For this experiment we have chosen to apply 30μM of each compound, which is 3 times the concentration required to inhibit ASP+ uptake by the DAT substrates d-amphetamine and dopamine. (Zapata et al., 2007) This experiment showed that compounds **1 - 3** had the strongest effect on ASP+ uptake by HEK-hDAT, which was significantly diminished to approximately 40% for compound **1**, 60% for compound **2** and compound **3** (all compounds $p < 0.001$ vs control intensity). Compound **4** and **5** showed a less significant reduction compared to controls ($p = 0.0037$ for compound **4**, and $p = 0.0024$ for compound **5**). With regard to compound **6** we were not able to determine an alteration of ASP+ uptake in HEK-hDAT. Since we have detected weak fluorescence intensities in the absence of ASP+ (data not shown), we have incubated compound **6** in dopaminergic neurons derived from mouse embryonic stem cells. (Martí et al., 2017)

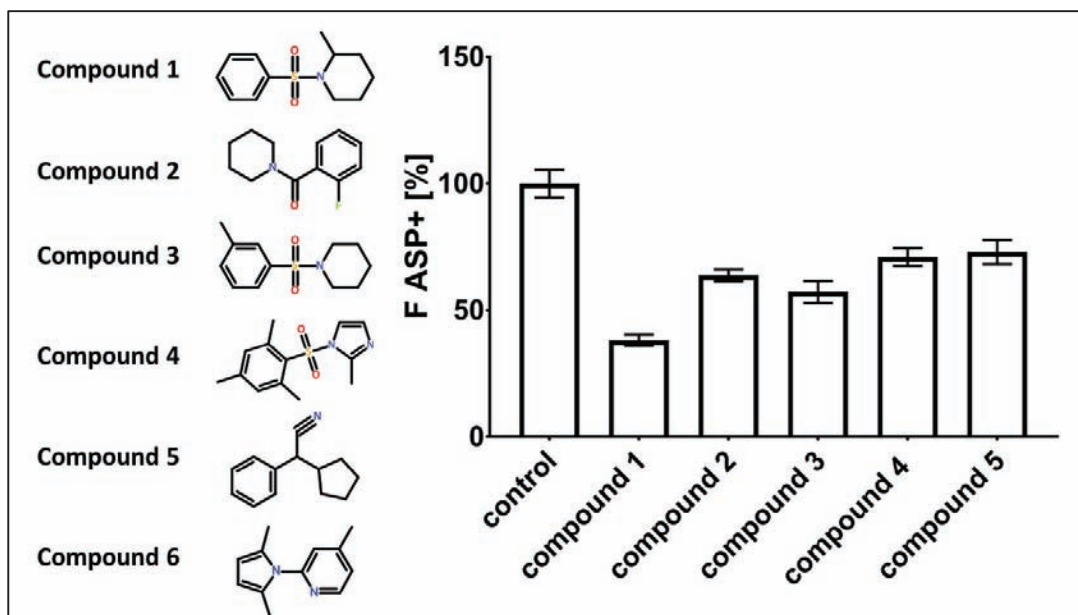


Figure 5.13 *In vitro* result, (a) HEK-hDAT were incubated for 10 min with 30 μ M of each compound prior addition of ASP+. Compounds 1 – 3 showed a significantly stronger effect on ASP+ uptake (***, $p < 0.001$) compared to compound 4 and 5. An effect of compound 6 could not be determined (n.d.) since the compound proved to be fluorescent when microscope settings for acquiring ASP+ images were applied.

ES mice cells were incubated with the compound 6. **Figure 5.14** shows exemplary live cell images of compound 6-labelled dopaminergic neurons, in which the compound predominantly stained globular structures on the soma and along neurites. Compound 6 fluorescence was found in globular, roundish as well as elongated structures in the soma and neurites, yet to be identified.

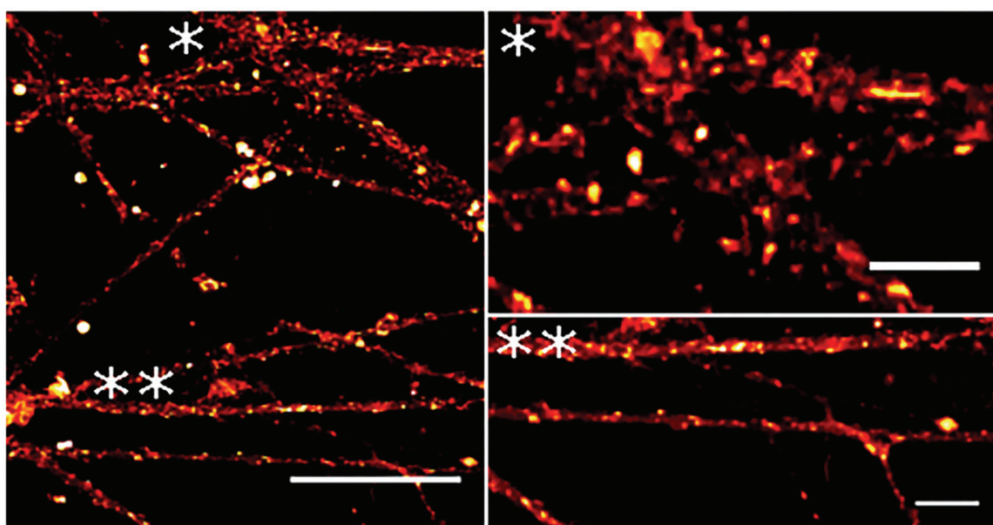


Figure 5.14 Exemplary images of compound 6 fluorescence in ES cell-derived dopaminergic neurons. Scale bar: 50 μ M. * shows the enlarged soma of a neuron, scale bar: 15 μ m. ** shows enlarged neurites, scale bar: 15 μ m.

To further characterize compound **1** – **3**, HEK-hDAT cells were incubated with each compound (0 μ M-30 μ M) for 10 min prior addition of 10 μ M ASP+ to the imaging chamber. As shown in **Figure 5.15**, the presence of compound **1** significantly dose-dependently diminished ASP+ uptake. A decreased ASP+ fluorescence to 50% \pm 2.67 of control values (SEM given) was measured at for 3 μ M compound **1**, and was maintained for higher concentrations (10 μ M: 41% \pm 2.42; 30 μ M: 38% \pm 2.25). In presence of compound **2**, already 1 μ M was enough to significantly diminish ASP+ fluorescence substrate (**Figure 5.15b**). At 1 μ M, ASP+ fluorescence decreased to 60% \pm 2.44 (SEM given) compared to control intensities. This fluorescence intensity remained alike when using higher concentrations of compound **2** (3 μ M: 56% \pm 2.48; 10 μ M: 55% \pm 2.09; 30 μ M: 64% \pm 2.39). Finally, incubation of HEK-hDAT with compound **3** also revealed a significant decrease of ASP+ uptake with increasing concentrations of the compound (**Figure 5.15c**). A significant reduction of ASP+ fluorescence started at 3 μ M (76 \pm 3.34; SEM given) and slightly increased at higher concentration with 30 μ M showing the strongest ASP+ uptake alteration compared to control conditions (10 μ M: 77 \pm 4.09; 30 μ M 57% \pm 4.35).

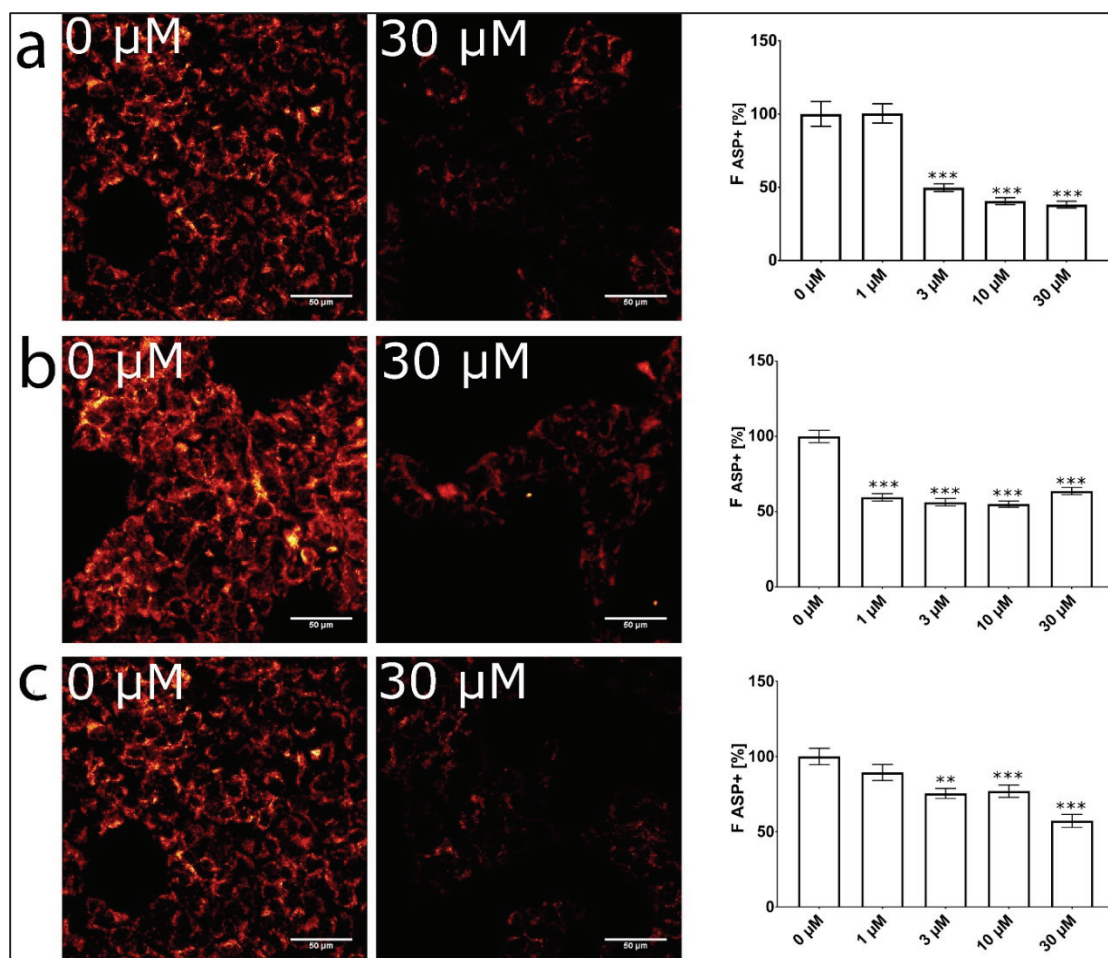


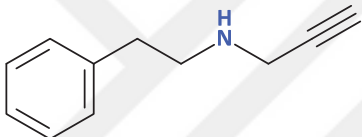
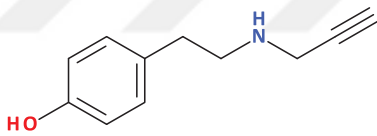
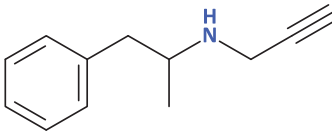
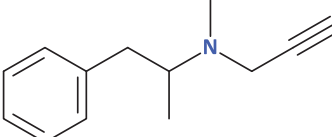
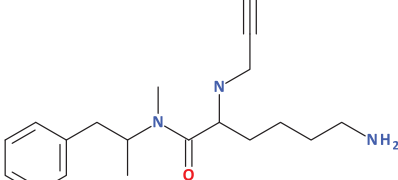
Figure 5.15 Alteration/inhibition of ASP+ uptake into HEK-hDAT cells. HEK-hDAT were treated for 10 min with different concentrations of compounds B (1), C (2) or D (3). All three compounds significantly reduced ASP+ uptake, (D) Representative fluorescent images of HEK-hDAT with 30 s incubation of 10μM ASP+ before and after incubation with the compounds. Bars represent means±SEMs of $N \geq 50$ ROIs taken from $N=3$ independent experiments ** $p \leq 0,01$, *** $p \leq 0,001$

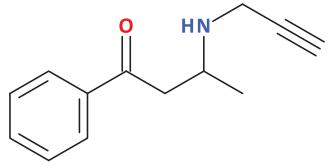
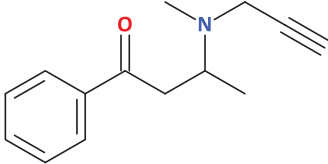
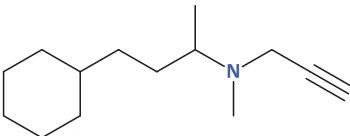

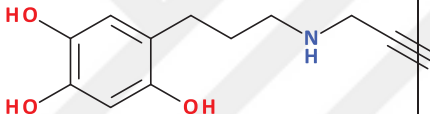
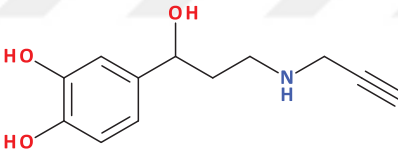
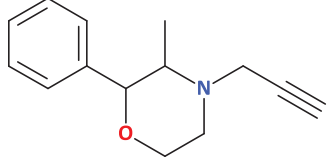
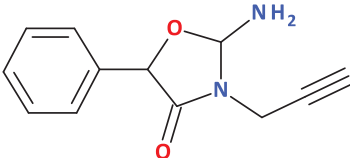
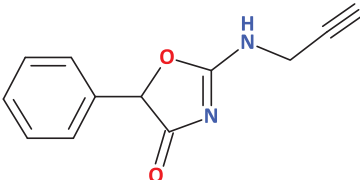
5.5. Novel hDAT Substrates/MAO Inhibitors with Potential Neuroprotective Activity

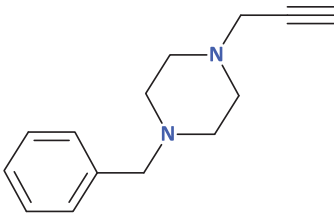
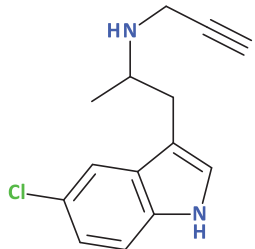
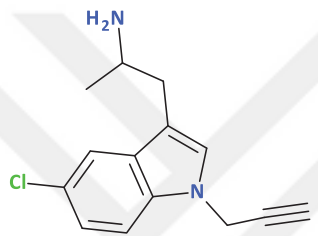
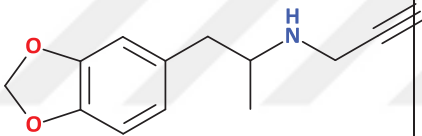
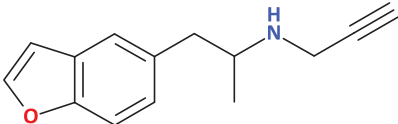
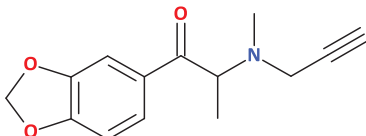
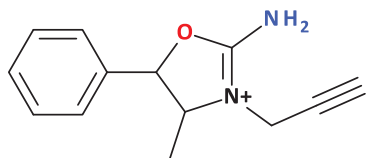
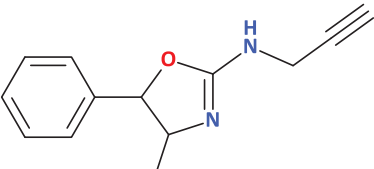
Some of the designed compounds having substrate-like properties have also shown good MAO-A and MAO-B inhibition. The results of docking studies are shown in Table 5. Out of twenty-two designed compounds, twelve compounds showed higher affinity for the hDAT-closed conformation. Based on our previous results (*in silico* and *in vitro*), we may suggest that these compounds would behave as hDAT substrates. These compounds have also shown good MAO activity. Much as rasagiline, MAO inhibition activity could lead

to neuroprotection. Most of the potential substrates showed higher affinity for MAO-A than MAO-B, which makes them MAO-A selective. Since these compounds have the propargylamine moiety attached to the amino group we might suggest that these compounds could increase Bcl-2 and decrease Bax activity. In the further research, they should be synthesized as tested *in vitro*.

Table 5.5 Docking results of novel compounds. Docking into hDATopen and hDAT closed to check for DAT-substrate behavior; Docking in MAO-A and MAO-B to check for MAO-inhibitory activity

COMPOUNDS		selective uptake into DA neurons		MAO inhibition	
		DAT closed	DAT open	MAO B	MAO A
		E kcal/mol	E kcal/mol	E kcal/mol	E kcal/mol
TK001		-7.17	-5.93	-5.74	-6.51
TK002		-7.07	-6.26	-6.11	-6.77
TK003		-7.17	-6.45	-6.32	-6.9
TK004		-6.45	-6.02	-6.39	-7.19
TK005		-2.45	-5.15	-6.48	-6.57

TK006		-7.11	-5.18	-7.13	-7.55
TK007		-5.96	-6.18	-6.95	-7.89
TK008		-6.15	-6.30	-7.02	-8.05
TK009		-6.30	-4.69	-6.74	-7.26
TK010		-5.37	-4.89	-6.6	-7.67
TK011		-5.98	-4.77	-7.14	-7.63
TK012		-6.00	-6.35	-6.99	-7.92
TK013		-5.84	-6.23	-6.55	-7.28
TK014		-6.19	-5.01	-7.025	-7.74

TK015		-5.99	-6.48	-6.52	-6.67
TK016		-6.17	-5.69	-7.96	-7.86
TK017		-3.97	-5.58	-7.2	-7.88
TK019		-7.13	-7.23	-6.69	-7.49
TK020		-6.85	-7.23	-7.19	-8.16
TK021		-5.65	-6.48	-6.85	-8.23
TK022		-6.14	-5.92	-7.01	-7.66
TK023		-7.28	-5.33	-7.31	-7.15

Compounds TK001, TK002, TK003, TK004, TK006, TK009, TK010, TK011, TK014, TK016, TK019, TK022 and TK023 are expected to be substrates of DAT, according to our docking results.

TK014 compound behaved like substrate, based on docking model, and have showed good affinities both for MAO-A and MAO-B, which is suggesting that it would act as non-selective MAO inhibitor (**Figure 5.16**). Compound TK019 which was designed by combining a structure of hDAT substrate MDMA and neuroprotective propargylamine group of rasagiline is shown on the **Figure 5.17**. Higher affinity for a hDAT-closed (-7.13 kcal/mol) than for hDAT-open (-7.23 kcal/mol) suggests that compound TK019 would behave as a hDAT substrate *in vitro*. This compound also shows slightly better affinity towards MAO-A (-7.49 kcal/mol) than MAO-B (-6.69), which makes it MAO-A selective. Only two compounds TK016 and TK023 are, like rasagiline, MAO-B selective. The compound TK016 (**Figure 5.18**) a derivative of pemoline has the highest MAO-B activity (-7.96 kcal/mol).

Using visualization we can see that all of the docked compounds are pulled into the hydrophobic pocket made from Tyr398, Tyr435 and FAD of MAO-B and Tyr407, Tyr444 and FAD of MAO-A. All of the compounds do interact with MAO-Bs' FAD, while with MAO-A that is not the case. With our docking studies we could not confirm whether these compounds are covalently binding for the FAD cofactor of MAO enzyme, like rasagiline, so we are not able to tell whether they are reversible or irreversible inhibitors. If that is the case (if these compounds could act as irreversible covalent inhibitors), then, logically, their affinity for MAO-B would be larger. This requires Molecular Dynamics Simulation, which is beyond the scope of this research, and could be done in the future studies. Compounds TK019 and TK016 in the binding sites of hDAT, MAO-A and MAO-B are shown on the pictures below.

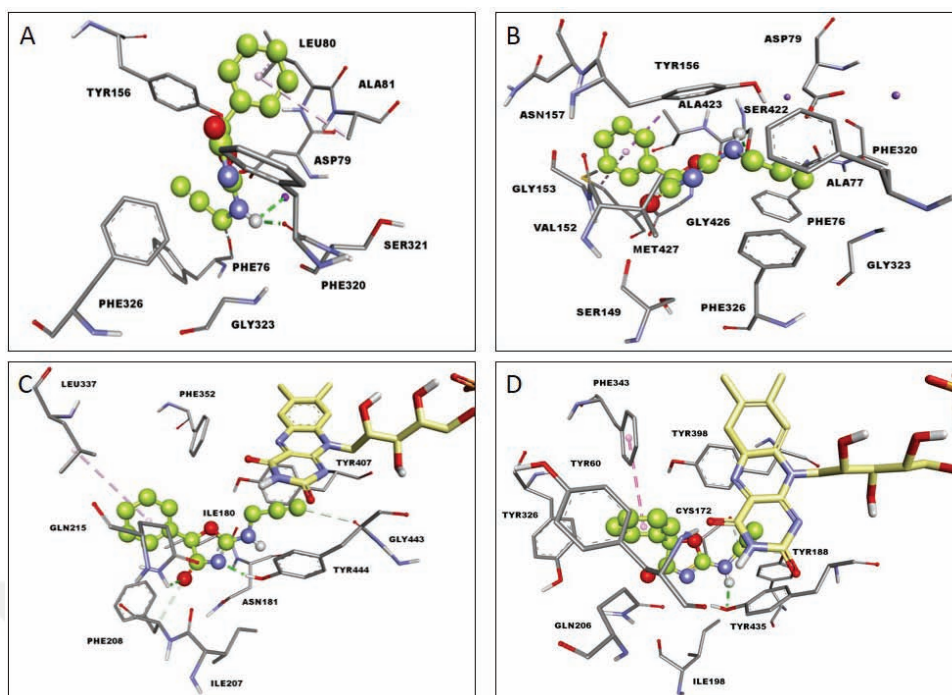


Figure 5.16 TK014; Important interactions of compound TK014 in the binding pocket of (A) hDAT-open, (B) hDAT-closed, (C) MAO-A and (D) MAO-B.

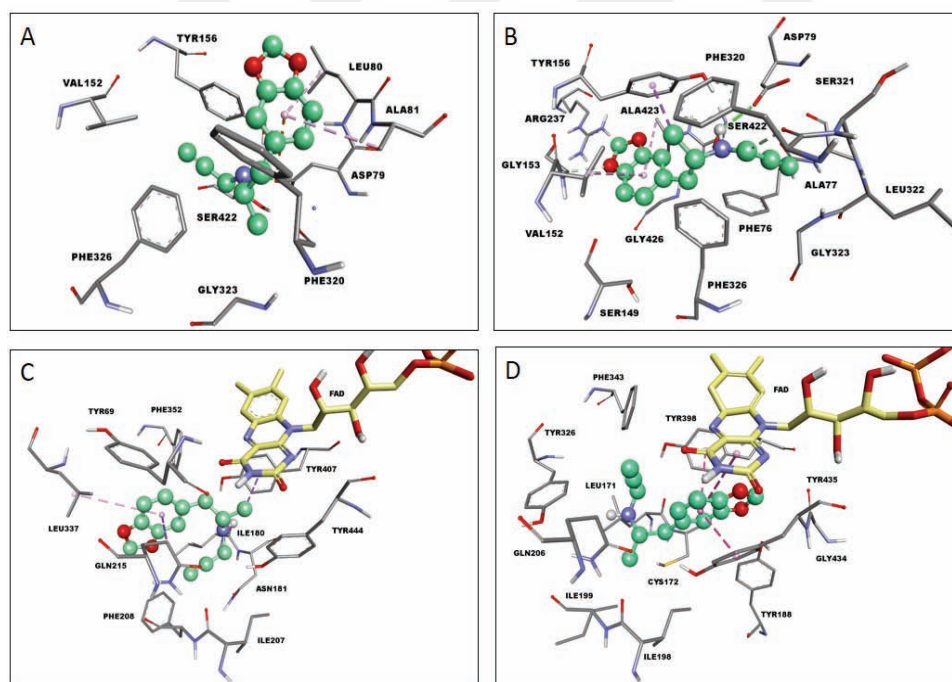


Figure 5.17 TK019; Important interactions of compound TK019 in the binding pocket of (A) hDAT-open, (B) hDAT-closed, (C) MAO-A and (D) MAO-B.

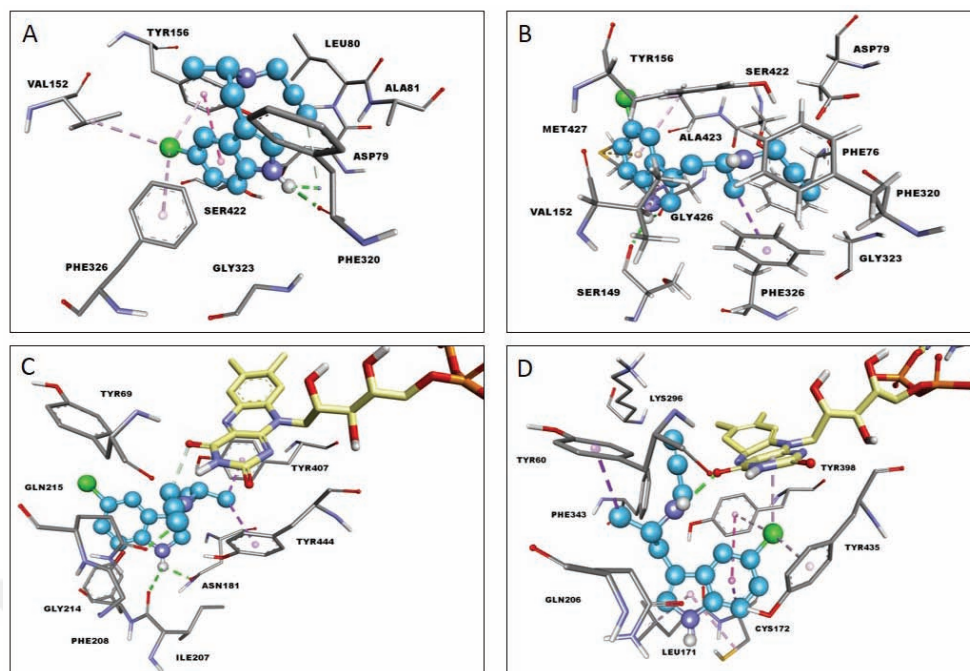


Figure 5.18 TK016; Important interactions of compound TK016 in the binding pocket of (A) hDAT-open, (B) hDAT-closed, (C) MAO-A and (D) MAO-B.

Continuing this research, these compounds should be further tested *in vitro* for their hDAT behavior, MAO-A and MAO-B activity, as well as neuroprotective effects. While the fundamental mechanisms that underlie PD still require elucidation, current opinion is that improved and targeted delivery of drugs inside the dopaminergic neuron are urgently required. Our *in silico* reconstruction of the human DAT and identification of five compounds that are effectively transported through the DAT provides a new avenue of research that may lead to improved anti PD drugs. The fact that these compounds possess some MAO inhibitory, antioxidant and anti-apoptotic properties, suggests that they may be suitable for reversing or delaying alpha-synuclein related neurodegeneration in the human brain.

6. CONCLUSION

Before the release of the X-ray structure of drosophila's DAT (dDAT)⁸, NSS transporters have been modeled on the structure of bacterial leucine transporter (LeuT) (Yamashita et al., 2005b), which shares an overall sequence similarity of about 20-25%. (Beuming et al., 2006; Forrest et al., 2006b; Indarte et al., 2008b; Ravna et al., 2006) LeuT and dDAT have several major differences, such as a kink in TM12 halfway across the membrane bilayer, a latch-like C-terminal domain that caps the cytoplasmic gate and a cholesterol molecule in the groove formed by TMs 1a, 5 and 7. The dDAT also co-transport a chloride anion with substrate, a peculiarity not shared by LeuT. (A. K. Kantcheva et al., 2013) After the dDAT structure release, a new homology model of hDAT has been recently published (Cheng et al., 2015; Cheng and Bahar, 2015b) proving higher reliability with respect to the previous ones. Following this strategy we have created a new homology model of the human dopamine transporter, to have a more precise model for structure based drug design purposes.

We speculated that since the inhibitors block the transporter in an outward open conformation (K. C. Schmitt et al., 2013), they could be docked more favorably in it, rather than in the closed conformation. On the other hand, the substrate should be able to bind the outward-open, the closed and the inward-open conformation. Accordingly, finding open and closed conformations of hDAT is helpful in the design of next generation anti-parkinsonian drugs.

We have investigated the conformational changes occurring in hDAT upon the binding of a substrate or inhibitors, mainly related to the closing of the pocket mediated by Phe320. These findings agree with X-ray structures published recently. (Wang et al., 2015) A previous study suggested that modafinil, which acts as an atypical inhibitor, keeps the hDAT in a closed conformation. (K. C. Schmitt et al., 2013) However, our results suggest that both cocaine and modafinil keep the transporter in an outward-open conformation,

whereas amphetamine causes closing of transporter. Furthermore, we suggest that cocaine and modafinil form more non-bonded interactions with hDAT which results in stronger binding affinity. The inhibitor keeps the transporter in the same conformation as the empty transporter. After 40 ns simulation we did not observe any major changes in the system that led to conformational change from occluded to inward-open conformation, so we speculated that there must be something else causing it, like binding of another substrate (Koldsø et al., 2013) or sodium being dragged by electrochemical gradient (Cheng and Bahar, 2015b; Tavoulari et al., 2016), but this is beyond of the scope of these research.

Furthermore, conformations that we have identified could be used for computational modeling. Using docking into these two conformations can indicate whether the compound is an inhibitor or a substrate. Based on docking of the known compounds into these two conformations we have determined differences between them. Namely, substrates show binding energies at around -7 kcal/mol (or more positive) for both hDAT conformations. The inhibitors show around -8 kcal/mol (or more negative) for open conformation and much less, or no binding for closed conformation (**APPENDIX A**). Lastly, we found a method to screen specifically for substrates, and we conclude that the best way is to take both protein conformations and ligands chemical properties into account.

In silico screening led us to choose six promising molecules out of 300,000 compounds, which indeed showed an effect on hDAT ASP⁺ transport *in vitro*. ASP⁺ has been shown to be translocated through plasma membrane not only by selective high-affinity transporters like DAT or SERT but also by low-affinity, high capacity monoamine transporters like OCT (organic cation transporter) and PMAT (plasma membrane monoamine transporter) and in addition by yet unknown uptake mechanisms.²³ Hence, the ASP⁺ transport rate mediated by high affinity transporters observed in different cellular systems accounts up to maximally 50 – 60 % of total accumulation into the cells. Therefore it is not possible to calculate accurate IC₅₀ values for the three most competing compounds. Rather we show that these compounds tested in our *in vitro* section inhibit ASP⁺ uptake to about 50% at concentrations within the same order of magnitude as do

the compounds in the computational calculations, i.e. the low micro-molar range. Our *in vitro*-experiments also identified one compound as a fluorescent DAT substrate, which is taken up into mouse ES cell-derived neurons and localizes to globular and slightly elongated structures, yet to be identified. In summary, this proves that the combination of *in silico* and *in vitro* studies is very effective and less time consuming and this approach can be used in the future to search for novel potent neuroprotective drugs that target dopaminergic neurons. After entering and accumulating in dopaminergic neurons, these compounds could target various proteins involved in neuroprotective or immunological mechanisms. They could target Monoamine Oxidase (MAO-B inhibitors), Glyceraldehyde-3-phosphate dehydrogenase (GADPH) or cytochrome c, among others. Alternatively, these compounds could bind heavy metal ions, calcium ions or ROS.(Akao et al., 2002a; Juárez Olgún et al., 2016a; Pavlin et al., 2016) Some authors have also suggested that the usage of DAT substrates could also be helpful for the treatment of cocaine addiction and might ameliorate the symptoms of stimulant withdrawal, thereby, facilitating abstinence. (Blough et al., 2014; Rothman, 2003) Continuing our work, we will screen these compounds for possible activities on enzymes in the cell (such as MAO, GADPH, caspases, cytochrome c, etc.) responsible for neurodegeneration/protection and look for other compounds able to target at the same time the hDAT transporter and other relevant proteins.

REFERENCES

- Abeliovich, A., Chen, C., Goda, Y., Silva, A.J., Stevens, C.F., Tonegawa, S., 1993. Modified hippocampal long-term potentiation in PKC gamma-mutant mice. *Cell* 75, 1253–1262.
- Acharya, C., Coop, A., MacKerell, J.E.P. and A.D., 2011. Recent Advances in Ligand-Based Drug Design: Relevance and Utility of the Conformationally Sampled Pharmacophore Approach [WWW Document]. *Curr. Comput. Aided Drug Des.* URL <http://www.eurekaselect.com/72953/article> (accessed 9.7.17).
- Ahn, B.-H., Rhim, H., Kim, S.Y., Sung, Y.-M., Lee, M.-Y., Choi, J.-Y., Wolozin, B., Chang, J.-S., Lee, Y.H., Kwon, T.K., Chung, K.C., Yoon, S.-H., Hahn, S.J., Kim, M.-S., Jo, Y.-H., Min, D.S., 2002. alpha-Synuclein interacts with phospholipase D isozymes and inhibits pervanadate-induced phospholipase D activation in human embryonic kidney-293 cells. *J. Biol. Chem.* 277, 12334–12342. <https://doi.org/10.1074/jbc.M110414200>
- Akao, Y., Maruyama, W., Yi, H., Shamoto-Nagai, M., Youdim, M.B., Naoi, M., 2002a. An anti-Parkinson's disease drug, N-propargyl-1 (R)-aminoindan (rasagiline), enhances expression of anti-apoptotic bcl-2 in human dopaminergic SH-SY5Y cells. *Neurosci. Lett.* 326, 105–108.
- Akao, Y., Maruyama, W., Yi, H., Shamoto-Nagai, M., Youdim, M.B.H., Naoi, M., 2002b. An anti-Parkinson's disease drug, N-propargyl-1(R)-aminoindan (rasagiline), enhances expression of anti-apoptotic bcl-2 in human dopaminergic SH-SY5Y cells. *Neurosci. Lett.* 326, 105–108.
- Aksenov, M.Y., Aksenova, M.V., Silvers, J.M., Mactutus, C.F., Booze, R.M., 2008. Different effects of selective dopamine uptake inhibitors, GBR 12909 and WIN 35428 on HIV-1 Tat toxicity in rat fetal midbrain neurons. *Neurotoxicology* 29, 971–977. <https://doi.org/10.1016/j.neuro.2008.06.003>
- Alder, B.J., Wainwright, T.E., 1959. Studies in Molecular Dynamics. I. General Method. *J. Chem. Phys.* 31, 459–466. <https://doi.org/10.1063/1.1730376>
- Andreas Kukol (Ed.), 2008. *Molecular Modeling of Proteins*. Humana Press, Hatfield, UK.
- Andrew R. Leach, 2001. *Molecular Modelling Principles and Applications*, 2nd ed. Glaxo Wellcome Research and Development, Pearson Education, Edinburgh, England.
- Bahr, B.A., Bendiske, J., 2002. The neuropathogenic contributions of lysosomal dysfunction. *J. Neurochem.* 83, 481–489.
- Baizabal, J.-M., Covarrubias, L., 2009. The embryonic midbrain directs neuronal specification of embryonic stem cells at early stages of differentiation. *Dev. Biol.* 325, 49–59. <https://doi.org/10.1016/j.ydbio.2008.09.024>
- Baranyi, M., Porceddu, P.F., Gölöncsér, F., Kulcsár, S., Otrókoci, L., Kittel, Á., Pinna, A., Frau, L., Huleatt, P.B., Khoo, M.-L., Chai, C.L.L., Dunkel, P., Mátyus, P., Morelli, M., Sperlágh, B., 2016. Novel (Hetero)arylalkenyl propargylamine compounds are protective in toxin-induced models of Parkinson's disease. *Mol. Neurodegener.* 11, 6. <https://doi.org/10.1186/s13024-015-0067-y>

- Barnham, K.J., Masters, C.L., Bush, A.I., 2004. Neurodegenerative diseases and oxidative stress. *Nat. Rev. Drug Discov.* 3, 205–214. <https://doi.org/10.1038/nrd1330>
- Basile, A.S., Janowsky, A., Golembiowska, K., Kowalska, M., Tam, E., Benveniste, M., Popik, P., Nikiforuk, A., Krawczyk, M., Nowak, G., Krieter, P.A., Lippa, A.S., Skolnick, P., Koustova, E., 2007. Characterization of the antinociceptive actions of bicifadine in models of acute, persistent, and chronic pain. *J. Pharmacol. Exp. Ther.* 321, 1208–1225. <https://doi.org/10.1124/jpet.106.116483>
- Beauchamp, K.A., Lin, Y.-S., Das, R., Pande, V.S., 2012. Are Protein Force Fields Getting Better? A Systematic Benchmark on 524 Diverse NMR Measurements. *J. Chem. Theory Comput.* 8, 1409–1414. <https://doi.org/10.1021/ct2007814>
- Beckman, J.S., Chen, J., Ischiropoulos, H., Crow, J.P., 1994. [23] Oxidative chemistry of peroxynitrite, in: *Methods in Enzymology, Oxygen Radicals in Biological Systems Part C*. Academic Press, pp. 229–240. [https://doi.org/10.1016/S0076-6879\(94\)33026-3](https://doi.org/10.1016/S0076-6879(94)33026-3)
- Benchimol, S., 2001. p53-dependent pathways of apoptosis. *Cell Death Differ.* 8, 1049–1051.
- Bento, A.P., Gaulton, A., Hersey, A., Bellis, L.J., Chambers, J., Davies, M., Krüger, F.A., Light, Y., Mak, L., McGlinchey, S., Nowotka, M., Papadatos, G., Santos, R., Overington, J.P., 2014. The ChEMBL bioactivity database: an update. *Nucleic Acids Res.* 42, D1083–D1090. <https://doi.org/10.1093/nar/gkt1031>
- Betarbet, R., Sherer, T.B., MacKenzie, G., Garcia-Osuna, M., Panov, A.V., Greenamyre, J.T., 2000. Chronic systemic pesticide exposure reproduces features of Parkinson's disease. *Nat. Neurosci.* 3, 1301–1306. <https://doi.org/10.1038/81834>
- Beuming, T., Kniazeff, J., Bergmann, M.L., Shi, L., Gracia, L., Raniszewska, K., Newman, A.H., Javitch, J.A., Weinstein, H., Gether, U., Loland, C.J., 2008. The binding sites for cocaine and dopamine in the dopamine transporter overlap. *Nat. Neurosci.* 11, 780–789. <https://doi.org/10.1038/nn.2146>
- Beuming, T., Shi, L., Javitch, J.A., Weinstein, H., 2006. A Comprehensive Structure-Based Alignment of Prokaryotic and Eukaryotic Neurotransmitter/Na⁺ Symporters (NSS) Aids in the Use of the LeuT Structure to Probe NSS Structure and Function. *Mol. Pharmacol.* 70, 1630–1642. <https://doi.org/10.1124/mol.106.026120>
- Billesbølle, C.B., Krüger, M.B., Shi, L., Quick, M., Li, Z., Stolzenberg, S., Kniazeff, J., Gotfryd, K., Mortensen, J.S., Javitch, J.A., Weinstein, H., Loland, C.J., Gether, U., 2015. Substrate-induced Unlocking of the Inner Gate Determines the Catalytic Efficiency of a Neurotransmitter:Sodium Symporter. *J. Biol. Chem.* 290, 26725–26738. <https://doi.org/10.1074/jbc.M115.677658>
- Binda, C., Wang, J., Pisani, L., Caccia, C., Carotti, A., Salvati, P., Edmondson, D.E., Mattevi, A., 2007. Structures of Human Monoamine Oxidase B Complexes with Selective Noncovalent Inhibitors: Saffinamide and Coumarin Analogs. *J. Med. Chem.* 50, 5848–5852. <https://doi.org/10.1021/jm070677y>
- Björklund, A., Lindvall, O., n.d. Replacing Dopamine Neurons in Parkinson's Disease: How did it happen? *J. Park. Dis.* 7, S23–S33. <https://doi.org/10.3233/JPD-179002>
- Blandini, F., 2005. Neuroprotection by rasagiline: a new therapeutic approach to Parkinson's disease? *CNS Drug Rev.* 11, 183–194.

- Blough, B.E., Landavazo, A., Partilla, J.S., Decker, A.M., Page, K.M., Baumann, M.H., Rothman, R.B., 2014. Alpha-ethyltryptamines as dual dopamine–serotonin releasers. *Bioorg. Med. Chem. Lett.* 24, 4754–4758. <https://doi.org/10.1016/j.bmcl.2014.07.062>
- Borre, L., Andreassen, T.F., Shi, L., Weinstein, H., Gether, U., 2014. The Second Sodium Site in the Dopamine Transporter Controls Cation Permeation and Is Regulated by Chloride. *J. Biol. Chem.* 289, 25764–25773. <https://doi.org/10.1074/jbc.M114.574269>
- Braak, H., Del Tredici, K., Rüb, U., De Vos, R.A., Steur, E.N.J., Braak, E., 2003. Staging of brain pathology related to sporadic Parkinson’s disease. *Neurobiol. Aging* 24, 197–211.
- Cabin, D.E., Shimazu, K., Murphy, D., Cole, N.B., Gottschalk, W., McIlwain, K.L., Orrison, B., Chen, A., Ellis, C.E., Paylor, R., Lu, B., Nussbaum, R.L., 2002. Synaptic vesicle depletion correlates with attenuated synaptic responses to prolonged repetitive stimulation in mice lacking alpha-synuclein. *J. Neurosci. Off. J. Soc. Neurosci.* 22, 8797–8807.
- Canet-Avilés, R.M., Wilson, M.A., Miller, D.W., Ahmad, R., McLendon, C., Bandyopadhyay, S., Baptista, M.J., Ringe, D., Petsko, G.A., Cookson, M.R., 2004. The Parkinson’s disease protein DJ-1 is neuroprotective due to cysteine-sulfenic acid-driven mitochondrial localization. *Proc. Natl. Acad. Sci. U. S. A.* 101, 9103–9108. <https://doi.org/10.1073/pnas.0402959101>
- Carvelli, L., Blakely, R.D., DeFelice, L.J., 2008. Dopamine transporter/syntaxin 1A interactions regulate transporter channel activity and dopaminergic synaptic transmission. *Proc. Natl. Acad. Sci. U. S. A.* 105, 14192–14197. <https://doi.org/10.1073/pnas.0802214105>
- Chen, C.C., Pogosyan, A., Zrinzo, L.U., Tisch, S., Limousin, P., Ashkan, K., Yousry, T., Hariz, M.I., Brown, P., 2006. Intra-operative recordings of local field potentials can help localize the subthalamic nucleus in Parkinson’s disease surgery. *Exp. Neurol.* 198, 214–221. <https://doi.org/10.1016/j.expneurol.2005.11.019>
- Cheng, F.-C., Kuo, J.-S., Chia, L.-G., Dryhurst, G., 1996. Elevated 5-S-cysteinyl dopamine/homovanillic acid ratio and reduced homovanillic acid in cerebrospinal fluid: possible markers for and potential insights into the pathoetiology of Parkinson’s disease. *J. Neural Transm.* 103, 433–446. <https://doi.org/10.1007/BF01276419>
- Cheng, M.H., Bahar, I., 2015a. Molecular Mechanism of Dopamine Transport by Human Dopamine Transporter. *Structure* 23, 2171–2181. <https://doi.org/10.1016/j.str.2015.09.001>
- Cheng, M.H., Bahar, I., 2015b. Molecular Mechanism of Dopamine Transport by Human Dopamine Transporter. *Structure* 23, 2171–2181. <https://doi.org/10.1016/j.str.2015.09.001>
- Cheng, M.H., Block, E., Hu, F., Cobanoglu, M.C., Sorkin, A., Bahar, I., 2015. Insights into the Modulation of Dopamine Transporter Function by Amphetamine, Orphenadrine, and Cocaine Binding. *Front. Neurol.* 6. <https://doi.org/10.3389/fneur.2015.00134>
- Chinta, S.J., Andersen, J.K., 2005. Dopaminergic neurons. *Int. J. Biochem. Cell Biol.* 37, 942–946. <https://doi.org/10.1016/j.biocel.2004.09.009>

- Clarke, G., Collins, R.A., Leavitt, B.R., Andrews, D.F., Hayden, M.R., Lumsden, C.J., McInnes, R.R., 2000. A one-hit model of cell death in inherited neuronal degenerations. *Nature* 406, 195–199. <https://doi.org/10.1038/35018098>
- Cook, C.D., Carroll, F.I., Beardsley, P.M., 2002. RTI 113, a 3-phenyltropine analog, produces long-lasting cocaine-like discriminative stimulus effects in rats and squirrel monkeys. *Eur. J. Pharmacol.* 442, 93–98.
- Coune, P.G., Schneider, B.L., Aebischer, P., 2012. Parkinson's Disease: Gene Therapies. *Cold Spring Harb. Perspect. Med.* 2. <https://doi.org/10.1101/cshperspect.a009431>
- Coyle, J.T., Puttfarcken, P., 1993a. Oxidative stress, glutamate, and neurodegenerative disorders. *Science* 262, 689–695.
- Coyle, J.T., Puttfarcken, P., 1993b. Oxidative stress, glutamate, and neurodegenerative disorders. *Science* 262, 689–695.
- Cozzi, N.V., Brandt, S.D., Daley, P.F., Partilla, J.S., Rothman, R.B., Tulzer, A., Sitte, H.H., Baumann, M.H., 2013. Pharmacological examination of trifluoromethyl ring-substituted methcathinone analogs. *Eur. J. Pharmacol.* 699, 180–187. <https://doi.org/10.1016/j.ejphar.2012.11.008>
- Cross, S., Cruciani, G., 2010. Molecular fields in drug discovery: getting old or reaching maturity? *Drug Discov. Today* 15, 23–32. <https://doi.org/10.1016/j.drudis.2008.12.006>
- Crossgrove, J., Zheng, W., 2004. Manganese toxicity upon overexposure. *NMR Biomed.* 17, 544–553. <https://doi.org/10.1002/nbm.931>
- Daniels, G.M., Amara, S.G., 1999. Regulated Trafficking of the Human Dopamine Transporter CLATHRIN-MEDIATED INTERNALIZATION AND LYSOSOMAL DEGRADATION IN RESPONSE TO PHORBOL ESTERS. *J. Biol. Chem.* 274, 35794–35801. <https://doi.org/10.1074/jbc.274.50.35794>
- Dauer, W., Przedborski, S., 2003. Parkinson's disease: mechanisms and models. *Neuron* 39, 889–909.
- Davies, R.W., Morris, B.J. (Eds.), 2004. *Molecular biology of the neuron*, 2nd ed. ed, Molecular and cellular neurobiology series. Oxford University Press, Oxford.
- Dekker, M.C.J., Bonifati, V., Duijn, V., M, C., 2003. Parkinson's disease: piecing together a genetic jigsaw. *Brain* 126, 1722–1733. <https://doi.org/10.1093/brain/awg172>
- Du, Y., Ma, Z., Lin, S., Dodel, R.C., Gao, F., Bales, K.R., Triarhou, L.C., Chernet, E., Perry, K.W., Nelson, D.L.G., Luecke, S., Phebus, L.A., Bymaster, F.P., Paul, S.M., 2001. Minocycline prevents nigrostriatal dopaminergic neurodegeneration in the MPTP model of Parkinson's disease. *Proc. Natl. Acad. Sci.* 98, 14669–14674. <https://doi.org/10.1073/pnas.251341998>
- Eriksen, J., Bjørn-Yoshimoto, W.E., Jørgensen, T.N., Newman, A.H., Gether, U., 2010. Postendocytic Sorting of Constitutively Internalized Dopamine Transporter in Cell Lines and Dopaminergic Neurons. *J. Biol. Chem.* 285, 27289–27301. <https://doi.org/10.1074/jbc.M110.131003>
- Fenollar-Ferrer, C., Stockner, T., Schwarz, T.C., Pal, A., Gotovina, J., Hofmaier, T., Jayaraman, K., Adhikary, S., Kudlacek, O., Mehdipour, A.R., Tavoulari, S., Rudnick, G., Singh, S.K., Konrat, R., Sitte, H.H., Forrest, L.R., 2014. Structure and Regulatory Interactions of the Cytoplasmic Terminal Domains of Serotonin Transporter. *Biochemistry (Mosc.)* 53, 5444–5460. <https://doi.org/10.1021/bi500637f>

- Fiser, A., 2010. Template-Based Protein Structure Modeling. *Methods Mol. Biol.* Clifton NJ 673, 73–94. https://doi.org/10.1007/978-1-60761-842-3_6
- Foltynie, T., Sawcer, S., Brayne, C., Barker, R.A., 2002. The genetic basis of Parkinson's disease. *J. Neurol. Neurosurg. Psychiatry* 73, 363–370.
- Forrest, L.R., Tang, C.L., Honig, B., 2006a. On the Accuracy of Homology Modeling and Sequence Alignment Methods Applied to Membrane Proteins. *Biophys. J.* 91, 508–517. <https://doi.org/10.1529/biophysj.106.082313>
- Forrest, L.R., Tang, C.L., Honig, B., 2006b. On the Accuracy of Homology Modeling and Sequence Alignment Methods Applied to Membrane Proteins. *Biophys. J.* 91, 508–517. <https://doi.org/10.1529/biophysj.106.082313>
- Foster, J.D., Yang, J.-W., Moritz, A.E., ChallaSivaKanaka, S., Smith, M.A., Holy, M., Wilebski, K., Sitte, H.H., Vaughan, R.A., 2012. Dopamine Transporter Phosphorylation Site Threonine 53 Regulates Substrate Reuptake and Amphetamine-stimulated Efflux. *J. Biol. Chem.* 287, 29702–29712. <https://doi.org/10.1074/jbc.M112.367706>
- Fontaine, T.M., Venda, L.L., Warrick, N., Christian, H.C., Brundin, P., Channon, K.M., Wade-Martins, R., 2008. The effect of α -synuclein knockdown on MPP+ toxicity in models of human neurons. *Eur. J. Neurosci.* 28, 2459–2473. <https://doi.org/10.1111/j.1460-9568.2008.06527.x>
- Ganellin, C.R., Lindberg, P., Mitscher, L.A., 1998. Glossary of terms used in medicinal chemistry. *Pure Appl Chem* 70, 1129–1143.
- Gardner, E.L., Liu, X., Paredes, W., Giordano, A., Spector, J., Lepore, M., Wu, K.-M., Froimowitz, M., 2006. A slow-onset, long-duration indanamine monoamine reuptake inhibitor as a potential maintenance pharmacotherapy for psychostimulant abuse: Effects in laboratory rat models relating to addiction. *Neuropharmacology* 51, 993–1003. <https://doi.org/10.1016/j.neuropharm.2006.06.009>
- Gibson, B.W., 2005. The human mitochondrial proteome: oxidative stress, protein modifications and oxidative phosphorylation. *Int. J. Biochem. Cell Biol.* 37, 927–934. <https://doi.org/10.1016/j.biocel.2004.11.013>
- Giepmans, B.N.G., Adams, S.R., Ellisman, M.H., Tsien, R.Y., 2006. The fluorescent toolbox for assessing protein location and function. *Science* 312, 217–224. <https://doi.org/10.1126/science.1124618>
- Glennon, R.A., 2014. Bath Salts, Mephedrone, and Methylenedioxypropylamphetamine as Emerging Illicit Drugs That Will Need Targeted Therapeutic Intervention, in: *Advances in Pharmacology*. Elsevier, pp. 581–620. <https://doi.org/10.1016/B978-0-12-420118-7.00015-9>
- Goldman, J.E., Yen, S.H., Chiu, F.C., Peress, N.S., 1983. Lewy bodies of Parkinson's disease contain neurofilament antigens. *Science* 221, 1082–1084.
- González, M.A., 2011. Force fields and molecular dynamics simulations. *Éc. Thématique Société Fr. Neutron.* 12, 169–200. <https://doi.org/10.1051/sfn/201112009>
- Goodsell, D.S., Morris, G.M., Olson, A.J., 1996. Automated docking of flexible ligands: applications of AutoDock. *J. Mol. Recognit. JMR* 9, 1–5. [https://doi.org/10.1002/\(SICI\)1099-1352\(199601\)9:1<1::AID-JMR241>3.0.CO;2-6](https://doi.org/10.1002/(SICI)1099-1352(199601)9:1<1::AID-JMR241>3.0.CO;2-6)
- Graham, D.G., Tiffany, S.M., Bell, W.R., Gutknecht, W.F., 1978. Autoxidation versus covalent binding of quinones as the mechanism of toxicity of dopamine, 6-

- hydroxydopamine, and related compounds toward C1300 neuroblastoma cells in vitro. *Mol. Pharmacol.* 14, 644–653.
- Graham, F.L., Smiley, J., Russell, W.C., Nairn, R., 1977. Characteristics of a human cell line transformed by DNA from human adenovirus type 5. *J. Gen. Virol.* 36, 59–72.
- Hadlock, G.C., Chu, P.-W., Walters, E.T., Hanson, G.R., Fleckenstein, A.E., 2010. Methamphetamine-Induced Dopamine Transporter Complex Formation and Dopaminergic Deficits: The Role of D2 Receptor Activation. *J. Pharmacol. Exp. Ther.* 335, 207–212. <https://doi.org/10.1124/jpet.110.166660>
- Halliwell, B., 2006. Oxidative stress and neurodegeneration: where are we now? *J. Neurochem.* 97, 1634–1658. <https://doi.org/10.1111/j.1471-4159.2006.03907.x>
- Halliwell, B., Gutteridge, J.M.C., 2015. *Free Radicals in Biology and Medicine*. Oxford University Press.
- Hansen, C., Li, J.-Y., 2012. Beyond α -synuclein transfer: pathology propagation in Parkinson's disease. *Trends Mol. Med.* 18, 248–255. <https://doi.org/10.1016/j.molmed.2012.03.002>
- Hastings, T.G., Zigmond, M.J., 1994. Identification of Catechol-Protein Conjugates in Neostriatal Slices Incubated with [³H]Dopamine: Impact of Ascorbic Acid and Glutathione. *J. Neurochem.* 63, 1126–1132. <https://doi.org/10.1046/j.1471-4159.1994.63031126.x>
- Hauser, R.A., 2011. Future Treatments for Parkinson's Disease: Surfing the PD Pipeline. *Int. J. Neurosci.* 121, 53–62. <https://doi.org/10.3109/00207454.2011.620195>
- Havel, T.F., Snow, M.E., 1991. A new method for building protein conformations from sequence alignments with homologues of known structure. *J. Mol. Biol.* 217, 1–7.
- Heal, D.J., Gosden, J., Smith, S.L., 2014. Dopamine reuptake transporter (DAT) “inverse agonism”--a novel hypothesis to explain the enigmatic pharmacology of cocaine. *Neuropharmacology* 87, 19–40. <https://doi.org/10.1016/j.neuropharm.2014.06.012>
- Hengartner, M.O., 2000. The biochemistry of apoptosis. *Nature* 407, 770–776. <https://doi.org/10.1038/35037710>
- Hong, W.C., Amara, S.G., 2013. Differential targeting of the dopamine transporter to recycling or degradative pathways during amphetamine- or PKC-regulated endocytosis in dopamine neurons. *FASEB J.* 27, 2995–3007. <https://doi.org/10.1096/fj.12-218727>
- Howell, L.L., Negus, S.S., 2014. Monoamine Transporter Inhibitors and Substrates as Treatments for Stimulant Abuse, in: *Advances in Pharmacology*. Elsevier, pp. 129–176. <https://doi.org/10.1016/B978-0-12-420118-7.00004-4>
- Hsu, M., Srinivas, B., Kumar, J., Subramanian, R., Andersen, J., 2005. Glutathione depletion resulting in selective mitochondrial complex I inhibition in dopaminergic cells is via an NO-mediated pathway not involving peroxynitrite: implications for Parkinson's disease. *J. Neurochem.* 92, 1091–1103. <https://doi.org/10.1111/j.1471-4159.2004.02929.x>
- Hughes, A.J., Daniel, S.E., Kilford, L., Lees, A.J., 1992. Accuracy of clinical diagnosis of idiopathic Parkinson's disease: a clinico-pathological study of 100 cases. *J. Neurol. Neurosurg. Psychiatry* 55, 181–184. <https://doi.org/10.1136/jnnp.55.3.181>

- Huleatt, P.B., Khoo, M.L., Chua, Y.Y., Tan, T.W., Liew, R.S., Balogh, B., Deme, R., Gölöncsér, F., Magyar, K., Sheela, D.P., Ho, H.K., Sperlágh, B., Mátyus, P., Chai, C.L.L., 2015. Novel arylalkenylpropargylamines as neuroprotective, potent, and selective monoamine oxidase B inhibitors for the treatment of Parkinson's disease. *J. Med. Chem.* 58, 1400–1419. <https://doi.org/10.1021/jm501722s>
- Hummerich, R., Reischl, G., Ehrlichmann, W., Machulla, H.-J., Heinz, A., Schloss, P., 2004. DASB -in vitro binding characteristics on human recombinant monoamine transporters with regard to its potential as positron emission tomography (PET) tracer. *J. Neurochem.* 90, 1218–1226. <https://doi.org/10.1111/j.1471-4159.2004.02585.x>
- Humphrey Rang, Maureen Dale, James Ritter, Rod Flower, 2007. Rang & Dale's Pharmacology, 6th ed. Churchill Livingstone.
- Huot, P., Fox, S.H., Brotchie, J.M., 2016. Dopamine Reuptake Inhibitors in Parkinson's Disease: A Review of Nonhuman Primate Studies and Clinical Trials. *J. Pharmacol. Exp. Ther.* 357, 562–569. <https://doi.org/10.1124/jpet.116.232371>
- Huot, P., Johnston, T.H., Gandy, M.N., Reyes, M.G., Fox, S.H., Piggott, M.J., Brotchie, J.M., 2012. The Monoamine Re-Uptake Inhibitor UWA-101 Improves Motor Fluctuations in the MPTP-Lesioned Common Marmoset. *PLOS ONE* 7, e45587. <https://doi.org/10.1371/journal.pone.0045587>
- Huot, P., Johnston, T.H., Lewis, K.D., Koprach, J.B., Reyes, M.G., Fox, S.H., Piggott, M.J., Brotchie, J.M., 2014. UWA-121, a mixed dopamine and serotonin re-uptake inhibitor, enhances l-DOPA anti-parkinsonian action without worsening dyskinesia or psychosis-like behaviours in the MPTP-lesioned common marmoset. *Neuropharmacology* 82, 76–87. <https://doi.org/10.1016/j.neuropharm.2014.01.012>
- Indarte, M., Madura, J.D., Surratt, C.K., 2008a. Dopamine transporter comparative molecular modeling and binding site prediction using the LeuT(Aa) leucine transporter as a template. *Proteins* 70, 1033–1046. <https://doi.org/10.1002/prot.21598>
- Indarte, M., Madura, J.D., Surratt, C.K., 2008b. Dopamine transporter comparative molecular modeling and binding site prediction using the LeuT(Aa) leucine transporter as a template. *Proteins* 70, 1033–1046. <https://doi.org/10.1002/prot.21598>
- Inyushin, M.U., Arencibia-Albite, F., de la Cruz, A., Vázquez-Torres, R., Colon, K., Sanabria, P., Jiménez-Rivera, C.A., 2013. New method to visualize neurons with DAT in slices of rat VTA using fluorescent substrate for DAT, ASP+. *J. Neurosci. Neuroengineering* 2, 98–103. <https://doi.org/10.1166/jnsne.2013.1040>
- Irwin, J.J., Sterling, T., Mysinger, M.M., Bolstad, E.S., Coleman, R.G., 2012. ZINC: A Free Tool to Discover Chemistry for Biology. *J. Chem. Inf. Model.* 52, 1757–1768. <https://doi.org/10.1021/ci3001277>
- Jankovic, J., Aguilar, L.G., 2008. Current approaches to the treatment of Parkinson's disease. *Neuropsychiatr. Dis. Treat.* 4, 743–757.
- Jardetzky, O., 1966. Simple allosteric model for membrane pumps. *Nature* 211, 969–970.
- Jastroch, M., Divakaruni, A.S., Mookerjee, S., Treberg, J.R., Brand, M.D., 2010. Mitochondrial proton and electron leaks. *Essays Biochem.* 47, 53–67. <https://doi.org/10.1042/bse0470053>

- Jenner, P., Mori, A., Hauser, R., Morelli, M., Fredholm, B.B., Chen, J.F., 2009. Adenosine, adenosine A2A antagonists, and Parkinson's disease. *Parkinsonism Relat. Disord.* 15, 406–413. <https://doi.org/10.1016/j.parkreldis.2008.12.006>
- Jęško, H., Lenkiewicz, A.M., Adamczyk, A., 2017. Treatments and compositions targeting α -synuclein: a patent review (2010-2016). *Expert Opin. Ther. Pat.* 27, 427–438. <https://doi.org/10.1080/13543776.2017.1261112>
- Jonathan Pevsner, 2015. *Bioinformatics and Functional Genomics*, 3rd Edition, 3rd ed. Wiley-Blackwell.
- Jonathan Pevsner, n.d. *Bioinformatics and Functional Genomics*, 2nd edition. ed. Wiley-Blackwell, Baltimore, Maryland.
- Jones, G., Willett, P., Glen, R.C., 1995. Molecular recognition of receptor sites using a genetic algorithm with a description of desolvation. *J. Mol. Biol.* 245, 43–53. [https://doi.org/10.1016/S0022-2836\(95\)80037-9](https://doi.org/10.1016/S0022-2836(95)80037-9)
- Jones, G., Willett, P., Glen, R.C., Leach, A.R., Taylor, R., 1997. Development and validation of a genetic algorithm for flexible docking1. *J. Mol. Biol.* 267, 727–748. <https://doi.org/10.1006/jmbi.1996.0897>
- Juárez Olguín, H., Calderón Guzmán, D., Hernández García, E., Barragán Mejía, G., 2016a. The Role of Dopamine and Its Dysfunction as a Consequence of Oxidative Stress. *Oxid. Med. Cell. Longev.* 2016, 1–13. <https://doi.org/10.1155/2016/9730467>
- Juárez Olguín, H., Calderón Guzmán, D., Hernández García, E., Barragán Mejía, G., 2016b. The Role of Dopamine and Its Dysfunction as a Consequence of Oxidative Stress. *Oxid. Med. Cell. Longev.* 2016. <https://doi.org/10.1155/2016/9730467>
- Kaczanowski, S., Zielenkiewicz, P., 2010. Why similar protein sequences encode similar three-dimensional structures? *Theor. Chem. Acc.* 125, 643–650. <https://doi.org/10.1007/s00214-009-0656-3>
- Kampman, K.M., 2008. The Search for Medications to Treat Stimulant Dependence. *Addict. Sci. Clin. Pract.* 4, 28–35.
- Kantcheva, A.K., Quick, M., Shi, L., Winther, A.-M.L., Stolzenberg, S., Weinstein, H., Javitch, J.A., Nissen, P., 2013. Chloride binding site of neurotransmitter sodium symporters. *Proc. Natl. Acad. Sci.* 110, 8489–8494. <https://doi.org/10.1073/pnas.1221279110>
- Kantcheva, A.K., Quick, M., Shi, L., Winther, A.-M.L., Stolzenberg, S., Weinstein, H., Javitch, J.A., Nissen, P., 2013. Chloride binding site of neurotransmitter sodium symporters. *Proc. Natl. Acad. Sci.* 110, 8489–8494. <https://doi.org/10.1073/pnas.1221279110>
- KEGG PATHWAY: Parkinson's disease - Homo sapiens (human) [WWW Document], n.d. URL http://www.genome.jp/kegg-bin/show_pathway?hsa05012 (accessed 7.29.17).
- Khalili-Araghi, F., Gumbart, J., Wen, P.-C., Sotomayor, M., Tajkhorshid, E., Schulten, K., 2009. Molecular dynamics simulations of membrane channels and transporters. *Curr. Opin. Struct. Biol.* 19, 128–137. <https://doi.org/10.1016/j.sbi.2009.02.011>
- Kim, J.-S., He, L., Lemasters, J.J., 2003. Mitochondrial permeability transition: a common pathway to necrosis and apoptosis. *Biochem. Biophys. Res. Commun.* 304, 463–470. [https://doi.org/10.1016/S0006-291X\(03\)00618-1](https://doi.org/10.1016/S0006-291X(03)00618-1)

- Kitchen, D.B., Decornez, H., Furr, J.R., Bajorath, J., 2004. Docking and scoring in virtual screening for drug discovery: methods and applications. *Nat. Rev. Drug Discov.* 3, 935–949. <https://doi.org/10.1038/nrd1549>
- Klein, C., Westenberger, A., 2012. Genetics of Parkinson's Disease. *Cold Spring Harb. Perspect. Med.* 2. <https://doi.org/10.1101/cshperspect.a008888>
- Klein, C., Westenberger, A., 2012. Genetics of Parkinson's Disease. *Cold Spring Harb. Perspect. Med.* 2, a008888–a008888. <https://doi.org/10.1101/cshperspect.a008888>
- Kohut, S.J., Fivel, P.A., Blough, B.E., Rothman, R.B., Mello, N.K., 2013. Effects of methcathinone and 3-Cl-methcathinone (PAL-434) in cocaine discrimination or self-administration in rhesus monkeys. *Int. J. Neuropsychopharmacol.* 16, 1985–1998. <https://doi.org/10.1017/S146114571300059X>
- Koldsø, H., Autzen, H.E., Grouleff, J., Schjøtt, B., 2013. Ligand Induced Conformational Changes of the Human Serotonin Transporter Revealed by Molecular Dynamics Simulations. *PLOS ONE* 8, e63635. <https://doi.org/10.1371/journal.pone.0063635>
- Kolinski, A., Betancourt, M.R., Kihara, D., Rotkiewicz, P., Skolnick, J., 2001. Generalized comparative modeling (GENECOMP): a combination of sequence comparison, threading, and lattice modeling for protein structure prediction and refinement. *Proteins* 44, 133–149.
- Krishnamurthy, H., Gouaux, E., 2012. X-ray structures of LeuT in substrate-free outward-open and apo inward-open states. *Nature* 481, 469–474. <https://doi.org/10.1038/nature10737>
- Kristensen, A.S., Andersen, J., Jørgensen, T.N., Sørensen, L., Eriksen, J., Loland, C.J., Strømgaard, K., Gether, U., 2011. SLC6 Neurotransmitter Transporters: Structure, Function, and Regulation. *Pharmacol. Rev.* 63, 585–640. <https://doi.org/10.1124/pr.108.000869>
- Kristensen, A.S., Andersen, J., Jørgensen, T.N., Sørensen, L., Eriksen, J., Loland, C.J., Strømgaard, K., Gether, U., 2011. SLC6 neurotransmitter transporters: structure, function, and regulation. *Pharmacol. Rev.* 63, 585–640. <https://doi.org/10.1124/pr.108.000869>
- Langston, J.W., Ballard, P., Tetrud, J.W., Irwin, I., 1983. Chronic Parkinsonism in humans due to a product of meperidine-analog synthesis. *Science* 219, 979–980.
- Lau, T., Proissl, V., Ziegler, J., Schloss, P., 2015. Visualization of neurotransmitter uptake and release in serotonergic neurons. *J. Neurosci. Methods* 241, 10–17. <https://doi.org/10.1016/j.jneumeth.2014.12.009>
- Lee, F.J., Liu, F., Pristupa, Z.B., Niznik, H.B., 2001. Direct binding and functional coupling of alpha-synuclein to the dopamine transporters accelerate dopamine-induced apoptosis. *FASEB J. Off. Publ. Fed. Am. Soc. Exp. Biol.* 15, 916–926.
- Lee, F.J.S., Pei, L., Moszczynska, A., Vukusic, B., Fletcher, P.J., Liu, F., 2007. Dopamine transporter cell surface localization facilitated by a direct interaction with the dopamine D2 receptor. *EMBO J.* 26, 2127–2136. <https://doi.org/10.1038/sj.emboj.7601656>
- Lee, V.M., Hartley, R.S., Trojanowski, J.Q., 2000. Neurobiology of human neurons (NT2N) grafted into mouse spinal cord: implications for improving therapy of spinal cord injury. *Prog. Brain Res.* 128, 299–307. [https://doi.org/10.1016/S0079-6123\(00\)28027-8](https://doi.org/10.1016/S0079-6123(00)28027-8)

- Lengauer, T., Rarey, M., 1996. Computational methods for biomolecular docking. *Curr. Opin. Struct. Biol.* 6, 402–406.
- L'Episcopo, F., Tirolo, C., Caniglia, S., Testa, N., Serra, P.A., Impagnatiello, F., Morale, M.C., Marchetti, B., 2010. Combining nitric oxide release with anti-inflammatory activity preserves nigrostriatal dopaminergic innervation and prevents motor impairment in a 1-methyl-4-phenyl-1, 2, 3, 6-tetrahydropyridine model of Parkinson's disease. *J. Neuroinflammation* 7, 83.
- Lin, Y.-C., Boone, M., Meuris, L., Lemmens, I., Van Roy, N., Soete, A., Reumers, J., Moisse, M., Plaisance, S., Drmanac, R., Chen, J., Speleman, F., Lambrechts, D., Van de Peer, Y., Tavernier, J., Callewaert, N., 2014. Genome dynamics of the human embryonic kidney 293 lineage in response to cell biology manipulations. *Nat. Commun.* 5. <https://doi.org/10.1038/ncomms5767>
- Linnane, A., Ozawa, T., Marzuki, S., Tanaka, M., 1989. MITOCHONDRIAL DNA MUTATIONS AS AN IMPORTANT CONTRIBUTOR TO AGEING AND DEGENERATIVE DISEASES. *The Lancet* 333, 642–645. [https://doi.org/10.1016/S0140-6736\(89\)92145-4](https://doi.org/10.1016/S0140-6736(89)92145-4)
- Linnane, A.W., Baumer, A., Maxwell, R.J., Preston, H., Zhang, C.F., Marzuki, S., 1990. Mitochondrial gene mutation: the ageing process and degenerative diseases. *Biochem. Int.* 22, 1067–1076.
- Lionta, E., Spyrou, G., Vassilatis, D.K., Cournia, Z., 2014. Structure-Based Virtual Screening for Drug Discovery: Principles, Applications and Recent Advances. *Curr. Top. Med. Chem.* 14, 1923–1938. <https://doi.org/10.2174/1568026614666140929124445>
- López-Arnau, R., Martínez-Clemente, J., Pubill, D., Escubedo, E., Camarasa, J., 2012. Comparative neuropharmacology of three psychostimulant cathinone derivatives: butylone, mephedrone and methylone: Neuropharmacology of cathinone derivatives. *Br. J. Pharmacol.* 167, 407–420. <https://doi.org/10.1111/j.1476-5381.2012.01998.x>
- Lotharius, J., Brundin, P., 2002. Pathogenesis of Parkinson's disease: dopamine, vesicles and alpha-synuclein. *Nat. Rev. Neurosci.* 3, 932–942. <https://doi.org/10.1038/nrn983>
- Luan, F., Cordeiro, M.N.D.S., Alonso, N., García-Mera, X., Caamaño, O., Romero-Duran, F.J., Yañez, M., González-Díaz, H., 2013. TOPS-MODE model of multiplexing neuroprotective effects of drugs and experimental-theoretic study of new 1,3-rasagiline derivatives potentially useful in neurodegenerative diseases. *Bioorg. Med. Chem.* 21, 1870–1879. <https://doi.org/10.1016/j.bmc.2013.01.035>
- Madras, B.K., Xie, Z., Lin, Z., Jassen, A., Panas, H., Lynch, L., Johnson, R., Livni, E., Spencer, T.J., Bonab, A.A., Miller, G.M., Fischman, A.J., 2006. Modafinil Occupies Dopamine and Norepinephrine Transporters in Vivo and Modulates the Transporters and Trace Amine Activity in Vitro. *J. Pharmacol. Exp. Ther.* 319, 561–569. <https://doi.org/10.1124/jpet.106.106583>
- Mandel, S., Weinreb, O., Amit, T., Youdim, M.B.H., 2005. Mechanism of neuroprotective action of the anti-Parkinson drug rasagiline and its derivatives. *Brain Res. Rev., Glial-Neuron Crosstalk in Neuroinflammation, Neurodegeneration and Neuroprotection* 48, 379–387. <https://doi.org/10.1016/j.brainresrev.2004.12.027>

- Manning-Bog, A.B., McCormack, A.L., Purisai, M.G., Bolin, L.M., Di Monte, D.A., 2003. Alpha-synuclein overexpression protects against paraquat-induced neurodegeneration. *J. Neurosci. Off. J. Soc. Neurosci.* 23, 3095–3099.
- Marco-Contelles, J., Unzeta, M., Bolea, I., Esteban, G., Ramsay, R.R., Romero, A., Martínez-Murillo, R., Carreiras, M.C., Ismaili, L., 2016. ASS234, As a New Multi-Target Directed Propargylamine for Alzheimer's Disease Therapy. *Front. Neurosci.* 10. <https://doi.org/10.3389/fnins.2016.00294>
- Marks, D.M., Pae, C.-U., Patkar, A.A., 2008. Triple Reuptake Inhibitors: The Next Generation of Antidepressants. *Curr. Neuropharmacol.* 6, 338–343. <https://doi.org/10.2174/157015908787386078>
- Martí, Y., Matthaues, F., Lau, T., Schloss, P., 2017. Methyl-4-phenylpyridinium (MPP+) differentially affects monoamine release and re-uptake in murine embryonic stem cell-derived dopaminergic and serotonergic neurons. *Mol. Cell. Neurosci.* 83, 37–45. <https://doi.org/10.1016/j.mcn.2017.06.009>
- Matthaues, F., Schloss, P., Lau, T., 2015. Differential Uptake Mechanisms of Fluorescent Substrates into Stem-Cell-Derived Serotonergic Neurons. *ACS Chem. Neurosci.* 6, 1906–1912. <https://doi.org/10.1021/acscchemneuro.5b00219>
- Mavel, S., Mincheva, Z., Méheux, N., Carcenac, Y., Guilloteau, D., Abarbri, M., Emond, P., 2012. QSAR study and synthesis of new phenyltropanes as ligands of the dopamine transporter (DAT). *Bioorg. Med. Chem.* 20, 1388–1395. <https://doi.org/10.1016/j.bmc.2012.01.014>
- McInnes, C., 2007. Virtual screening strategies in drug discovery. *Curr. Opin. Chem. Biol., Analytical Techniques / Mechanisms* 11, 494–502. <https://doi.org/10.1016/j.cbpa.2007.08.033>
- McNaught, K.S.P., Olanow, C.W., Halliwell, B., Isacson, O., Jenner, P., 2001. Failure of the ubiquitin–proteasome system in Parkinson's disease. *Nat. Rev. Neurosci.* 2, 589–594. <https://doi.org/10.1038/35086067>
- Menzies, R.A., Gold, P.H., 1971. The Turnover of Mitochondria in a Variety of Tissues of Young Adult and Aged Rats. *J. Biol. Chem.* 246, 2425–2429.
- Millan, M.J., 2009. Dual- and triple-acting agents for treating core and co-morbid symptoms of major depression: novel concepts, new drugs. *Neurotherapeutics* 6, 53–77. <https://doi.org/10.1016/j.nurt.2008.10.039>
- Milletti, F., Storchi, L., Goracci, L., Bendels, S., Wagner, B., Kansy, M., Cruciani, G., 2010. Extending pKa prediction accuracy: High-throughput pKa measurements to understand pKa modulation of new chemical series. *Eur. J. Med. Chem.* 45, 4270–4279. <https://doi.org/10.1016/j.ejmech.2010.06.026>
- Moroy, G., Sperandio, O., Rielland, S., Khemka, S., Druart, K., Goyal, D., Perahia, D., Miteva, M.A., 2015. Sampling of conformational ensemble for virtual screening using molecular dynamics simulations and normal mode analysis. *Future Med. Chem.* 7, 2317–2331. <https://doi.org/10.4155/fmc.15.150>
- Morris, G.M., Goodsell, D.S., Halliday, R.S., Huey, R., Hart, W.E., Belew, R.K., Olson, A.J., 1998. Automated docking using a Lamarckian genetic algorithm and an empirical binding free energy function. *J. Comput. Chem.* 19, 1639–1662.
- Morris, G.M., Huey, R., Lindstrom, W., Sanner, M.F., Belew, R.K., Goodsell, D.S., Olson, A.J., 2009. AutoDock4 and AutoDockTools4: Automated docking with selective receptor flexibility. *J. Comput. Chem.* 30, 2785–2791. <https://doi.org/10.1002/jcc.21256>

- Murphy, M.P., Smith, R.A., 2000. Drug delivery to mitochondria: the key to mitochondrial medicine. *Adv. Drug Deliv. Rev.* 41, 235–250.
- Mysinger, M.M., Carchia, M., Irwin, J.J., Shoichet, B.K., 2012. Directory of Useful Decoys, Enhanced (DUD-E): Better Ligands and Decoys for Better Benchmarking. *J. Med. Chem.* 55, 6582–6594. <https://doi.org/10.1021/jm300687e>
- Nayak, L., Henchcliffe, C., 2008. Rasagiline in treatment of Parkinson's disease. *Neuropsychiatr. Dis. Treat.* 4, 23–32.
- Newmeyer, D.D., Ferguson-Miller, S., 2003. Mitochondria. *Cell* 112, 481–490. [https://doi.org/10.1016/S0092-8674\(03\)00116-8](https://doi.org/10.1016/S0092-8674(03)00116-8)
- Nikolic, K., Mavridis, L., Djikic, T., Vucicevic, J., Agbaba, D., Yelekci, K., Mitchell, J.B.O., 2016. Drug Design for CNS Diseases: Polypharmacological Profiling of Compounds Using Cheminformatic, 3D-QSAR and Virtual Screening Methodologies. *Front. Neurosci.* 10, 265. <https://doi.org/10.3389/fnins.2016.00265>
- Oczkowska, A., Kozubski, W., Lianeri, M., Dorszewska, J., 2013. Mutations in PRKN and SNCA Genes Important for the Progress of Parkinson's Disease. *Curr. Genomics* 14, 502–517. <https://doi.org/10.2174/1389202914666131210205839>
- Olanow, C.W., Brundin, P., 2013. Parkinson's Disease and Alpha Synuclein: Is Parkinson's Disease a Prion-Like Disorder? *Mov. Disord.* 28, 31–40. <https://doi.org/10.1002/mds.25373>
- Ou, X.-M., Lu, D., Johnson, C., Chen, K., Youdim, M.B.H., Rajkowska, G., Shih, J.C., 2009. Glyceraldehyde-3-Phosphate Dehydrogenase–Monoamine Oxidase B-Mediated Cell Death-Induced by Ethanol is Prevented by Rasagiline and 1-R-Aminoindan. *Neurotox. Res.* 16, 148–159. <https://doi.org/10.1007/s12640-009-9064-7>
- Oz, M., Libby, T., Kivell, B., Jaligam, V., Ramamoorthy, S., Shippenberg, T.S., 2010. Real-time, spatially resolved analysis of serotonin transporter activity and regulation using the fluorescent substrate, ASP+. *J. Neurochem.* 114, 1019–1029. <https://doi.org/10.1111/j.1471-4159.2010.06828.x>
- Palmer, A.E., Tsien, R.Y., 2006. Measuring calcium signaling using genetically targetable fluorescent indicators. *Nat. Protoc.* 1, 1057–1065. <https://doi.org/10.1038/nprot.2006.172>
- Park, S.U., Ferrer, J.V., Javitch, J.A., Kuhn, D.M., 2002. Peroxynitrite Inactivates the Human Dopamine Transporter by Modification of Cysteine 342: Potential Mechanism of Neurotoxicity in Dopamine Neurons. *J. Neurosci.* 22, 4399–4405.
- Pasternak, B., Svanström, H., Nielsen, N.M., Fugger, L., Melbye, M., Hviid, A., 2012. Use of calcium channel blockers and Parkinson's disease. *Am. J. Epidemiol.* 175, 627–635. <https://doi.org/10.1093/aje/kwr362>
- Pavlin, M., Repič, M., Vianello, R., Mavri, J., 2016. The Chemistry of Neurodegeneration: Kinetic Data and Their Implications. *Mol. Neurobiol.* 53, 3400–3415. <https://doi.org/10.1007/s12035-015-9284-1>
- Pearce, R.K.B., Smith, L.A., Jackson, M.J., Banerji, T., Scheel-Krüger, J., Jenner, P., 2002. The monoamine reuptake blocker brasofensine reverses akinesia without dyskinesia in MPTP-treated and levodopa-primed common marmosets. *Mov. Disord.* 17, 877–886. <https://doi.org/10.1002/mds.10238>
- Peng, J., Stevenson, F.F., Doctrow, S.R., Andersen, J.K., 2005. Superoxide Dismutase/Catalase Mimetics Are Neuroprotective against Selective Paraquat-

- mediated Dopaminergic Neuron Death in the Substantia Nigra
 IMPLICATIONS FOR PARKINSON DISEASE. *J. Biol. Chem.* 280, 29194–29198. <https://doi.org/10.1074/jbc.M500984200>
- Penmatsa, A., Wang, K.H., Gouaux, E., 2013. X-ray structure of dopamine transporter elucidates antidepressant mechanism. *Nature* 503, 85–90.
- Perier, C., Vila, M., 2012. Mitochondrial Biology and Parkinson's Disease. *Cold Spring Harb. Perspect. Med.* 2. <https://doi.org/10.1101/cshperspect.a009332>
- Phillips, J.C., Braun, R., Wang, W., Gumbart, J., Tajkhorshid, E., Villa, E., Chipot, C., Skeel, R.D., Kalé, L., Schulten, K., 2005. Scalable molecular dynamics with NAMD. *J. Comput. Chem.* 26, 1781–1802. <https://doi.org/10.1002/jcc.20289>
- Piana, S., Klepeis, J.L., Shaw, D.E., 2014. Assessing the accuracy of physical models used in protein-folding simulations: quantitative evidence from long molecular dynamics simulations. *Curr. Opin. Struct. Biol.* 24, 98–105. <https://doi.org/10.1016/j.sbi.2013.12.006>
- Pj, G., 1985. A computational procedure for determining energetically favorable binding sites on biologically important macromolecules. *J. Med. Chem.* 28, 849–857. <https://doi.org/10.1021/jm00145a002>
- Polymeropoulos, M.H., Lavedan, C., Leroy, E., Ide, S.E., Dehejia, A., Dutra, A., Pike, B., Root, H., Rubenstein, J., Boyer, R., Stenroos, E.S., Chandrasekharappa, S., Athanassiadou, A., Papapetropoulos, T., Johnson, W.G., Lazzarini, A.M., Duvoisin, R.C., Iorio, G.D., Golbe, L.I., Nussbaum, R.L., 1997. Mutation in the α -Synuclein Gene Identified in Families with Parkinson's Disease. *Science* 276, 2045–2047. <https://doi.org/10.1126/science.276.5321.2045>
- Rahman, A., 1964. Correlations in the Motion of Atoms in Liquid Argon. *Phys. Rev.* 136, A405–A411. <https://doi.org/10.1103/PhysRev.136.A405>
- Ramamoorthy, S., Shippenberg, T.S., Jayanthi, L.D., 2011. Regulation of Monoamine Transporters: Role of Transporter Phosphorylation. *Pharmacol. Ther.* 129, 220–238. <https://doi.org/10.1016/j.pharmthera.2010.09.009>
- Raval, A., Piana, S., Eastwood, M.P., Dror, R.O., Shaw, D.E., 2012. Refinement of protein structure homology models via long, all-atom molecular dynamics simulations. *Proteins Struct. Funct. Bioinforma.* 80, 2071–2079. <https://doi.org/10.1002/prot.24098>
- Ravna, A.W., Jaroczyk, M., Sylte, I., 2006. A homology model of SERT based on the LeuT(Aa) template. *Bioorg. Med. Chem. Lett.* 16, 5594–5597. <https://doi.org/10.1016/j.bmcl.2006.08.028>
- Ravna, A.W., Sylte, I., 2012. Homology modeling of transporter proteins (carriers and ion channels). *Methods Mol. Biol. Clifton NJ* 857, 281–299. https://doi.org/10.1007/978-1-61779-588-6_12
- Reddy, A.S., Pati, S.P., Kumar, P.P., Pradeep, H.N., Sastry, G.N., 2007. Virtual screening in drug discovery -- a computational perspective. *Curr. Protein Pept. Sci.* 8, 329–351.
- Reith, M.E.A., Blough, B.E., Hong, W.C., Jones, K.T., Schmitt, K.C., Baumann, M.H., Partilla, J.S., Rothman, R.B., Katz, J.L., 2015. Behavioral, biological, and chemical perspectives on atypical agents targeting the dopamine transporter. *Drug Alcohol Depend.* 147, 1–19. <https://doi.org/10.1016/j.drugalcdep.2014.12.005>
- Reith, M.E.A., Blough, B.E., Hong, W.C., Jones, K.T., Schmitt, K.C., Baumann, M.H., Partilla, J.S., Rothman, R.B., Katz, J.L., 2015. Behavioral, biological, and

- chemical perspectives on atypical agents targeting the dopamine transporter. *Drug Alcohol Depend.* 147, 1–19.
<https://doi.org/10.1016/j.drugalcdep.2014.12.005>
- Rester, U., 2008. From virtuality to reality - Virtual screening in lead discovery and lead optimization: a medicinal chemistry perspective. *Curr. Opin. Drug Discov. Devel.* 11, 559–568.
- Richard B. Silverman, 2004. *The Organic Chemistry of Drug Design*, 2nd ed. Elsevier, Academic Press.
- Rijk, M.C. de, Breteler, M.M.B., Graveland, G.A., Ott, A., Grobbee, D.E., Meche, F.G.A. van der, Hofman, A., 1995. Prevalence of Parkinson's disease in the elderly The Rotterdam Study. *Neurology* 45, 2143–2146.
<https://doi.org/10.1212/WNL.45.12.2143>
- Robertson, S.D., Matthies, H.J., Galli, A., 2009a. A closer look at amphetamine induced reverse transport and trafficking of the dopamine and norepinephrine transporters. *Mol. Neurobiol.* 39, 73–80. <https://doi.org/10.1007/s12035-009-8053-4>
- Robertson, S.D., Matthies, H.J.G., Galli, A., 2009b. A Closer Look at Amphetamine-Induced Reverse Transport and Trafficking of the Dopamine and Norepinephrine Transporters. *Mol. Neurobiol.* 39, 73–80.
<https://doi.org/10.1007/s12035-009-8053-4>
- Rolletschek, A., Chang, H., Guan, K., Czyz, J., Meyer, M., Wobus, A.M., 2001. Differentiation of embryonic stem cell-derived dopaminergic neurons is enhanced by survival-promoting factors. *Mech. Dev.* 105, 93–104.
- Rothman, R.B., 2003. (+)-Fenfluramine and Its Major Metabolite, (+)-Norfenfluramine, Are Potent Substrates for Norepinephrine Transporters. *J. Pharmacol. Exp. Ther.* 305, 1191–1199. <https://doi.org/10.1124/jpet.103.049684>
- Sali, A., Blundell, T.L., 1993. Comparative protein modelling by satisfaction of spatial restraints. *J. Mol. Biol.* 234, 779–815. <https://doi.org/10.1006/jmbi.1993.1626>
- Sanderson, M.J., Smith, I., Parker, I., Bootman, M.D., 2014. *Fluorescence Microscopy*. Cold Spring Harb. Protoc. 2014, pdb.top071795.
<https://doi.org/10.1101/pdb.top071795>
- Schloss, P., Matthäus, F., Lau, T., 2015. Shine bright: considerations on the use of fluorescent substrates in living monoaminergic neurons in vitro. *Neural Regen. Res.* 10, 1383.
- Schmeichel, B.E., Zemlan, F.P., Berridge, C.W., 2013. A Selective Dopamine Reuptake Inhibitor Improves Prefrontal Cortex-Dependent Cognitive Function: Potential Relevance to Attention Deficit Hyperactivity Disorder. *Neuropharmacology* 64, 321–328. <https://doi.org/10.1016/j.neuropharm.2012.07.005>
- Schmitt, K.C., Rothman, R.B., Reith, M.E.A., 2013. Nonclassical Pharmacology of the Dopamine Transporter: Atypical Inhibitors, Allosteric Modulators, and Partial Substrates. *J. Pharmacol. Exp. Ther.* 346, 2–10.
<https://doi.org/10.1124/jpet.111.191056>
- Schmitt, K.C., Rothman, R.B., Reith, M.E.A., 2013. Nonclassical Pharmacology of the Dopamine Transporter: Atypical Inhibitors, Allosteric Modulators, and Partial Substrates. *J. Pharmacol. Exp. Ther.* 346, 2–10.
<https://doi.org/10.1124/jpet.111.191056>
- Schwartz, J.W., Blakely, R.D., DeFelice, L.J., 2003. Binding and Transport in Norepinephrine Transporters REAL-TIME, SPATIALLY RESOLVED

- ANALYSIS IN SINGLE CELLS USING A FLUORESCENT SUBSTRATE. *J. Biol. Chem.* 278, 9768–9777. <https://doi.org/10.1074/jbc.M209824200>
- Seddik, A., Holy, M., Weissensteiner, R., Zdrzil, B., Sitte, H.H., Ecker, G.F., 2013. Probing the Selectivity of Monoamine Transporter Substrates by Means of Molecular Modeling. *Mol. Inform.* 32, 409–413. <https://doi.org/10.1002/minf.201300013>
- Shaw, G., Morse, S., Ararat, M., Graham, F.L., 2002. Preferential transformation of human neuronal cells by human adenoviruses and the origin of HEK 293 cells. *FASEB J. Off. Publ. Fed. Am. Soc. Exp. Biol.* 16, 869–871. <https://doi.org/10.1096/fj.01-0995fje>
- Singh, S.K., Piscitelli, C.L., Yamashita, A., Gouaux, E., 2008. A competitive inhibitor traps LeuT in an open-to-out conformation. *Science* 322, 1655–1661. <https://doi.org/10.1126/science.1166777>
- Singh, S.K., Yamashita, A., Gouaux, E., 2007. Antidepressant binding site in a bacterial homologue of neurotransmitter transporters. *Nature* 448, 952–956. <https://doi.org/10.1038/nature06038>
- Sinko, W., de Oliveira, C., Williams, S., Van Wynsberghe, A., Durrant, J.D., Cao, R., Oldfield, E., McCammon, J.A., 2011. Applying Molecular Dynamics Simulations to Identify Rarely Sampled Ligand-bound Conformational States of Undecaprenyl Pyrophosphate Synthase, an Antibacterial Target: Identifying Rare States of UPPS. *Chem. Biol. Drug Des.* 77, 412–420. <https://doi.org/10.1111/j.1747-0285.2011.01101.x>
- Sitte, H.H., Huck, S., Reither, H., Boehm, S., Singer, E.A., Pifl, C., 1998. Carrier-mediated release, transport rates, and charge transfer induced by amphetamine, tyramine, and dopamine in mammalian cells transfected with the human dopamine transporter. *J. Neurochem.* 71, 1289–1297.
- Son, S.-Y., Ma, J., Kondou, Y., Yoshimura, M., Yamashita, E., Tsukihara, T., 2008. Structure of human monoamine oxidase A at 2.2-Å resolution: the control of opening the entry for substrates/inhibitors. *Proc. Natl. Acad. Sci. U. S. A.* 105, 5739–5744. <https://doi.org/10.1073/pnas.0710626105>
- Sorkina, T., Caltagarone, J., Sorkin, A., 2013. Flotillins regulate membrane mobility of the dopamine transporter but are not required for its protein kinase C dependent endocytosis. *Traffic Cph. Den.* 14, 709–724. <https://doi.org/10.1111/tra.12059>
- Sousa, S.F., Fernandes, P.A., Ramos, M.J., 2006. Protein-ligand docking: current status and future challenges. *Proteins* 65, 15–26. <https://doi.org/10.1002/prot.21082>
- Spyrakis, F., Benedetti, P., Decherchi, S., Rocchia, W., Cavalli, A., Alcaro, S., Ortuso, F., Baroni, M., Cruciani, G., 2015. A Pipeline To Enhance Ligand Virtual Screening: Integrating Molecular Dynamics and Fingerprints for Ligand and Proteins. *J. Chem. Inf. Model.* 55, 2256–2274. <https://doi.org/10.1021/acs.jcim.5b00169>
- Spyrakis, F., Cavasotto, C.N., 2015. Open challenges in structure-based virtual screening: Receptor modeling, target flexibility consideration and active site water molecules description. *Arch. Biochem. Biophys.* 583, 105–119. <https://doi.org/10.1016/j.abb.2015.08.002>
- Spyrakis, F., Cellini, B., Bruno, S., Benedetti, P., Carosati, E., Cruciani, G., Micheli, F., Felici, A., Cozzini, P., Kellogg, G.E., Voltattorni, C.B., Mozzarelli, A., 2014. Targeting cystalysin, a virulence factor of *treponema denticola*-supported

- periodontitis. *ChemMedChem* 9, 1501–1511.
<https://doi.org/10.1002/cmdc.201300527>
- Spyrakis, F., Felici, P., Bayden, A.S., Salsi, E., Miggiano, R., Kellogg, G.E., Cozzini, P., Cook, P.F., Mozzarelli, A., Campanini, B., 2013a. Fine tuning of the active site modulates specificity in the interaction of O-acetylserine sulfhydrylase isozymes with serine acetyltransferase. *Biochim. Biophys. Acta BBA - Proteins Proteomics* 1834, 169–181. <https://doi.org/10.1016/j.bbapap.2012.09.009>
- Spyrakis, F., Felici, P., Bayden, A.S., Salsi, E., Miggiano, R., Kellogg, G.E., Cozzini, P., Cook, P.F., Mozzarelli, A., Campanini, B., 2013b. Fine tuning of the active site modulates specificity in the interaction of O-acetylserine sulfhydrylase isozymes with serine acetyltransferase. *Biochim. Biophys. Acta BBA - Proteins Proteomics* 1834, 169–181. <https://doi.org/10.1016/j.bbapap.2012.09.009>
- Spyrakis, F., Singh, R., Cozzini, P., Campanini, B., Salsi, E., Felici, P., Raboni, S., Benedetti, P., Cruciani, G., Kellogg, G.E., Cook, P.F., Mozzarelli, A., 2013c. Isozyme-Specific Ligands for O-acetylserine sulfhydrylase, a Novel Antibiotic Target. *PLoS ONE* 8, e77558. <https://doi.org/10.1371/journal.pone.0077558>
- Stayte, S., Rentsch, P., Tröscher, A.R., Bamberger, M., Li, K.M., Vissel, B., 2017. Activin A Inhibits MPTP and LPS-Induced Increases in Inflammatory Cell Populations and Loss of Dopamine Neurons in the Mouse Midbrain In Vivo. *PLoS ONE* 12. <https://doi.org/10.1371/journal.pone.0167211>
- Susin, S.A., Lorenzo, H.K., Zamzami, N., Marzo, I., Snow, B.E., Brothers, G.M., Mangion, J., Jacotot, E., Costantini, P., Loeffler, M., Larochette, N., Goodlett, D.R., Aebersold, R., Siderovski, D.P., Penninger, J.M., Kroemer, G., 1999. Molecular characterization of mitochondrial apoptosis-inducing factor. *Nature* 397, 441–446. <https://doi.org/10.1038/17135>
- Sveinbjornsdottir, S., 2016. The clinical symptoms of Parkinson’s disease. *J. Neurochem.* 139, 318–324. <https://doi.org/10.1111/jnc.13691>
- Swerdlow, R.H., Parks, J.K., Miller, S.W., Tuttle, J.B., Trimmer, P.A., Sheehan, J.P., Bennett, J.P., Davis, R.E., Parker, W.D., 1996. Origin and functional consequences of the complex I defect in Parkinson’s disease. *Ann. Neurol.* 40, 663–671. <https://doi.org/10.1002/ana.410400417>
- Szewczyk, A., Wojtczak, L., 2002. Mitochondria as a pharmacological target. *Pharmacol. Rev.* 54, 101–127.
- Tanner, C.M., Kamel, F., Ross, G.W., Hoppin, J.A., Goldman, S.M., Korell, M., Marras, C., Bhudhikanok, G.S., Kasten, M., Chade, A.R., Comyns, K., Richards, M.B., Meng, C., Priestley, B., Fernandez, H.H., Cambi, F., Umbach, D.M., Blair, A., Sandler, D.P., Langston, J.W., 2011. Rotenone, Paraquat, and Parkinson’s Disease. *Environ. Health Perspect.* 119, 866–872. <https://doi.org/10.1289/ehp.1002839>
- Tavoulari, S., Margheritis, E., Nagarajan, A., DeWitt, D.C., Zhang, Y.-W., Rosado, E., Ravera, S., Rhoades, E., Forrest, L.R., Rudnick, G., 2016. Two Na⁺ Sites Control Conformational Change in a Neurotransmitter Transporter Homolog. *J. Biol. Chem.* 291, 1456–1471. <https://doi.org/10.1074/jbc.M115.692012>
- Tieu, K., Ischiropoulos, H., Przedborski, S., 2003. Nitric Oxide and Reactive Oxygen Species in Parkinson’s Disease. *IUBMB Life* 55, 329–335. <https://doi.org/10.1080/1521654032000114320>
- Tizzano, J.P., Stribling, D.S., Perez-Tilve, D., Strack, A., Frassetto, A., Chen, R.Z., Fong, T.M., Shearman, L., Krieter, P.A., Tschöp, M.H., Skolnick, P., Basile,

- A.S., 2008. The triple uptake inhibitor (1R,5S)-(+)-1-(3,4-dichlorophenyl)-3-azabicyclo[3.1.0] hexane hydrochloride (DOV 21947) reduces body weight and plasma triglycerides in rodent models of diet-induced obesity. *J. Pharmacol. Exp. Ther.* 324, 1111–1126. <https://doi.org/10.1124/jpet.107.133132>
- Török, N., Majláth, Z., Szalárdy, L., Vécsei, L., 2016. Investigational α -synuclein aggregation inhibitors: hope for Parkinson's disease. *Expert Opin. Investig. Drugs* 25, 1281–1294. <https://doi.org/10.1080/13543784.2016.1237501>
- Totrov, M., Abagyan, R., 2008. Flexible ligand docking to multiple receptor conformations: a practical alternative. *Curr. Opin. Struct. Biol.* 18, 178–184. <https://doi.org/10.1016/j.sbi.2008.01.004>
- Underwood, J., Simon Cross, 2009. *General and Systematic Pathology*, 5th ed. Churchill Livingstone, Edinburgh.
- Vaughan, R.A., Foster, J.D., 2013. Mechanisms of dopamine transporter regulation in normal and disease states. *Trends Pharmacol. Sci.* 34. <https://doi.org/10.1016/j.tips.2013.07.005>
- Vyas, V.K., Ukawala, R.D., Ghatge, M., Chintha, C., 2012. Homology Modeling a Fast Tool for Drug Discovery: Current Perspectives. *Indian J. Pharm. Sci.* 74, 1–17. <https://doi.org/10.4103/0250-474X.102537>
- Walters, W.P., Stahl, M.T., Murcko, M.A., 1998. Virtual screening—an overview. *Drug Discov. Today* 3, 160–178.
- Wang, K.H., Penmatsa, A., Gouaux, E., 2015. Neurotransmitter and psychostimulant recognition by the dopamine transporter. *Nature* 521, 322–327. <https://doi.org/10.1038/nature14431>
- Wang, X., Figueroa, B.E., Stavrovskaya, I.G., Zhang, Y., Sirianni, A.C., Zhu, S., Day, A.L., Kristal, B.S., Friedlander, R.M., 2009. Methazolamide and Melatonin Inhibit Mitochondrial Cytochrome C Release and Are Neuroprotective in Experimental Models of Ischemic Injury. *Stroke J. Cereb. Circ.* 40, 1877–1885. <https://doi.org/10.1161/STROKEAHA.108.540765>
- Wang, X., Zhu, S., Pei, Z., Drozda, M., Stavrovskaya, I.G., Del Signore, S.J., Cormier, K., Shimony, E.M., Wang, H., Ferrante, R.J., Kristal, B.S., Friedlander, R.M., 2008. Inhibitors of Cytochrome c Release with Therapeutic Potential for Huntington's Disease. *J. Neurosci. Off. J. Soc. Neurosci.* 28, 9473–9485. <https://doi.org/10.1523/JNEUROSCI.1867-08.2008>
- Warren, G.L., Andrews, C.W., Capelli, A.-M., Clarke, B., LaLonde, J., Lambert, M.H., Lindvall, M., Nevins, N., Semus, S.F., Senger, S., Tedesco, G., Wall, I.D., Woolven, J.M., Peishoff, C.E., Head, M.S., 2006. A critical assessment of docking programs and scoring functions. *J. Med. Chem.* 49, 5912–5931. <https://doi.org/10.1021/jm050362n>
- Webb, B., Sali, A., 2016. Comparative Protein Structure Modeling Using MODELLER. *Curr. Protoc. Bioinforma.* 54, 5.6.1-5.6.37. <https://doi.org/10.1002/cpbi.3>
- Weiner, P.K., Kollman, P.A., 1981. AMBER: Assisted model building with energy refinement. A general program for modeling molecules and their interactions. *J. Comput. Chem.* 2, 287–303. <https://doi.org/10.1002/jcc.540020311>
- Weiner, S.J., Kollman, P.A., Case, D.A., Singh, U.C., Ghio, C., Alagona, G., Profeta, S., Weiner, P., 1984. A new force field for molecular mechanical simulation of nucleic acids and proteins. *J. Am. Chem. Soc.* 106, 765–784. <https://doi.org/10.1021/ja00315a051>

- Weinreb, O., Mandel, S., Bar-Am, O., Yogev-Falach, M., Avramovich-Tirosh, Y., Amit, T., Youdim, M.B.H., 2009. Multifunctional neuroprotective derivatives of rasagiline as anti-Alzheimer's disease drugs. *Neurother. J. Am. Soc. Exp. Neurother.* 6, 163–174. <https://doi.org/10.1016/j.nurt.2008.10.030>
- Wersinger, C., Sidhu, A., 2003. Attenuation of dopamine transporter activity by alpha-synuclein. *Neurosci. Lett.* 340, 189–192.
- Wiemerslage, L., Schultz, B.J., Ganguly, A., Lee, D., 2013. Selective degeneration of dopaminergic neurons by MPP⁺ and its rescue by D2 autoreceptors in *Drosophila* primary culture. *J. Neurochem.* 126, 529–540. <https://doi.org/10.1111/jnc.12228>
- Wimalasena, D.S., Perera, R.P., Heyen, B.J., Balasooriya, I.S., Wimalasena, K., 2008. Vesicular Monoamine Transporter Substrate/Inhibitor Activity of MPTP/MPP⁺ Derivatives: A Structure–Activity Study. *J. Med. Chem.* 51, 760–768. <https://doi.org/10.1021/jm070875p>
- Yamashita, A., Singh, S.K., Kawate, T., Jin, Y., Gouaux, E., 2005a. Crystal structure of a bacterial homologue of Na⁺/Cl⁻-dependent neurotransmitter transporters. *Nature* 437, 215–223. <https://doi.org/10.1038/nature03978>
- Yamashita, A., Singh, S.K., Kawate, T., Jin, Y., Gouaux, E., 2005b. Crystal structure of a bacterial homologue of Na⁺/Cl⁻-dependent neurotransmitter transporters. *Nature* 437, 215–223. <https://doi.org/10.1038/nature03978>
- Yin, D., MacKerell, A.D., 1998. Combined ab initio/empirical approach for optimization of Lennard–Jones parameters. *J. Comput. Chem.* 19, 334–348. [https://doi.org/10.1002/\(SICI\)1096-987X\(199802\)19:3<334::AID-JCC7>3.0.CO;2-U](https://doi.org/10.1002/(SICI)1096-987X(199802)19:3<334::AID-JCC7>3.0.CO;2-U)
- Youdim, M.B.H., Edmondson, D., Tipton, K.F., 2006. The therapeutic potential of monoamine oxidase inhibitors. *Nat. Rev. Neurosci.* 7, 295–309. <https://doi.org/10.1038/nrn1883>
- Yuan, J., Yankner, B.A., 2000. Apoptosis in the nervous system. *Nature* 407, 802–809. <https://doi.org/10.1038/35037739>
- Zapata, A., Kivell, B., Han, Y., Javitch, J.A., Bolan, E.A., Kuraguntla, D., Jaligam, V., Oz, M., Jayanthi, L.D., Samuvel, D.J., Ramamoorthy, S., Shippenberg, T.S., 2007. Regulation of dopamine transporter function and cell surface expression by D3 dopamine receptors. *J. Biol. Chem.* 282, 35842–35854. <https://doi.org/10.1074/jbc.M611758200>
- Zhao, Y., Quick, M., Shi, L., Mehler, E.L., Weinstein, H., Javitch, J.A., 2010. Substrate-dependent proton antiport in neurotransmitter:sodium symporters. *Nat. Chem. Biol.* 6, 109–116. <https://doi.org/10.1038/nchembio.284>
- Zvejniece, L., Svalbe, B., Vavers, E., Makrecka-Kuka, M., Makarova, E., Liepins, V., Kalvinsh, I., Liepinsh, E., Dambrova, M., 2017. S-phenylpiracetam, a selective DAT inhibitor, reduces body weight gain without influencing locomotor activity. *Pharmacol. Biochem. Behav.* <https://doi.org/10.1016/j.pbb.2017.07.009>

CURRICULUM VITAE

Personal Information

Name Surname : Teodora Đikić
Place and Date of Birth : 20.06.1988
Belgrade, Serbia



Education

Undergraduate Education : Faculty of Pharmacy, University of Belgrade, Serbia
Graduate Education : Faculty of Pharmacy, University of Belgrade, Serbia

Foreign Language Skills : Serbian (native speaker)
English (advanced speaker),
Turkish (basic)

Work Experience

September 2014 - September 2017

Kemal Yelekçi, Kadir Has University, Istanbul, Turkey

Employed on the project "*In silico* reconstruction of the dopamine transporter and design of new drugs with neuroprotective properties"; funded under the EU Marie Curie Framework 7,

Contact:

Telephone : +905367940636
E-mail Address : teodora.djik88@gmail.com

List of Publications:

Human Dopamine Transporter: The first implementation of a combined in silico/in vitro approach revealing the substrate and inhibitor specificities; Teodora Djikic, Yasmina Marti, Francesca Spyraakis, Thorsten Lau, Paolo Benedetti, Gavin Davey, Patrick Schloss and Kemal Yelekci - under review

Synthesis, Molecular Modelling and Anticancer Activity of Diflunisal Derivatives as Cyclooxygenase Enzyme Inhibitors; Göknül Pelin Coşkun, Teodora Djikic, Nezaket Türkel, Kemal Yelekçi, Fikretin Şahin, Ş. Güniz Küçükgülzel – under review

Synthesis, Anticancer Activity and Molecular Modeling of Etodolac-Thioether Derivatives as Potent Methionine Aminopeptidase (type II) Inhibitors; Isil Coruh, Ozge Cevik, Kemal Yelekci, Teodora Djikic, S. Guniz Kuçukguzel - under review

Drug design for CNS diseases: polypharmacological profiling of compounds using cheminformatic, 3D-QSAR and virtual screening methodologies; Katarina Nikolic , Lazaros Mavridis, Teodora Djikic, Jelica Vucicevic, Danica Agbaba, Kemal Yelekci and John B O Mitchell. *Frontiers in Neuroscience* Published on 25. May 2016, doi:10.3389/fnins.2016.00265

Synthesis and Screening of Human Monoamine Oxidase-A Inhibitor Effect of New 2-Pyrazoline and Hydrazone Derivatives; B. Evranos-Aksoz, İ. Baysal, S. Yabanoglu Ciftci, T. Djikic, K. Yelekci, G. Ucar, *Arch Pharm (Weinheim)*. 2015 Oct;348(10):743-56. doi: 10.1002/ardp.201500212

List of Presentations:

- Oral presentations:

National Symposium in Neuroscience, “*In silico modeling of dopamine transporter and in vitro testing*”; Sakarya, Turkey, May 2017

Turkish BIOVIA (ACCELRY'S) Seminar: “*In silico modeling of dopamine transporter using Accelrys Discovery Studio*”; Istanbul, Turkey, March 2015

- Poster presentations:

American Chemical Society (ACS) meeting: “***In silico* modeling of dopamine transporter and design of novel neuroprotective agents**”; Philadelphia, USA, August 2016

International Symposium on Pharmaceutical Sciences (ISOPS-11): “**Novel reversible and selective pyrazoline based hMAO-A inhibitors: synthesis, docking studies and biological evaluation**”; Ankara, Turkey, June 2015

RICT 2015, International Conference on Medicinal Chemistry, “***In silico* modeling of human dopamine transporter and design of novel inhibitors**”; Avignon, France, July 2015

3rd International BAU Drug Design Congress: “**Synthesis, Characterization and Molecular Docking of New Diflunisal 1,2,4-Triazole- 3-Thiones**”; Istanbul, Turkey, May 2015

APPENDIX A

Table A. 1 Docking results of known inhibitors docked into 10 conformations extracted from MD simulation of hDAT-cocaine complex and graphs representing docking results into 10 different conformations with error bars (SE for Autodock = ± 2 kcal/mol)

hDAT open (cocaine bound)					
compound	hDATopen1	hDATopen2	hDATopen3	hDATopen4	hDATopen5
	AutoDock ΔG (kcal/mol)				
benzotropin	-8.65	-7.99	-8.33	-7.97	-8.09
bupropion	-6.27	-6.38	-6.9	-6.28	-6.89
citalopram	-7.37	-7.4	-6.6	-5.99	-8.52
cocaine	-7.47	-7.54	-7.62	-7.19	-7.74
duloxetine	-7.6	-7.86	-8.15	-6.86	-8.36
GBR-12783	-8.03	-9.45	-9.14	-7.92	-9.24
modafinil	-6.76	-6.33	-6.72	-6.46	-7.23
rimcazole	-6.57	-8.17	-7.73	-8.09	-8.29
RTI-55	-6.16	-7.8	-8.46	-7.72	-7.98
sertalin	-8.37	-7.88	-8.92	-7.62	-8.81
sibutramin	-6.99	-6.49	-6.83	-6.53	-7.3
trimipramin	-8.35	-7.19	-7.35	-7.35	-7.75
vanorexin	-8.05	-5.22	-6.72	-8.05	-6.88

hDAT open (cocaine bound)					
compound	hDATopen6	hDATopen7	hDATopen8	hDATopen9	hDATopen10
	AutoDock ΔG (kcal/mol)				
benzotropin	-7.76	-6.96	-7.11	-7.2	-6.37
bupropion	-6.31	-6.36	-5.89	-5.79	-5.66
citalopram	-6.47	-6.79	-6.84	-6.17	-5.63
cocaine	-7.57	-6.87	-6.76	-6.55	-6.57
duloxetine	-7.02	-7.04	-7.12	-6.73	-5.98
GBR-12783	-7.42	-7.75	-7.38	-6.98	-7.17
modafinil	-6.82	-5.96	-5.8	-5.56	-5.28
rimcazole	-6.49	-9.16	-8.44	-7.83	-7.62
RTI-55	-7.59	-6.3	-6.69	-6.04	-5.81
sertalin	-7.13	-7.8	-7.67	-7.17	-6.73
sibutramin	-6.99	-6.55	-6.66	-6.43	-6.34
trimipramin	-7.7	-7.46	-7.54	-7.12	-6.84
vanorexin	-7.75	-7.2	-6.47	-6.79	-6.52

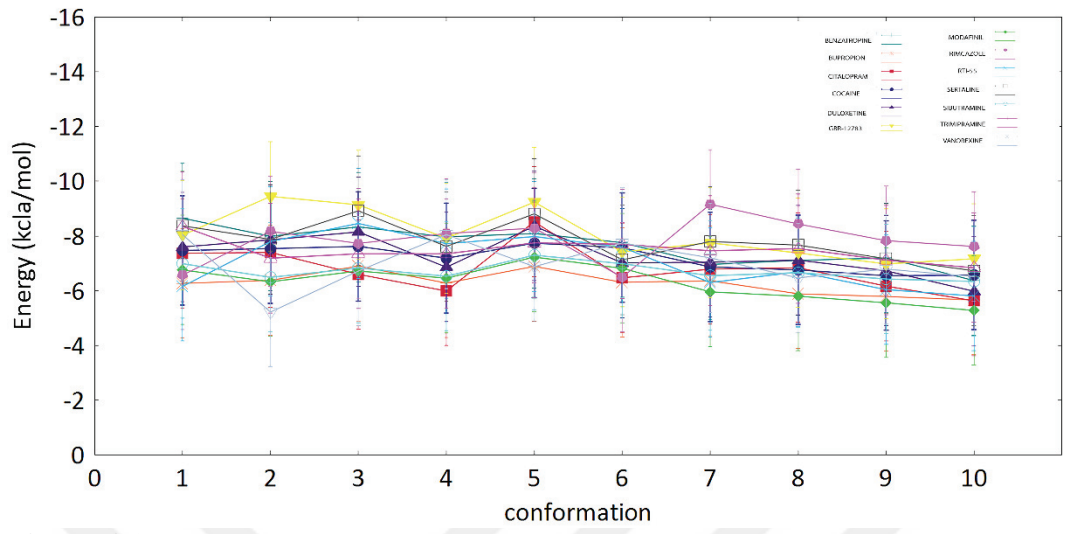


Figure A1: graphs representing docking results into 10 different conformations with error bars (SE for Autodock = ± 2 kcal/mol)

Table A.2 Docking results of known inhibitors docked into 10 conformations extracted from MD simulation of hDAT-modafinil complex and graphs representing docking results into 10 different conformations with error bars (standard error (SE) for Autodock = ± 2 kcal/mol)

hDAT open (modafinil bound)					
compound	hDATopen1	hDATopen2	hDATopen3	hDATopen4	hDATopen5
	AutoDock ΔG (kcal/mol)				
benzotropin	-8.94	-8.2	-8.09	-8.58	-8.61
bupropion	-8.03	-7.61	-6.43	-6.69	-6.94
citalopram	-8.73	-7.5	-7.09	-7.22	-8.76
cocaine	-8.33	-7.14	-6.99	-7.35	-8.31
duloxetine	-9.32	-8	-8.06	-7.65	-8.69
GBR-12783	-10.21	-9.6	-7.66	-9.03	-10.53
modafinil	-7.74	-7.02	-6.83	-7.52	-7.87
rimcazole	-9.71	-8.53	-9.3	-9.62	-10.09
RTI-55	-7.4	-7.42	-6.74	-6.62	-8.31
sertalin	-7.72	-7.88	-8.33	-8.87	-9.19
sibutramin	-8.09	-6.69	-6.92	-7.08	-7.61
trimipramin	-8.14	-7.46	-7.42	-8.1	-8.2
vanorexin	-11.69	-8.22	-9.6	-8.1	-9.77

hDAT open (modafinil bound)					
compound	hDATopen1	hDATopen2	hDATopen3	hDATopen4	hDATopen5
	AutoDock ΔG (kcal/mol)				
benzotropin	-8.02	-8.03	-8.11	-8.19	-8.9
bupropion	-6.59	-6.87	-6.73	-6.61	-6.82
citalopram	-6.86	-7.06	-7.39	-6.96	-8.24
cocaine	-6.65	-7.34	-7.3	-7.45	-7.31
duloxetine	-6.97	-7.11	-7.46	-7.36	-8.02
GBR-12783	-8.17	-9.43	-8.87	-9.35	-9.45
modafinil	-6.43	-6.79	-7.02	-6.79	-7.47
rimcazole	-8.85	-8.89	-9.02	-9.25	-8.51
RTI-55	-6.94	-6.87	-7.27	-7	-7.16
sertalin	-7.47	-7.6	-7.95	-7.79	-9
sibutramin	-6.79	-7.17	-7.25	-7.23	-7.04
trimipramin	-7	-7.62	-8.18	-7.88	-7.14
vanorexin	-8.45	-8.24	-8.12	-8.22	-8.76

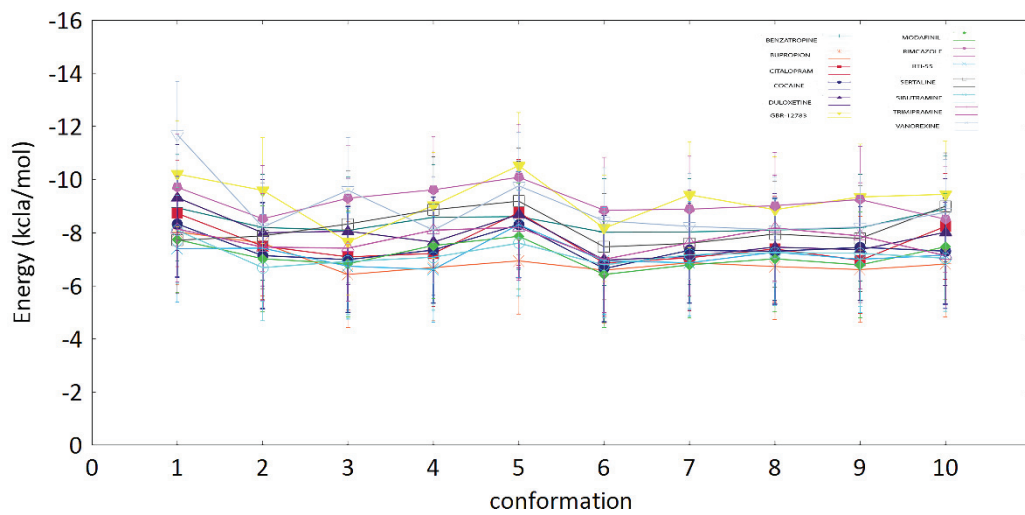


Figure A.2: graphs representing docking results into 10 different conformations with error bars (standard error (SE) for Autodock = ± 2 kcal/mol)

Table A.3 Docking results of known inhibitors docked into 10 conformations extracted from MD simulation of hDAT-amphetamine complex and graphs representing docking results into 10 different conformations with error bars (SE for Autodock = ± 2 kcal/mol)

hDAT closed (amphetamine bound)					
compounds	hDATclosed 1	hDATclosed 2	hDATclosed 3	hDATclosed 4	hDAT closed 5
	AutoDock ΔG (kcal/mol)				
6-OH-dopamin	-5.87	-5.55	-5.72	-5.58	-5.76
amphetamine	-6.26	-6.3	-6.5	-6.11	-6.34
cathinon	-6.53	-6.45	-6.7	-6.3	-6.48
dopamin	-6	-6.45	-6.23	-6.22	-5.6
fenflouramine	-6.78	-6.98	-6.98	-6.59	-6.94
FN102	5.54	-8.05	-6.99	-6.27	-5.9
metcathinone	-6.56	-6.39	-6.45	-6.41	-6.58
MDA	-7.04	-7.18	-7.22	-6.76	-6.9
metamphetamine	-6.37	-6.39	-6.49	-6.24	-6.44
MNAP	-8.01	-9.47	-8.56	-7.58	-7.79
MPTP	-6.39	6.32	-6.15	-6.28	-5.42
octopamine	-5.94	-6.02	-6.22	-5.98	-5.62

hDAT closed (amphetamine bound)					
compounds	hDATclosed 6	hDATclosed 7	hDATclosed 8	hDATclosed 9	hDATclosed 10
	AutoDock ΔG (kcal/mol)				
6-OH-dopamin	-6.01	-6.07	-4.82	-4.24	-5.10
amphetamine	-6.16	-6.34	-5.29	-5.75	-5.37
cathinon	-6.28	-6.58	-5.59	-5.42	-5.48
dopamin	-5.94	-5.96	-5.26	-5.86	-5.20
fenflouramine	-5.91	-6.63	-4.93	-4.85	-5.48
FN102	-6.93	-6.66	-6.06	-6.25	-6.30
metcathinone	-6.35	-6.73	-5.00	-5.41	-5.55
MDA	-6.79	-7.14	-5.27	-6.58	-5.29
metamphetamine	-6.3	-6.42	-4.89	-5.73	-5.35
MNAP	-7.33	-7.73	-5.29	-7.08	-6.75
MPTP	-6.15	-5.52	-5.14	-4.85	-5.20
octopamine	-5.77	-6	-5.18	-5.86	-5.03

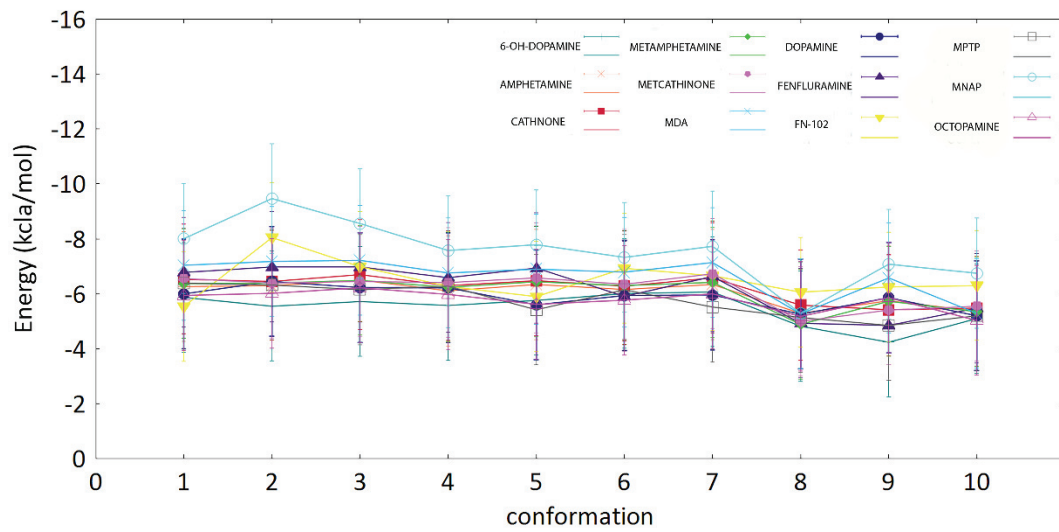


Figure A3 graphs representing docking results into 10 different conformations with error bars (standard error (SE) for Autodock = ± 2 kcal/mol)

APPENDIX B

Table B.1 150 best candidates extracted after flexible SBV and pharmacophore LBSD and their docking results into hDAT open and hDAT closed conformation

Candidate	H (1)	H*DRY*H (1)	H*O*DRY (1)	Glob-Prod (1)	Glob-Sum (1)	hDATclosed		hDATopen	
						Auto Dock (ΔG)	Auto Dock (Ki)	Auto Dock (ΔG)	Auto Dock (Ki)
AE_848_0229 8042	0.55463	0.28174	0.03783	0.30429	1.02987	-5.85	51.84	-5.36	118.06
AN_967_1548 8224	0.65468	0.3006	0.03767	0.31093	0.999299	-6.07	35.65	-5.41	108.34
AS_871_4228 2905	0.73289	0.31288	0.03707	0.31511	0.993179	-6.42	19.77	-5.39	112.41
AE_848_3701 8148	0.59787	0.18055	0.07604	0.36994	0.978111	-2.15	26650	-7.22	5.13
AE_641_0067 4038	0.66378	0.29176	0.03581	0.30785	0.964827	-6.33	22.93	-4.96	232.18
AP_124_4102 7793	0.68147	0.29204	0.03538	0.30795	0.960955	-6.72	11.87	-6.16	30.29
AE_848_1182 8165	0.54502	0.12771	0.05714	0.32613	0.946725	4.6	/	-7.86	1.73
AP_263_4291 1275	0.68266	0.28064	0.0342	0.30389	0.94023	-5.55	85.1	-5.44	103.57
AO_801_4107 7282	0.62435	0.25479	0.03392	0.29426	0.935656	-6.53	16.36	-5.6	77.96
AI_204_31721 050	0.65489	0.27331	0.0338	0.30122	0.931054	-6.09	34.24	-4.89	260.91
AF_399_1512 8622	0.608	0.24658	0.03318	0.29106	0.923082	-4.92	248.94	-5.55	86.07
AP_263_4141 7746	0.6037	0.21538	0.09388	0.4141	0.917514	-1.22	12677 0	-7.11	6.14
AQ_390_1163 3955	0.67621	0.26649	0.03241	0.29869	0.915882	-6.59	14.73	-5.55	84.94
AP_263_4077 8092	0.66743	0.26493	0.03243	0.29811	0.913497	-4.7	356.75	-6.45	18.79
AP_355_4347 0009	0.65674	0.26086	0.03265	0.29658	0.909086	-6.5	16.66	-4.69	231.26
AO_840_4271 7981	0.64605	0.25787	0.03234	0.29544	0.904511	-5.82	53.97	-4.69	363.21
AG_803_4086 9717	0.67136	0.25954	0.03168	0.29607	0.90396	-6.22	27.57	-5.19	156.08
AJ_333_09217 054	0.66883	0.21107	0.09002	0.41234	0.903779	-6.29	24.51	-6.33	13.72
AO_854_4347 9173	0.70455	0.25708	0.03063	0.29514	0.90352	-6.12	32.58	-5.02	209.5
AK_968_0969 3021	0.67821	0.2589	0.03144	0.29583	0.903084	-6	4.07	-6	4.13
AE_641_0056 6009	0.64552	0.25686	0.03197	0.29505	0.900805	-5.06	194.63	-3.95	1270
AP_124_4338 2881	0.61619	0.24383	0.03223	0.28998	0.899483	1.32		-7.05	6.83
AH_034_3246 4035	0.55841	0.23664	0.03198	0.2871	0.898799	-5.97	42.02	-4.77	320.95
AP_263_4341 1891	0.66074	0.25522	0.03215	0.29442	0.897835	-6.2	28.37	-5.07	190.84
AI_942_13331 922	0.63905	0.25319	0.03167	0.29364	0.894691	0.65		-6.24	26.88
AP_263_4194 6528	0.65757	0.25322	0.0316	0.29365	0.894278	-6.05	36.97	-6.2	28.72
AG_690_0970 8032	0.61938	0.2507	0.03185	0.29267	0.893878	-5.17	161.48	-4.22	812.77
AG_455_0268 8033	0.60497	0.24106	0.03186	0.28887	0.892256	-5.49	94.64	-4.84	284.82

AP_263_4261 1020	0.6445	0.25185	0.03137	0.29312	0.891423	-5.69	67.05	-5.58	81.6
AF_399_1503 0041	0.64835	0.25198	0.03132	0.29317	0.891415	-3.85	1510	-6.44	18.92
AC_907_2501 4313	0.74207	0.24106	0.02823	0.28887	0.888997	-7.11	6.15	-5.77	58.77
AJ_292_37095 006	0.63515	0.24815	0.03148	0.29168	0.888005	-4.93	242.7	-6.22	27.7
AE_848_3320 6048	0.61358	0.2429	0.03159	0.28961	0.886634	-6.13	32.08	-4.96	233.3
AE_406_4105 6245	0.68516	0.24854	0.03012	0.29183	0.886561	-0.38	52666 0	-7.16	5.6
AG_205_0178 3022	0.64804	0.24619	0.03058	0.29091	0.880755	-4.87	269.33	-4.01	1150
AP_355_4346 9976	0.67266	0.24504	0.02991	0.29046	0.879791	-6.83	9.91	-5.18	159.23
AP_263_4217 3199	0.64286	0.2452	0.03075	0.29052	0.879736	-1.97	35970	-6.58	15.06
AH_262_3422 7043	0.62328	0.24099	0.03112	0.28885	0.878339	-6.64	13.67	-5.48	96.38
AO_365_4336 8475	0.64714	0.24466	0.03041	0.29031	0.878012	-6	39.73	-5.68	68.92
AO_840_4271 7980	0.65714	0.2433	0.03048	0.28977	0.87557	-5.8	55.91	-4.61	418.06
AG_690_1370 5992	0.66756	0.23914	0.03091	0.28811	0.875272	-6.61	14.31	-5.4	110.43
AP_263_4337 1037	0.59607	0.2157	0.08669	0.39902	0.87228	-0.57	38261 0	-7.13	5.98
AK_968_4094 1130	0.66879	0.23958	0.03059	0.28828	0.872064	-6.64	13.68	-5.59	80.44
AO_080_4094 3604	0.66442	0.24068	0.03009	0.28872	0.870982	-6.39	20.87	-5.67	69.29
AG_670_3458 3003	0.59483	0.21515	0.03015	0.27813	0.869621	-5.64	73.06	-5.13	172.47
AN_512_1326 4022	0.625	0.22548	0.03055	0.28251	0.869221	-5.44	103.76	-5.26	138.78
AG_205_0675 5020	0.67595	0.23686	0.02917	0.28719	0.865767	-5.83	53.73	-6.17	30.1
AE_848_0127 3028	0.68234	0.23589	0.02902	0.2868	0.865508	-6.26	25.73	-4.85	280.67
AP_355_4346 9991	0.68759	0.23616	0.02935	0.2869	0.86431	1.1	/	-4.85	278.04
AP_836_4122 0120	0.59413	0.23316	0.03025	0.28568	0.863338	-6.27	25.34	-5.04	203.3
AC_907_3412 7026	0.68985	0.23397	0.0295	0.28602	0.860374	-6	39.96	-4.94	240.95
AG_690_1131 0128	0.58242	0.22479	0.03015	0.28222	0.860014	-6.2	28.68	-5.18	160.37
AP_906_4125 1032	0.6209	0.23361	0.02965	0.28587	0.858882	-7.38	3.89	-6.16	30.29
AE_641_0064 7044	0.64057	0.23306	0.02912	0.28564	0.857217	-6.39	20.8	-5.36	117.43
AI_204_31718 012	0.65269	0.22892	0.02977	0.28394	0.854748	-6.28	24.74	-5.1	181.97
AA_516_3001 2024	0.5852	0.22115	0.02954	0.28069	0.852693	-5.06	195.25	-4.04	1090
AT_051_4342 1379	0.67127	0.23039	0.02901	0.28455	0.852277	-6.58	15.07	-5.53	88.84
AN_967_1548 8221	0.63615	0.22991	0.02916	0.28435	0.851662	-5.42	106.51	-6.24	26.66
AG_690_1154 8859	0.57814	0.17797	0.07909	0.39006	0.85133	-2.85	8150	-7.35	4.09
AA_516_1243 2250	0.6293	0.22913	0.02923	0.28403	0.850758	-5.5	93.61	-5.17	65.12
AH_262_1466 8001	0.61582	0.21907	0.02954	0.27981	0.848352	-2.03	32560	-4.81	297.64
AB_337_1303 6269	0.62928	0.22321	0.0294	0.28156	0.846529	-6.66	13.08	-6	40.05
AN_329_4100 6735	0.71484	0.21061	0.02491	0.27616	0.846273	-6.66	13.17	-6.09	34.47

AE_406_4105 6053	0.68121	0.2259	0.02839	0.28269	0.845069	-0.38	52666 0	-7.16	5.6
AP_263_1016 6001	0.64658	0.22567	0.0281	0.28259	0.844775	-6.97	7.73	-6.26	25.88
AG_690_1166 8987	0.62111	0.22524	0.02892	0.28241	0.84391	-6.55	15.73	-6.53	16.48
AG_690_3444 0051	0.59888	0.21999	0.02929	0.2802	0.843706	6.1		-7	7.36
AN_153_4330 9816	0.56059	0.1859	0.083	0.39245	0.843599	-3.64	2140	-6.73	11.58
AG_690_3617 0003	0.57949	0.21666	0.02922	0.27878	0.842305	-1.47	83970	-6.45	18.67
AP_263_4217 3350	0.63626	0.22146	0.0291	0.28082	0.84158	-5.8	56.44	-6.15	31.21
AT_057_4348 5877	0.59281	0.22247	0.02902	0.28125	0.841542	-4.32	686.36	-5.86	50.93
AO_080_4344 1536	0.66188	0.22356	0.02784	0.28171	0.841237	-7.08	6.47	-5.76	60.28
AP_501_4230 2470	0.60885	0.22385	0.02869	0.28183	0.840874	-6.3	24.02	-6.98	7.7
AS_662_4341 2992	0.65096	0.22357	0.02853	0.28171	0.839935	-6.29	24.52	-5.06	193.8
AO_365_4132 9037	0.6226	0.22294	0.0287	0.28145	0.8396	-0.58	37279 0	-6.71	12.08
AG_205_3700 7234	0.63732	0.2225	0.02789	0.28126	0.838452	-7.48	3.31	-7.16	5.86
AE_842_3392 0018	0.56914	0.21858	0.02897	0.2796	0.838287	-5.5	92.9	-5.12	176.24
AN_698_4211 4533	0.62195	0.22155	0.0287	0.28086	0.837869	-6.02	38.37	-5.65	71.8
AO_854_4000 3386	0.64407	0.22225	0.02794	0.28116	0.837713	-6.9	8.74	-5.5	92.47
AH_262_3422 8052	0.60899	0.22202	0.02845	0.28106	0.837232	-5.33	123.21	-4.23	797.83
AC_907_3412 6064	0.60212	0.21868	0.02884	0.27964	0.836614	-5.9	47.65	-5.35	120.38
AH_034_1196 3070	0.63026	0.22177	0.02842	0.28095	0.836485	-7.01	7.3	-5.54	87.22
AR_360_4276 0709	0.68248	0.21764	0.02706	0.2792	0.836047	-8.13	1.1	-7.15	5.71
AI_204_31698 019	0.56622	0.2093	0.02875	0.27559	0.834123	-0.05		-5.95	43.47
AG_670_1190 0026	0.59444	0.21739	0.02862	0.27909	0.833023	0.12		-5.66	7.52
AP_355_4346 9975	0.64112	0.21886	0.02818	0.27972	0.832529	-6.21	27.93	-4.8	302.87
AQ_432_4143 6196	0.65254	0.21928	0.02803	0.2799	0.831771	-6.56	15.44	-6.25	26.35
AF_399_4210 0404	0.66624	0.21446	0.02627	0.27783	0.831767	-7.13	5.94	-5.71	65.15
AO_854_4346 3999	0.713	0.20512	0.02458	0.27374	0.831102	-7.47	3.34	-6.25	26.43
AB_337_1303 6340	0.62037	0.21886	0.02779	0.27972	0.830987	-6.56	15.67	-6.14	31.5
AR_422_4287 5228	0.61768	0.21869	0.02783	0.27965	0.83062	-5.74	61.54	-5.93	44.85
AI_298_32870 013	0.61503	0.2184	0.02785	0.27952	0.830057	-1.12	150.61	-6.4	20.36
AP_263_4261 0973	0.63164	0.21814	0.02798	0.27941	0.829717	-6.27	25.41	-6.49	17.53
AG_205_1236 7041	0.6645	0.21746	0.02822	0.27912	0.829662	-6.68	12.67	-6.4	20.48
AO_365_4336 8753	0.58609	0.21645	0.02827	0.27869	0.828798	-6.33	23.04	-5.93	45.29
AC_907_2500 5104	0.66952	0.21761	0.0276	0.27918	0.828764	-6.82	10.01	-5.34	121.4
AP_065_4344 1414	0.64221	0.21448	0.02842	0.27784	0.828501	-6.2	28.6	-5.69	67.62
AB_337_1303 6243	0.62	0.21725	0.02759	0.27903	0.828034	-5.04	201.46	-6	40.25

AN_465_4336 9193	0.50377	0.10846	0.08502	0.37499	0.82802	-0.98	19086 0	-7.09	6.33
AE_848_3273 1037	0.62953	0.21682	0.02733	0.27885	0.827955	-7.39	3.8	-6.15	31.24
AR_360_4025 0962	0.65829	0.21337	0.0263	0.27736	0.827884	-6.39	20.8	-5.49	93.85
AK_918_1190 7023	0.66316	0.21593	0.02702	0.27846	0.827656	-6.76	11.06	-2.47	15520
AE_641_1284 5202	0.59913	0.21658	0.02798	0.27875	0.827242	-2.68	8030	-7.26	4.75
AI_942_13331 780	0.65614	0.21635	0.02729	0.27865	0.827027	-6.05	36.89	-6.24	26.88
AO_854_4010 8228	0.64898	0.21624	0.02726	0.2786	0.826891	-6.54	16.1	-5.42	106.84
AF_960_0043 7050	0.62647	0.21617	0.02761	0.27857	0.825866	-6.58	15.08	-5.1	183.14
AS_871_1133 6720	0.65119	0.21292	0.02639	0.27717	0.82537	-6.62	14.15	-5.32	126.29
AG_690_1116 9080	0.61397	0.21538	0.02793	0.27823	0.825242	-3.48	2820	-5.22	148.57
AK_968_1173 8113	0.62678	0.21536	0.0272	0.27822	0.825137	-6.26	25.79	-6.92	8.4
AQ_390_1330 4011	0.58039	0.20927	0.02832	0.27557	0.825028	-6.96	7.95	-5.3	130.42
AS_871_4347 5907	0.64039	0.21542	0.02734	0.27825	0.824766	-6.04	37.36	-5.42	105.81
AJ_292_14129 264	0.67266	0.20748	0.0253	0.27479	0.824102	-3.87	1460	-5.73	63.3
AJ_333_13050 048	0.63092	0.21466	0.0271	0.27792	0.823991	-5.42	106.1	-6.01	39.28
AI_204_31757 058	0.65136	0.21506	0.02767	0.27809	0.823892	-5.36	117.1	-4.31	695.46
AP_355_4347 0025	0.64578	0.21352	0.0267	0.27743	0.823821	-6.6	14.55	-5.69	67.42
AG_690_0759 0015	0.61042	0.21644	0.01747	0.22357	0.823778	-6.13	32.19	-6.06	36.26
AN_689_4174 1334	0.57814	0.2063	0.02822	0.27426	0.823345	44.52		-6.08	34.89
AJ_292_41723 218	0.62286	0.2137	0.02752	0.2775	0.82129	-6.9	8.7	-5.88	48.76
AP_355_4346 9975	0.62534	0.2134	0.02768	0.27737	0.821241	-6.21	27.93	-4.8	302.87
AA_516_1243 2331	0.64908	0.21004	0.02804	0.27591	0.820845	-5.98	41.54	-5.93	45.27
AE_848_3250 3063	0.61154	0.21211	0.02782	0.27681	0.820374	-6.34	22.34	-5.1	181.91
AN_329_4334 1637	0.58917	0.21255	0.02769	0.277	0.820062	-4.58	440.37	-5.12	176.38
AP_263_4341 2431	0.61504	0.21291	0.02715	0.27716	0.819889	-4.37	342.47	-5.59	80.27
AO_080_4337 8446	0.61166	0.21264	0.02743	0.27704	0.81929	-5.53	88.2	-4.28	229.17
AI_204_31727 034	0.61521	0.21052	0.02787	0.27612	0.819142	1.22		-6.6	14.44
AH_487_4143 4858	0.61822	0.21225	0.02699	0.27687	0.818882	-2.06	31.01	-5.44	102.75
AJ_292_40891 136	0.49767	0.13979	0.07705	0.37365	0.818605	0.67		-6.47	17.98
AP_124_4338 2878	0.6215	0.21209	0.02697	0.2768	0.818597	-7.1	6.29	-6.65	13.4
AE_562_4329 2961	0.66587	0.20507	0.02513	0.27372	0.81831	-6.9	8.73	-6.26	25.75
AJ_333_09218 036	0.58524	0.18422	0.06373	0.35374	0.818088	-0.17	74655 0	-6.48	17.87
AN_329_4100 6789	0.70463	0.20153	0.02599	0.27213	0.816702	-6.66	13.17	-6.09	34.47
AG_690_4044 8673	0.62543	0.20892	0.02777	0.27542	0.816664	-6.25	26.25	-5.98	41.07
AP_355_4347 1872	0.6285	0.21029	0.02654	0.27602	0.816558	-4.73	343.09	-6.03	37.91

AT_057_4346 9072	0.61162	0.21068	0.02744	0.27619	0.816184	-4.32	686.36	-5.86	50.93
AH_262_3233 8004	0.58994	0.21004	0.02756	0.27591	0.815981	-7.16	5.6	-5.44	103.4
AT_051_4342 2518	0.6523	0.20745	0.02593	0.27477	0.814239	-5.18	160.37	-4.29	720.88
AI_204_31701 041	0.67017	0.20922	0.0265	0.27555	0.814103	-6.56	15.42	-5.59	80.11
AO_854_1291 0145	0.67295	0.2099	0.02709	0.27585	0.813958	-6.43	19.32	-5.27	138.21
AM_879_1174 1391	0.64305	0.20684	0.02582	0.2745	0.813943	-6.54	16.04	-5.38	114.01
AG_205_0587 9010	0.63528	0.20967	0.02684	0.27575	0.813687	-7.15	5.79	-6.22	27.36
AN_689_4174 1341	0.58545	0.20896	0.0274	0.27544	0.813519	-0.06	89816 0	-6.09	34.47
AF_399_4090 8294	0.6071	0.20918	0.02752	0.27553	0.813263	-3.02	6090	-6.03	38.02
AP_836_4122 0284	0.64665	0.20575	0.02559	0.27402	0.813212	-7.25	4.85	-5.88	48.71
AG_690_1288 5322	0.63556	0.20845	0.02743	0.27521	0.813102	-6.56	15.57	-6.81	10.26
AP_263_4001 7925	0.63517	0.20857	0.02728	0.27527	0.812358	-7.59	2.74	-6.08	34.89
AP_124_4338 2867	0.6355	0.20849	0.02667	0.27523	0.811583	-6.26	25.78	-6.05	37.02
AR_685_4330 6310	0.62427	0.2086	0.02697	0.27528	0.811445	-5.43	104.63	-6.07	35.65
AK_968_1377 9206	0.57569	0.20713	0.02739	0.27463	0.81128	-5.36	118.75	-4.69	366.31
AN_604_1428 2001	0.61282	0.20665	0.02741	0.27442	0.810939	-6.4	20.53	-5.58	80.63
AO_476_4340 7263	0.59979	0.19386	0.0274	0.26864	0.810258	-5.35	119.74	-6.36	21.13

APPENDIX C

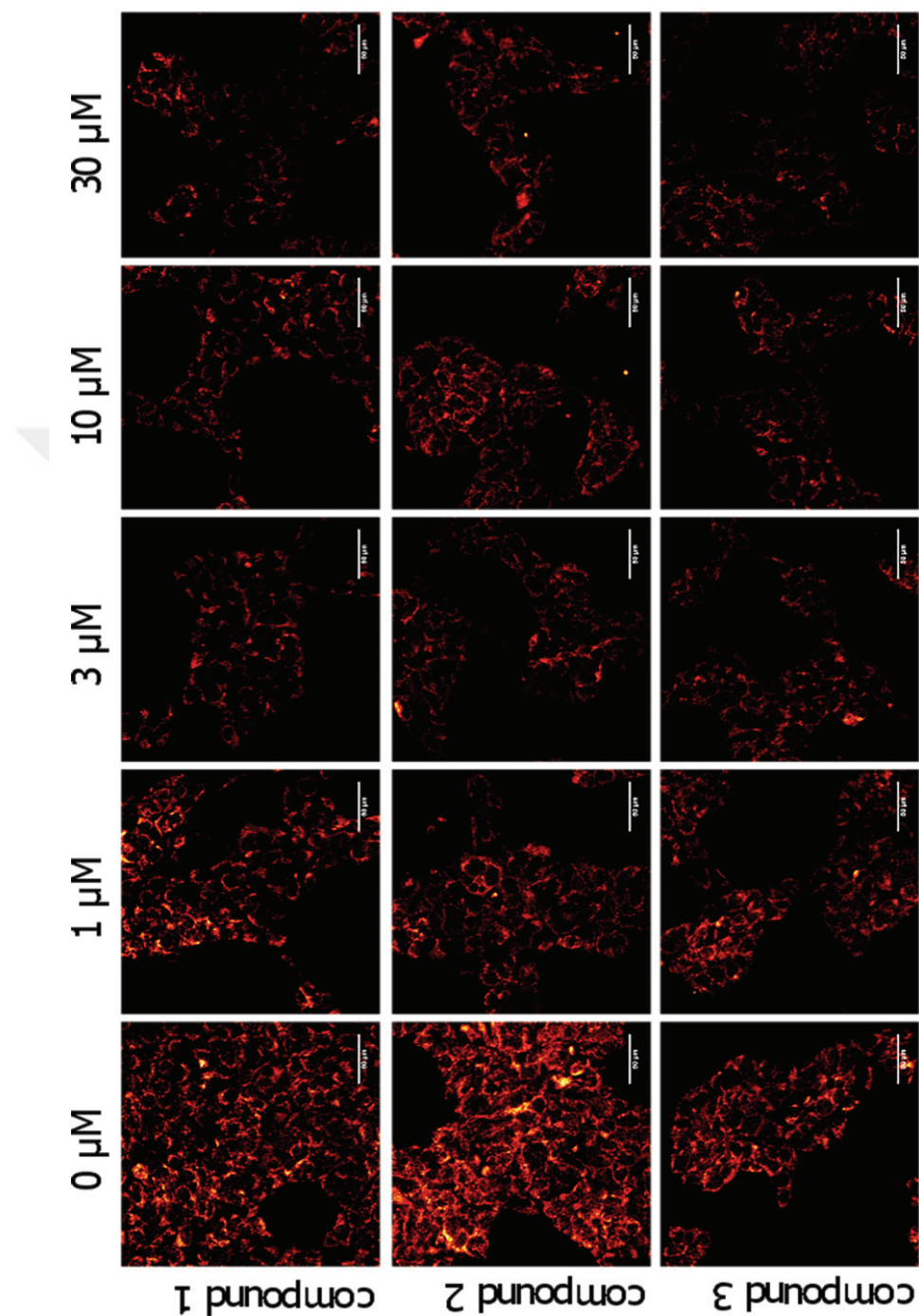


Figure C.1 HEK-hDAT were treated for 10 min with different concentrations (1 μM, 3 μM, 10 μM and 30 μM) of compounds **1**, **2** or **3**. Representative fluorescent images of HEK-hDAT with 30 s incubation of 10 μM ASP+ before and after incubation with the compounds.

